The Mixture Formation Process In The Gas Fuelled Engine

Politechnika Lubelska
Wydział Mechaniczny
ul. Nadbystrzycka 36
20-618 LUBLIN

Łukasz Grabowski
Mirosław Wendeker

The Mixture Formation Process In The Gas Fuelled Engine

Politechnika Lubelska
Lublin 2010

Recenzent: prof. dr hab. inż. Piotr Tarkowski

Redakcja i skład: Łukasz Grabowski

Publikacja wydana za zgodą Rektora Politechniki Lubelskiej

ISBN: 978-83-62596-07-2

Wydawca: Politechnika Lubelska
ul. Nadbystrzycka 38D, 20-618 Lublin
Realizacja: Biblioteka Politechniki Lubelskiej
Ośrodek ds. Wydawnictw i Biblioteki Cyfrowej
ul. Nadbystrzycka 36A, 20-618 Lublin
tel. (81) 538-46-59, email: wydawca@pollub.pl
www.biblioteka.pollub.pl
Druk: Wydawnictwo-Drukarnia „Liber Duo"
ul. Długa 5, 20-346 Lublin

Contents

1. Gas supply system in combustion engines

1.1 Introduction

Gaseous fuels have been used to supply internal combustion engines since motorization started. The construction, developed by Nikolaus August Otto in 1862, was fuelled by coal gas. It is the prototype of the currently used gasoline engines.

Despite the advantages of gaseous fuels in the quality of combustion (especially CO_2 emissions), liquid fuels: petrol and diesel have remained the basic type of fuel for decades. Factors that favor the dominance of liquid fuels in automotive industry are their high energy density and low costs of their extraction, processing and storage. For example, the gasoline calorific value is approximately 38.6 MJ/m^3 under normal conditions, whereas that of LPG is approximately 36.6 MJ/m^3, but at a pressure of 0.8 MPa. However, the effective storage of methane takes place only at a pressure above 20 MPa. For the last twenty years, gaseous fuels have continued to replace oil-based liquid fuels. This trend is due to declining oil resources and continuously increasing oil prices [12, 58]. In 2008, the prices reached $150 per barrel and the analysis of long-term trends, published by Globtrex.com [17], indicates that in 2-3 years, oil prices can reach their new peak values of around $200 per barrel. The analyses presented in the work [62] show that both present and future conventional oil resources will satisfy the actual needs for the next 50 years. However, the largest oil consumers are required to follow efficient and sustainable management of this raw material. The natural response to the situation is a constantly increasing share of alternative fuels in road transport. The viable alternatives to conventional fuels are liquefied propane-butane (LPG), as its physical and chemical properties enable easy storage, and compressed natural gas - CNG. LPG is a primary end-product produced in petroleum refining and is the most common alternative source of power in automotive vehicles. However, using compressed natural gas as an automotive fuel can enable to become independent of petroleum-based fuels [31]. The existing natural gas deposits are an important advantage. The data given in the study [42] shows that the reserves and proven natural gas resources are sufficient enough for nearly 900 years (at current consumption rate). According to the EU Directorate-General for Energy and Transport, in 2020 the share of CNG in the overall fuel market is assumed to amount to 10% [18]. Further research on alternative fuels has focused on hydrogen which was called a fuel of the future. For road transport, it can be used both in hydrogen fuel cells and piston engines. Hydrogen is characterized by good properties as an automotive fuel, including high heat of combustion, wide flammability limits, low ignition energy, and highself ignition temperature. For several years, automotive companies like BMW or Mazda [103, 104] have been intensively engaged in the development of hydrogen fuelled engines.

The use of alternative fuels, besides economic values, is particularly important due to exhaust gas emissions regulations. [86]. The United Nations Framework Convention on Climate Change (UNFCCC) clearly defines the objectives and principles of cooperation among countries to prevent climate changes. Particular emphasis is placed to reduce the emissions of greenhouse gases, e.g. carbon dioxide.

Comparing the chemical composition of conventional and alternative fuels, in the case of gas fuels, the mass share of carbon in a molecule decreases in favor of hydrogen and looks as follows: $C_1H_{1,89}O_{0,016}$ for gasoline, $C_1H_{1,86}O_{0,005}$ for diesel, $C_1H_{2,525}$ for LPG and C_1H_4 for CNG. Due to the decreasing share of coal in the fuels, the combustion of gaseous fuels is accompanied by reduced carbon dioxide emissions into the atmosphere. The data in the work [98, 99] shows that replacing gasoline with LPG will decrease CO_2 emissions by about 12%, whereas with natural gas by about 20%. In the report on reducing carbon dioxide emissions strategy by AEGPL Europe, the authors state a several percent improvement in the case of LPG fuelled SI engines [1]. A comparable reduction in CO_2 emissions in relation to gasoline was obtained after testing in Australia vehicles supplied with propane-butane and natural gas [41]. Similar results confirming the benefits of the change of gasoline for gaseous fuel are given in the work [10].

The information in a report by ARAL Ltd. confirms the common use of LPG to fuel vehicles. German forecasts indicate that the number of LPG fuelled vehicles is going to increase five times in the next six years [77].

The above analyses show that at present gaseous fuels are becoming a basic kind of fuel, which implies the development of gas supply systems for automotive engines. The most common are sequential injection systems, where due to low fuel energy density and ease of installation, LPG is injected into the intake manifold.

Gasoline injection systems have been studied especially with respect to air-fuel mixture formation and the influence on the process of factors such as the parameters of a sprayed gasoline stream (macroscopic – a spray angle and range; microscopic – a spray spectrum), an intake system structure, a droplet movement, a fuel film [40, 43, 90, 69]. The study has demonstrated a complex relationship between fuel injection parameters and engine operation results.

Due to high cost of studies of that type, companies producing gas installations refrain from carrying them out. The literature offers an insufficient number of studies on the impact of LPG injection parameters on the process of mixture formation. In modern gas installations, injection time and the start of a gaseous fuel injection into the intake manifold are copied from gasoline injection systems. The correction of injection time results only from a different physical state of aggregation of the fuel dosed. The process of air-gas mixture formation differs significantly from that of the original fuel.

Air-gas mixture formation depends, e.g. on the construction of the intake manifold and a fuel supply method, or the design of a gas supply system. Elements to dose gas can be injectors that are mounted directly on inlet pipes, as it is in the Koltec Necam installation. However, in most cases, these are injectors or a fuel injection unit connected to the manifold with pipes and injection nozzles. The injection nozzle is often mounted too far away from the axis of each cylinder intake valve. There is no research on the mixture formation process and the influence gas installation assembly parameters have on this process. In the case of LPG supply, there is no difficulty in the accumulation of a liquid fuel phase in the intake manifold. Therefore, it seems that placing the gas injector further away from the inlet valve axis should improve the mixture formation process in a cylinder by its better homogenization. Gas installations are mounted in workshops and based on engineering practice it turns out that moving away of the injection nozzle due to problems with system installation deteriorates engine operation.

The assessment of how much the way a gas injector is installed influences the quality of engine operation was what mostly influenced the author to write this monograph.

1.2 Fuel injection systems

The development of gasoline supply systems caused implementation of gas installations of next generations. This development results mainly from continuous tightening of exhaust gas emission standards for vehicles [33, 59, 73, 74]. LPG fuelled vehicles are required to meet the same standards with respect to toxic emissions as when they work on gasoline. For instance, for M1 category vehicles [72] manufactured in accordance with EURO IV standards since January 1, 2005, the exhaust gas toxicity must not exceed the values given in Table 1.1. during an official certification.

Tab. 1.1 Permissible emission of exhaust components into the atmosphere according to EURO IV [57]

carbon monoxide [g/km]	**hydrocarbons [g/km]**	**nitric oxides [g/km]**
1,0	0,1	0,08

Reviewing the latest versions of gas installations, the first generation of LPG installation can be compared to a carburetor supply system. The second generation reflects a single-point gasoline injection, whereas the third and fourth generations match the operation principles of a multi-point gasoline injection.

Nowadays, the fourth-generation systems are the most common, as they can be mounted in new vehicles. At the same time this type of installation provides a precise dosage of fuel so that EURO IV emission standards can be met [56].

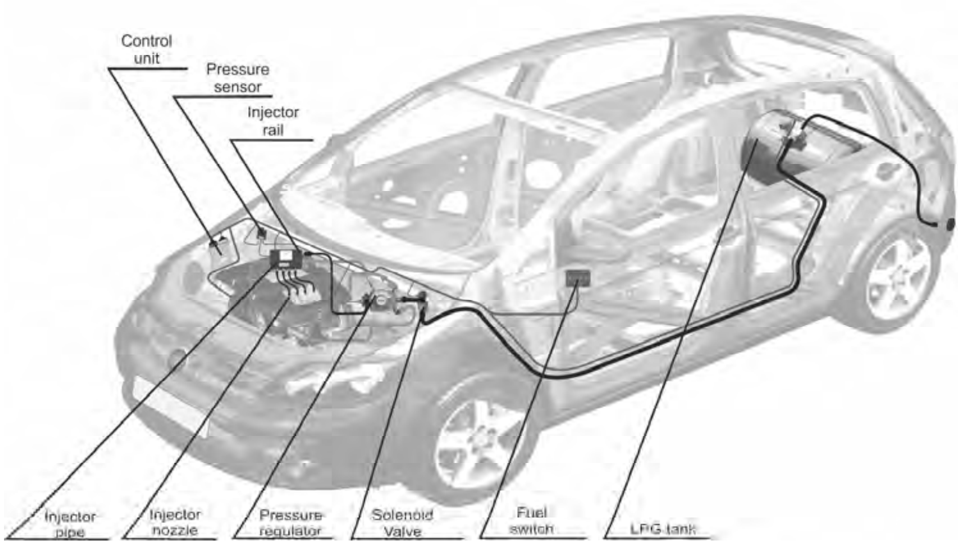

Fig. 1.1 Typical LPG injection system in a vehicle

The principle of operation of gas injection systems is as follows. LPG liquid fuel flows from a tank to a reducer-evaporator where is evaporated to become a gas. Its pressure is reduced. Then, the evaporated LPG of a suitable pressure (usually about 0.1 MPa of overpressure in relation to the pressure in an inlet manifold) reaches injectors. In most cases, they are combined on a common injection rail and the gas is supplied to a manifold through pipes and nozzles [51, 83]. The properties of the injectors of the fourth generation system are comparable with the ones currently used in gasoline-fuelled vehicles. Figure 1.2 presents a time diagram for the course of gas injection into inlet pipes as a function of the angle of crankshaft rotation. A control unit sets the duration of a gas injection, based on the time of gasoline injection, and appropriately adjusts it with respect to the temperature and pressure of a gas phase.

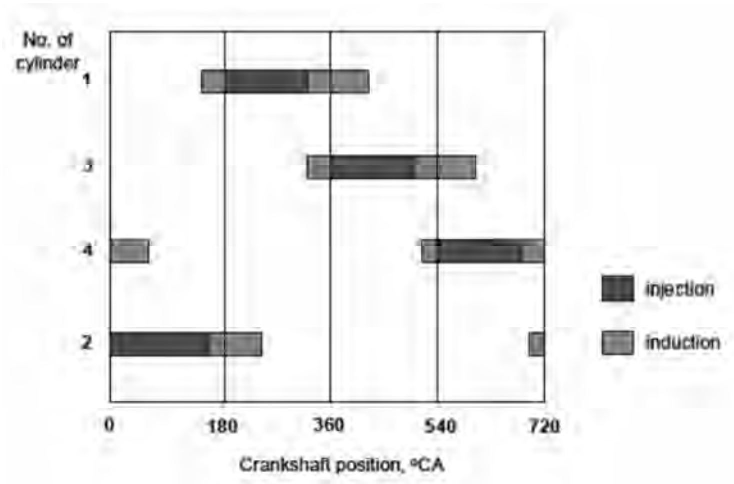

Fig. 1.2 Sequential gas injection [35]

1.3 LPG properties

Tab. 1.2 Properties of propane and butane

PROPANE C_3H_8	**BUTHANE C_4H_{10}**
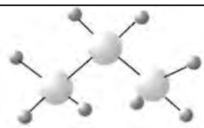	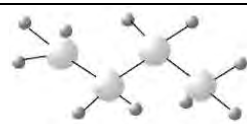
According to PN-C-96008;1998: • amount of C_3, min, % (m/m) – 90.0, • calorific value, min, kJ/kg - 45 640, • density at a temperature of 15.6°C, min, t/m^3 - 0,495.	**According to PN-C-96008;1998:** • amount of C4, min, % (m/m) – 95.0, • calorific value, min, kJ/kg - 44 800, • density at the temperature of 15.6°C, min, t/m^3 - 0,564.
Vapour pressure, MPa: • at the temperature of 15°C, min – 0.20, • at the temperature of 70°C, max – 3.04.	**Vapour pressure, MPa:** • at the temperature of 40°C, max – 0.47, • at the temperature of 70°C, max – 1.08.
Theoretical need for air: • L_t = 15.59 kg area.	**Theoretical need for air:** • L_t = 15.37 kg area.

2. Mixture formation process in automotive engines

2.1 Air-gasoline mixture formation process

Comparing supply systems based on gasoline and gas, many similarities with respect to the control methods can be observed [75]. However, gas-dynamic processes in an inlet system vary in a significant way.

Describing a gasoline injection system in an engine the stages of gasoline injection, mixture formation in the inlet system and in the cylinder need to be addressed [2, 44, 90]. Referring to fuel injection, the parameters of fuel flow are important [34, 39, 85]. They fall into three groups:

- gasoline volume flow and gasoline mass,
- flow microstructure,
- flow macrostructure.

Research results on the influence of injector geometry on the parameters of gasoline flow are presented in the work [92]. It has been demonstrated that more openings in the injector increase flow volume and the degree of fuel atomization.

The mixture formation in an intake manifold is accompanied by fuel film formation, as after injection fuel is not completely carried along by flowing air. Thus, gasoline accumulates in the inlet pipe as non-evaporated liquid. The subject of indirect gasoline injection was described, e.g. in [3, 13, 91]. The present research has shown that fuel film formation has got an adverse impact on mixture composition in the dynamic stages of engine operation. That is why gasoline injectors are mounted as close as possible to an inlet valve.

The next stage of mixture formation takes place inside cylinders. Fuel is delivered as aerosol, gas mixture and liquid fuel flowing down due to gravity. The re-search results on this issue are presented in [41].

During research, the following observations have been made:

- the mass of liquid fuel supplied to a cylinder depends on an injection dose and air speed,
- there is no liquid fuel in a cylinder under full load,
- mixture swirl reduces the size of droplets and to some extent, reduces the fuel mass.

Similar results have been obtained during the tests described in [52]. Using computational fluid dynamics (CFD), the impact of an air swirl on the mass of liquid fuel phase in a cylinder with the use of a SCV valve installed in a manifold has been simulated and tested.

It has been proven that the change of the position of the CSV valve (fig. 2.1) significantly influences the extent to which gasoline mixes with air in a cylinder. The flow of air-fuel mixture through a suitably shaped air intake pipe supports the mixing process. This contributes to a better mixture homogenization in a cylinder. It has been noted that the mass of fuel droplets in a cylinder decreased by 10% compared with the results for the CSV valve in a closed position.

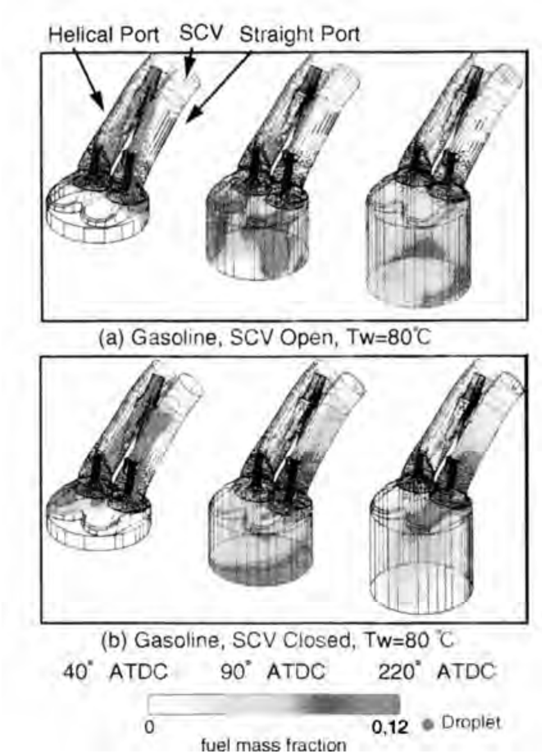

Fig. 2.1 Differences in mixture homogenization for various arrangements of inlet pipes: a) SCV valve opened, b) SCV valve closed [52]

The changes in the distribution and degree of air-fuel mixture homogenization in an engine that result from alternating valve timing gear are given in [9]. The tests were done for varied values of the inlet valve lift, i.e. less than 1.5 mm and 3 mm. In order to record any changes during filling, optical methods enabling quickchanging processes recording were used. It has been demonstrated that an average fuel droplet diameter increases as the value of an intake valve lift decreases (fig. 2.2).

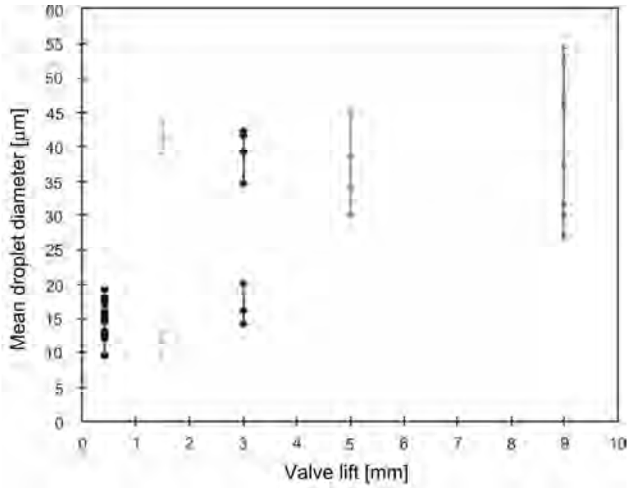

Fig. 2.2 Dependence of a droplet diameter on an intake valve lift [9]

The analysis of the velocity and turbulence in a cylinder [9] explains why a fuel droplet diameter increases. It has been found that turbulence intensity increases for small values of an intake valve lift (fig. 2.3), which is manifested by swirl vortices and tumble vortices that occur inside a cylinder.

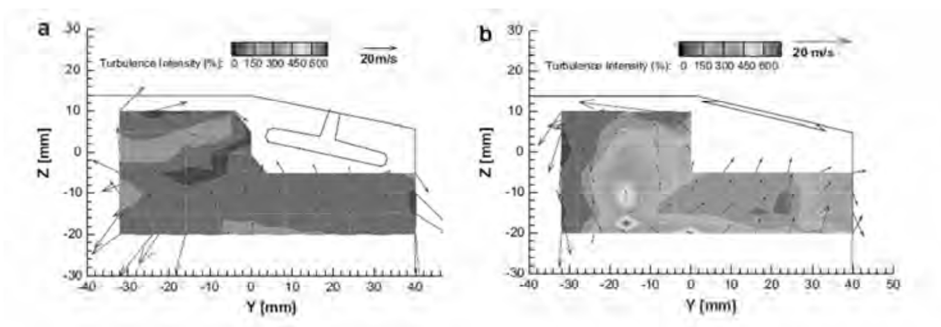

Fig. 2.3 Fuel mixture speed and its turbulence for the two variants of intake valve opening: a) 9 mm, b) 0.4 mm [9]

The nature of a filling process depends to a large extent on the geometry of an intake manifold [9]. Vehicles with a fuel injection system are most often equipped with asymmetric intake manifolds with an air intake that is asymmetric to all intake pipes axes in a manifold (photo 2.1). There are many studies that describe how manifold geometric factors influence a mass flow rate through an intake valve [20, 43, 65, 68, 93]. A filling process is examined with the use of computational simulations and optical methods [4, 24, 67].

The effectiveness of computational fluid mechanics to simulate flow through an intake manifold was described by Genesan [22]. The author developed a model of an asymmetric intake manifold for a four cylinder engine. He tested a mass flow rate through an intake valve under steady states for varied values of an intake valve lift. The experimental verification showed that these calculations are identical with the measurements of a real object.

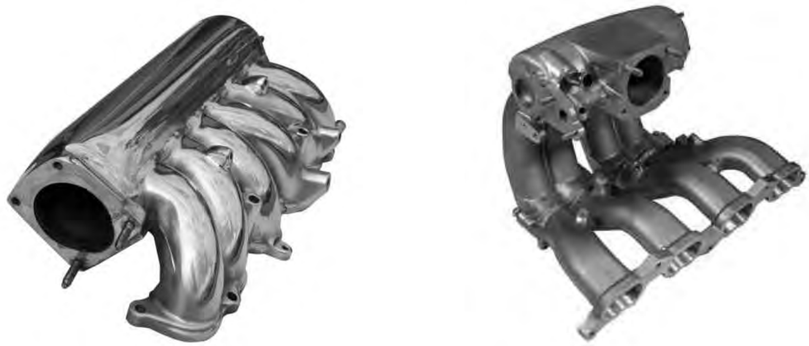

a) **b)**

Photo. 2.1 Intake manifold: a) asymmetric view, b) symmetric view [101] [102]

The simulation research results to show how an intake system geometry influences cylinder filling are given in [21]. The examination was done for three varied inlet pipes and two speeds. Better cylinder filling was when a pipe with a larger section was used (see fig. 2.5, geometry in 2). If its section was smaller (fig. 2.4, geometry in 1), the fuel mixed better with air because the kinetic energy of turbulence increased.

The authors of the work in [64] measured optically a filling process. They tested several variants of flow for varied values of an intake valve lift, as shown in photo 2.2

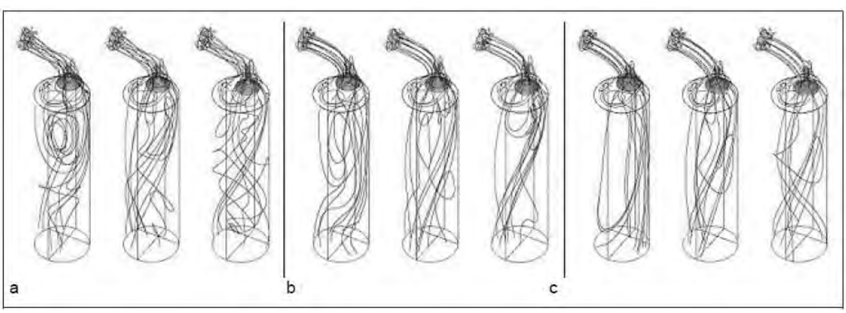

Fig. 2.4 Velocity vector mapping for the intake valve lifts: 1 mm, 5 mm, 9 mm a) geometry no 1, b) geometry no 2, c) geometry no 3 [21]

It was shown that the greatest kinetic energy of turbulence is for an angle of 60° and an intake valve lift of 75% and 100% (fig. 2.6), which implies that a fuel mixes the most efficiently with air in such a design.

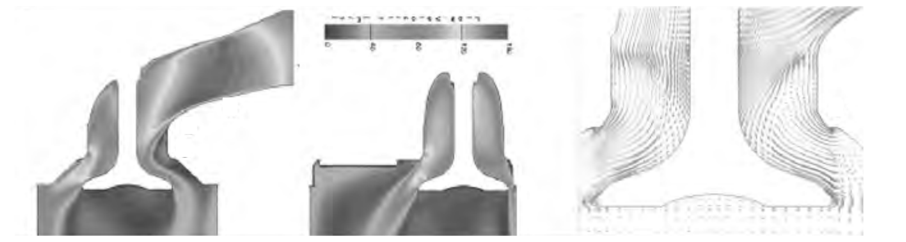

a)

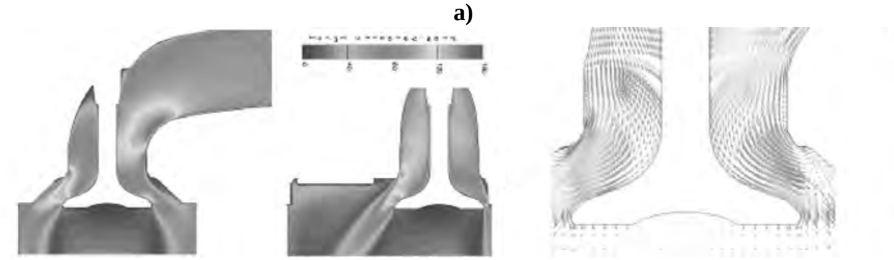

b)

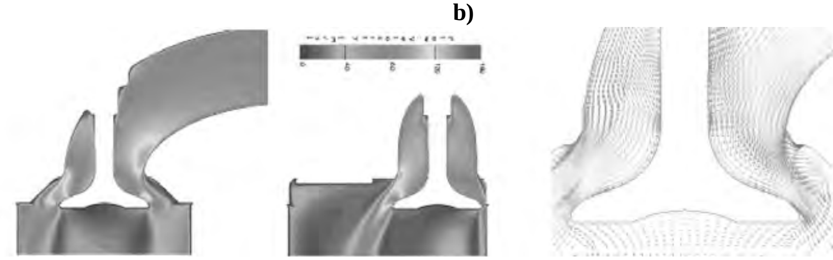

c)

Fig. 2.5 Distribution of velocity vectors for the three intake pipe designs: a) geometry no 1, b) geometry no 2, c) geometry no 3 [21]

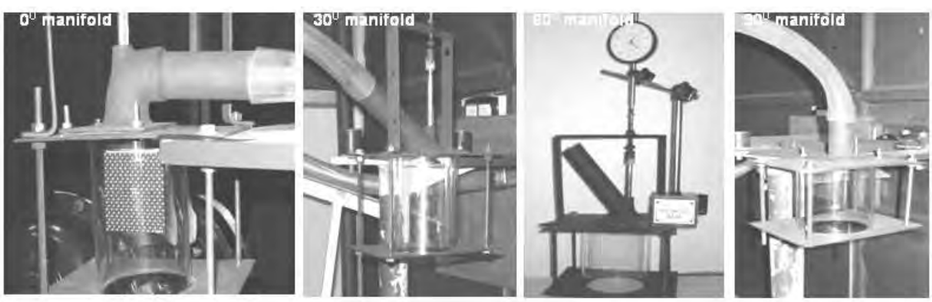

Photo 2.2 Tested inlet pipe designs [64]

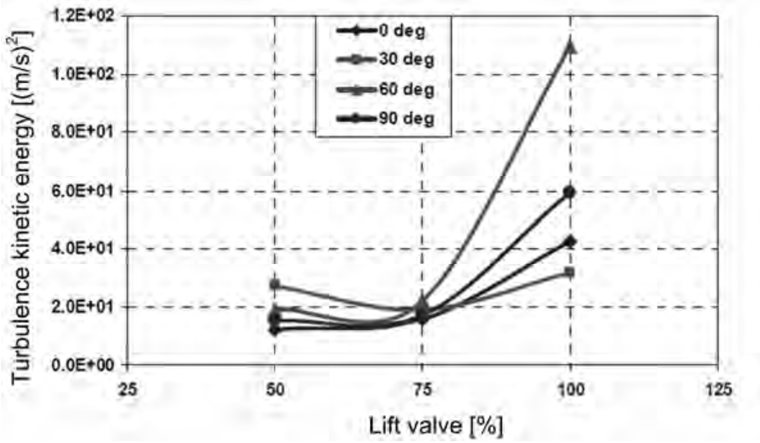

Fig. 2.6 Turbulence energy depending on an intake pipe geometry and intake valve lift [64]

An injection system in a multi-cylinder engine should ensure a mixture composition to be as similar as possible in each cylinder. The results presented by Lenz [48] indicate that a mixture composition varies most between cylinders when speed and load are low (fig. 2.7).

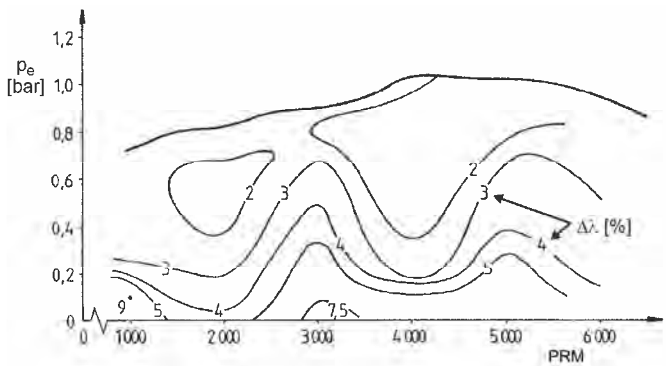

Fig. 2.7 Dependence of the dispersion of a mixture composition $\Delta\lambda$ on working conditions of an engine supplied by an injection [48]

Those differences in the mixture distribution in a cylinder and in the dispersion between cylinders, following the impact of injection parameters on a filling process, affect significantly combustion and toxic gases formation. These issues were described in detail in [13, 25, 52 96]. Merola [60] showed that the change in fuel injection pressure significantly influences flame propagation speed and with this binding affects the emission of toxic gases. As injection pressure increased, the emissions of hydrocarbons and carbon monoxide decreased definitely.

Gold et al. [23] provided the results concerning mixture formation in an SI engine where the change in a petrol early injection angle α_w caused an injection onto a closed or open intake valve. It was found that while injecting onto a closed intake valve, adjusting α_w only slightly affects exhaust gas composition. When injecting onto an open valve however, a change in the injection angle increases the emissions of HC and NO_x because of a greater variability of fuel fraction. The best results were obtained for α_w of 0° CA (start of intake stroke).

The piston engine is a dynamic object and its operation is accompanied by many phenomena of mass and energy accumulation. Precise gasoline dosing depends on the place where an injector is mounted. In indirect gasoline injection systems, injectors are mounted as close as possible to an intake valve. To a certain extent, this helps, to avoid changes in mixture composition reaching a cylinder, in transient states with sudden changes in dosing. [5, 88]. Dynamic phenomena are compensated for in control algorithms [30, 63].

It can be concluded that in gasoline injection systems injectors are mounted as close as possible to the intake valve due to the dynamic operation states. This may, however, cause a liquid fuel phase in a cylinder. The filling process was enhanced by: increasing injection pressure, fuel injection onto an open intake valve, changing an intake valve lift, changing valve timing and using an appropriate intake manifold design. By contrast, moving a gasoline injector away would definitely enhance the homogenization of mixture in a combustion chamber.

2.2 Air-gas mixture formation process

The available literature suggests that gaseous fuel compared to gasoline significantly changes the filling process in SI engines [81, 82, 95]. The effects include changes in volumetric efficiency η_v resulting from varied values of early injection angle and are given in the present work [45]. The authors demonstrated that the cylinder is filled most efficiently for αw angle of 0º (start of intake stroke). The tests were carried out for one value of rotational speed and two values of a throttle position angle. In all cases, similar dependence was obtained. The lowest values of the η_v coefficient were obtained for the boundary values of the α_w angle (fig. 2.8).

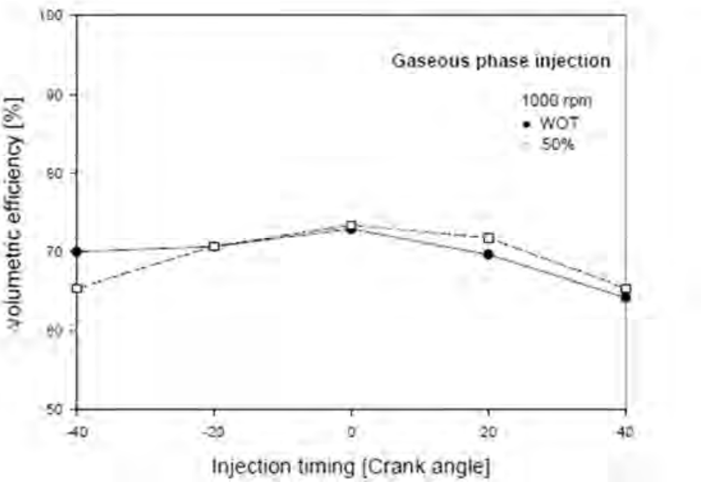

Fig. 2.8 Dependence of volumetric efficiency η_v on an early injection angle for the two values of a throttle opening angle [45]

The same researchers examined also how a fuel physical state influences the filling process in LPG engines. [46]. It was noted that this factor did not influence engine volumetric efficiency $\eta_{v.}$ Later, the results obtained were compared with those obtained when the so-called second generation installation supplied an engine (fig. 2.9). It was demonstrated that the farther away a gas dispenser from an intake valve axis was mounted, the more engine operation deteriorated.

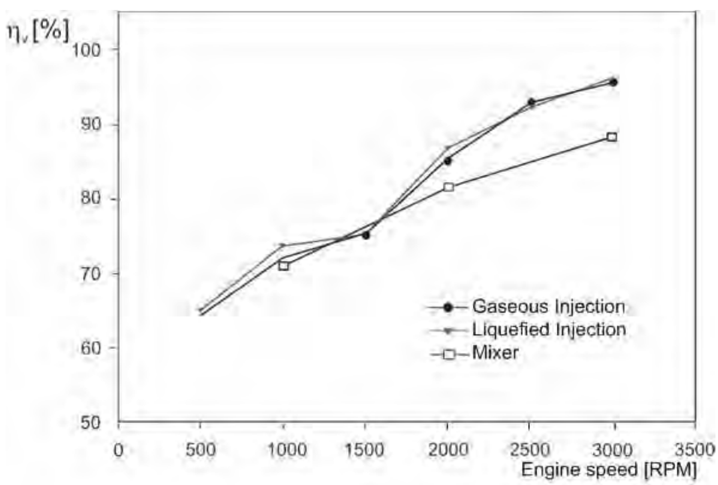

Fig 2.9 Dependence of volumetric efficiency η_v on a method to supply an engine by LPG as a function of engine rotational speed [46]

A propane-butane injection technique was described in detail in [35, 36]. Simultaneous and sequential injections as well as the impact early injection angle has got on SI engine operation were tested. It was demonstrated that if the injection technique changes (from simultaneous into sequential), no significant changes in the torque of the tested operating conditions are noted. It was found, however, that for a certain range of early injection angles, engine operation deteriorates because of misfire. Particularly considerable deterioration was noted when the engine was fuelled with a lean mixture (λ=1.2). Based on the analysis of the concentration of toxic gases, it was noted that the best fuel distribution occurs for early injection angles. As a result, a minimum concentration of CO, increased concentration of NO_x and increased mean indicated cylinder pressure are noted. These effects are due to increased completeness of combustion. The tests were done for a constant distance between the injector and the inlet valve axis.

The authors showed in their works [19, 38] how the temporary nature of LPG injection influences SI engine operation. The papers [7, 45] provide the research results on the composition of exhaust gases that were obtained for the engine fuelled by LPG. In both cases, the emissions of hydrocarbons and carbon dioxide were reduced by more than 20% compared with the results obtained in the case of gasoline fuelling.

The results published in the work [14] confirm the advantages of LPG in terms of volumetric concentration of carbon monoxide in the exhaust gas. The tests were done for one value of rotational speed with a completely open throttle. It was noted that the concentration of CO was significantly reduced in the case of LPG compared with gasoline, especially for lean mixtures (fig. 2.10).

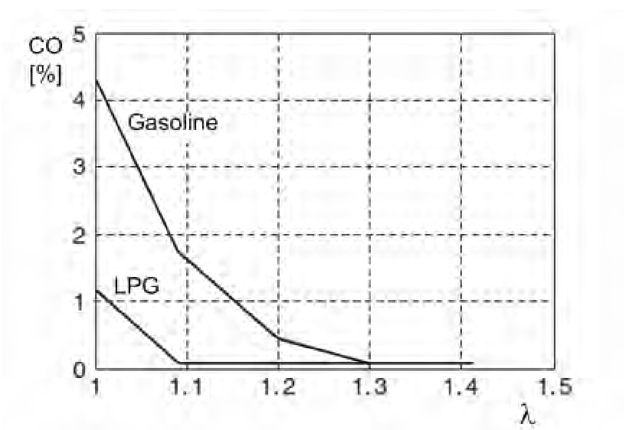

Fig. 2.10 Dependence of CO concentration in exhaust gases on an excess air ratio for gasoline and LPG [14]

The use of computational fluid dynamics for examining of the filling process in gas-fuelled engines is described in [4, 8, 78, 79]. Cylinder filling with air-fuel mixture depends on the geometry of a gas dosing system, i.e. diameter and length of an injection pipe, diameter of an injection nozzle, or the distance between the injection nozzle and the axis of the intake valve. Changing the injection nozzle diameter influences real time needed to dose gaseous fuel to the intake pipe [75]. It was demonstrated that gas outflows twice longer from the injection nozzle, which influences directly fuel flow into the cylinder.

The article [78] analyses how the geometry of an injection nozzle for natural gas that is mounted in an intake manifold can influence the fuel distribution in a cylinder. The research was done for five different nozzles (fig. 2.11) and varied intake valve lifts.

Fig. 2.11 The tested injection nozzles [78]

As shown, more openings in the injection nozzle can improve how fuel is carried within a cylinder. The best results are for three, four and five openings, depending on an intake valve lift.

2.3 Summary

The review of the state-of-art leads to the following conclusions:

1. The principle of operation of propane-butane injection systems resembles gasoline systems. However, gas injection into the intake manifold considerably changes mixture formation. This applies especially to the engine volumetric efficiency and fuel distribution in the cylinder.
2. The available research results confirm that engine filling with mixture of air and propane-butane depends on geometry and time. In relation to the geometry of an LPG supply system, the impact of factors such as the injector nozzle diameter and the diameter and length of the injection pipe were examined. Also, timing of the injection process significantly affects the filling process, which directly influences combustion and exhaust gas composition.
3. Scientific literature offers limited information on the impact the distance between the injection nozzle and the axis of the intake valve has got on the mixture formation in an SI engine fuelled by injected propane-

butane. As this distance increases, mixing of fuel with air can be enhanced, but at the same time mixture composition can be dispersed between cylinders in an engine with asymmetric intake manifold. In addition, the distance between the gas injector and the axis of the intake valve may adversely affect engine operation in dynamic states.

4. Examinations that can clarify how the distance between an injection nozzle and the axis of an intake valve can influence a filling process in an engine should be two-stage. First, there should be testing a real object in a test house. Based on the studies on different distances of injection nozzles, it is possible to record direct results including the changes in exhaust gases composition. Computational fluid dynamics is a reliable research tool to learn about the reasons for any differences in the tested concentrations of exhaust gas components. The previous section described when such tools can be used to analyze flow phenomena in engines.
5. Research factors, to be considered, include: engine load and rotational speed, number of cylinders, an intake system design. The intensity of feedback flows from a cylinder into an intake manifold is the highest for low load and rotational speed. Additionally, to test the impact of an early injection angle on each of the tested variants of nozzle installation, stand tests need to be carried out. The tested object should be a multi-cylinder engine with an asymmetric intake manifold.

In this monograph, the author attempted to clarify the reasons for the deterioration of engine operation as a result of increasing the distance between a gas injection nozzle and an intake valve axis.

3. Test stand

3.1 Introduction

This chapter describes the research object, designed propane-butane injection system, and additional measurement systems built in the test stand to conduct research. It outlines how to maintain the required engine operation state.

3.2 Engine test bed

Experimental research was done at a test stand in the test house at the Department of Internal Combustion Engines and Transport at Lublin University of Technology (photo 3.1).

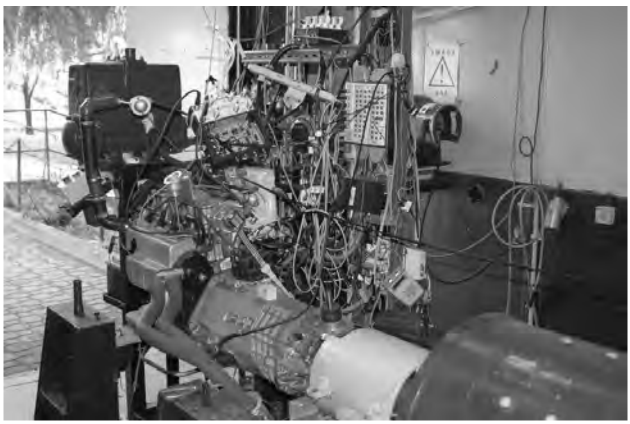

Photo 3.1 Test stand

A scheme of the test stand is given in photo 3.1. The test stand includes an engine brake, the tested object (a gasoline engine - Holden C20LE), measurement and control systems. The test stand enables the research engine to be fuelled by both gasoline and gaseous fuels like LPG or CNG.Engine test stand

At the test stand there is no possibility to condition the environment by adjusting pressure, temperature and humidity. However, there is a ventilation and exhaust gas system. The tests lasted several hours and no important changes of the above mentioned parameters were noted. The recorded values are as follows:

- air temperature 25 ± 2° C
- barometric pressure 101 ± 3 kPa,
- relative humidity 64 ± 3%.

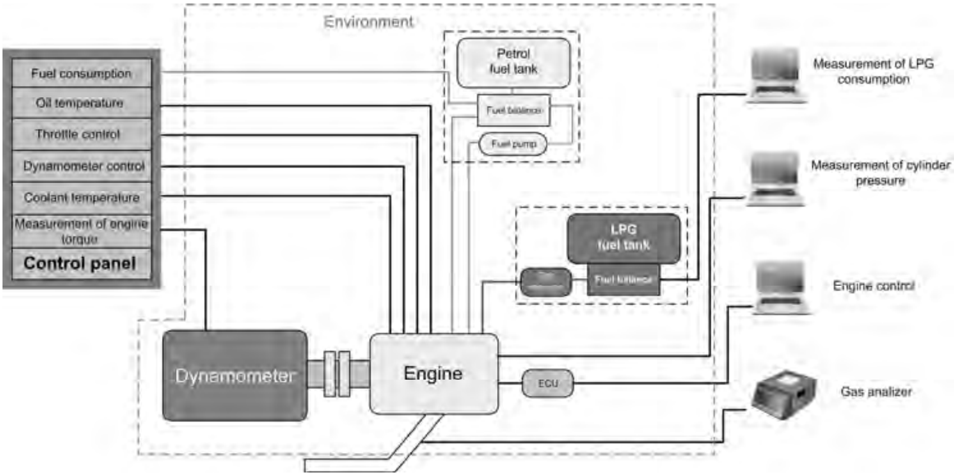

Fig. 3.1 Test stand scheme

The air temperature in the inlet system was measured with a Pt100 resistance sensor mounted in the cumulative manifold. The temperature was 39 ± 2 °C.

ADAM 5510 temperature regulation system, controlled with a microprocessor, stabilized the engine coolant temperature. The system allows the required engine thermal state to be maintained with an accuracy of 1 °C. A Danffos EVSIM 20 Solenoid is mounted on the heat exchanger which transfers heat to an external cooling installation in the test house. The coolant temperature is measured with the use of a Fe-CuNi thermocouple. The test stand cannot stabilize the temperature of engine lubricating oil. During testing, lubricating oil temperature is controlled in the oil sump with the use of a Pt100 resistance temperature sensor. LPG temperature in the tank equaled ambient temperature. Exhaust gas temperature was measured with a NiCr-NiAl thermocouple.

Engine load was obtained with the use of the SAK-670 N electric brake (maxi-mum power of 80 kW and maximum speed of 6,500 rpm) manufactured by VEB Elbtalwerk. The brake works with the AMX 231-CYM microprocessor device by Automex which controls the throttle torque, speed and position. During the tests, one of the brake controlling modes was used to stabilize the given crankshaft rotational speed of the engine by adjusting the brake magnetic current for a fixed throttle opening angle [66].

Tab. 3.1 SAC-N-670 Engine Brake Specifications

Manufacturer	VEB ELBTALWERK
Brake	GpFp 11h
Peak current intensity	200 A
Supply voltage	380 V
Generator voltage	32 V
Received power range	5,5 kW to 80 kW
Operation temperature	40°C
Peak rotational speed	6500 rpm
Brake controller	Controller by APATOR – Toruń with the DML/MN thyristor driving system compatible with DC engines

The throttle position was changed with the use of the PTT-20 controller that was operated from the module of the AMX 201 throttle controller manufactured by Automex. The device enables the throttle position to be precisely set with an accuracy of 1%.

Gas mass consumption was measured with the WPT 24C scales by Radwag and Wagawin software. Table 3.2 shows the most important measurement parameters and their values. Toxic components in exhaust gas were measured by means of a gas analyzer Pierburg HGA 400. Its measurement characteristic is given in Table 3.3.

An OPTRAND sensor with an ignition plug adapter was used [54] to measure indicated pressure. This sensor was specially developed to measure the pressure in piston engines. It is based on the changes in the intensity of luminous light that is transmitted by two adjacent fibers. One of them is connected with the LED diode and the other with a photo-detector. Any changes in the intensity of the light received by the photodiode are due to changes in the intensity of the light reflected by a steel membrane that is deformed by pressure.

Tab. 3.2 Summary of major quantities measured

Measured quantity	**Sensor**	**Accuracy**
Rotational velocity	Reluctant sensor	± 1 rpm
Torque	Strain gauge	± 1 Nm
Throttle position	Potentiometer	± 1%
Fuel consumption per hour	Tensometric sensor	± 0,01 kg/h
Gas consumption per hour	strain gauge	± 0,1 kg/h
Coolant temperature	Fe-CuNi Thermocouple	± 0,1 °C

Tab. 3.2 Summary of major quantities measured - continued

Measured quantity	**Sensor**	**Accuracy**
Oil temperature	Pt 100	± 0,1 °C
Exhaust gas temperature	NiCr-NiAl Thermocouple	± 5 °C
Air temperature in the inlet manifold	Pt 100	± 0,1 °C
Air pressure in the inlet manifold	Tensometric sensor	± 2 kPa

Tab. 3.3 Measurement characteristic of the HGA 400 gas analyzer

Component	**Measuring range**	**Resolution**	**Accuracy**
CO	0…10% vol.	± 0,01% vol.	< 1.2% vol. ± 0,06% ≥ 1,2% vol. ± 5%
CO_2	0…20% vol.	± 0,1% vol.	< 10% vol. ± 0,5% ≥ 10% vol. ± 5%
HC	0…20000 ppm vol.	± 1 ppm vol.	< 220 ppm vol. ± 11 ppm vol. ≥ 220 ppm vol. ± 5%
O_2	0…22% vol.	± 0,01% vol.	< 2% vol. ± 0,1% vol. ≥ 2% vol. ± 5%
NO_x	0…5000 ppm vol.	± 1 ppm vol.	< 500 ppm vol. ± 50 ppm vol. ≥ 500 ppm vol. ± 10%

Fig. 3.2 Ignition spark plug adapted for mounting the Optrand fiber-optic sensors [55]

Tab. 3.4 Properties of the Optrand sensor

Measuring range	0-70 MPa
Distructive pressure	2 x measuring range
Sensor output signal	analogue intensity signal ranging from 0,5 V to 5V
Diagnostic output signal	analogue intensity signal ranging from 0 to 3,6 V
Membrane resonance frequency	≥120 kHz
Permissible frequency	from 0,01 Hz to 15 kHz or from 0,01 Hz to 5 kHz
S/N ratio	2000:1 (for 15 kHz)
Pressure carrier	gas or liquid
Output impedance	250 Ω
Power	9 ÷18 V
Power consumption	50 mA (max. 85 mA)
Permissible acceleration	100 g

A crankshaft rotation angle was measured with the MH420-6 optoelectronic rotary code MH420 converter by Megatron with a 10-bit converter that can determine the location of a crankshaft with a resolution of 512 dots per rotation (as the sensor cooperates with the camshaft, which rotates twice slower than the crankshaft, the effective measurement resolution of 1024 points per rotation decreases twice). A converter, designed by the author, converted a digital signal coded with Grey's code into an analogue signal that was changing within the range of -5 ÷ 5 V. Then, this signal and other quick-changing signals were recorded with a data acquisition station.

3.3 Research object

A four-cylinder, four-stroke engine in a row set-up C20LE Holden (photo 3.2) was tested. The engine is equipped with a standard multi-point fuel injection into an intake manifold. Its displacement is 1998 cm^3, compression ratio 8.8:1. The engine has two valves per cylinder which are driven by a camshaft via hydraulic tappets. The valve timing is shown in table 3.6. The engine is based on a direct ignition system (DIS).

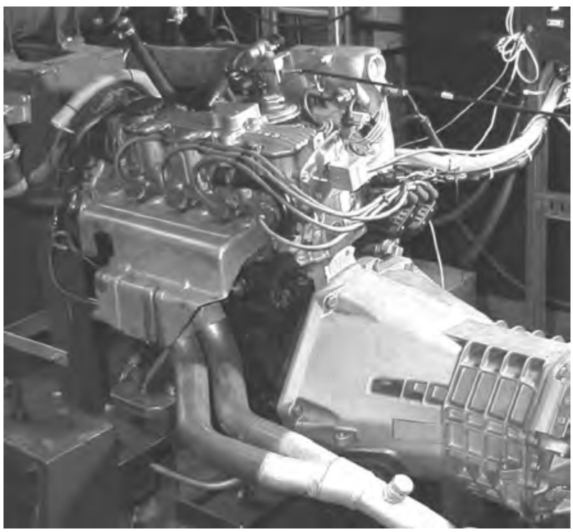

Photo. 3.2 Research object on the test stand

An engine for testing was manufactured in 1998. Its serial number is 25171217. The selected engine specification is given in Table 3.5:

Tab. 3.5 Holden engine specification

<u>Basic properties:</u>	
Manufacturer	Holden
Engine code	C20LE
Model	2,O MPFI
Type	4-stroke with a spark ignition
Number and cylinder design	4, in line
Cylinder diameter/ piston stroke	86/86 mm
Engine displacement	1998 cm^3
Compression ratio	8.8:1
Max engine power	77 kW at 5200 rpm
Max torque	164 Nm at 2600 rpm
Idle rotation	800 ±50 rpm
Cylinder sequence	1-3-4-2
Ignition type	DIS (Direct Ignition System)
<u>Camshaft mechanism:</u>	
Valve location	in a head
Camshaft location	on the head top
Camshaft drive	belt
Valve clearance	non-adjustable (hydraulic control)

Tab. 3.6 Phases of the engine timing C20LE

	Opening	**Closing**	**Opening angle**
Intake valve	23° before TDC	71° after BDC	274°
Outlet valve	60° before BDC	35° after TDC	274°

Tab. 3.7 Sensors and regulatory systems in the engine controlling system

Sensors	**Regulatory systems**
crankshaft location sensor	injectors (4)
throttle position sensor	an ignition system (DIS)
coolant temperature sensor	a fuel pump
inlet manifold temperature sensor	a step motor with an air by-pass valve
oxygen sensor (lambda sensor)	
speed sensor (mounted in a gearbox)	

3.4 Gas injection system

The research was done using a developed supply system based on propane-butane. The supply system consists of the following elements: a gas tank, a laboratory controller, controlling software, an injection system, an evaporator-reducer, solenoid valves, measuring transducers.

The DTS-700 laboratory controller (photo 3.3) which cooperates with the ENGWIN software controlled the engine. Communication between the controller and a PC was provided by means of a CAN transmission protocol. This device and its software adjusted engine operation parameters including injection time, a start injection angle, an ignition advance angle, additional air valve location.

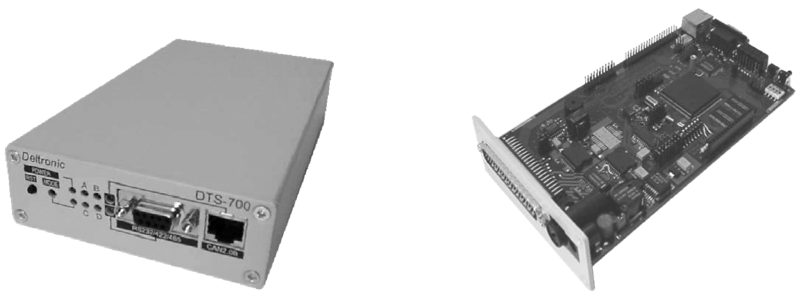

a) **b)**

Photo. 3.3 Measurement and control system DTS-700: a) view from the side of the connectors, b) the electronic systems

The controller enables:

- signals of the classic board sensors (manifold pressure, throttle position, engine temperature, signals from narrow- and wide-ranged oxygen sensors) to be measured,
- injectors to be controlled,
- ignition with a DIS to be controlled directly or indirectly,
- other regulatory elements including an additional air valve to be controlled,
- self-diagnosis,
- the support of transmission with a personal computer with the following interfaces:
  - RS-232,
  - RS-485/422,
  - CAN 2.0.B.

The speed of the control unit allows quick-changing signals at a dozen several kHz frequencies to be measured, control with a frequency up to 1 kHz and the data at 1 Mb/s (for the CAN 2.0B interface) to be transmitted.

The propane-butane injection system installed at the tests stand was PEGAS, the GTP01 model, manufactured by DT Gas System (photo 3.4). Technical details for this device are shown in Table 3.7. This device supplies gas to a four cylinder engine. Its each section is operated by two electro-magnets that cooperate with flap valves.

Tab. 3.7 PEGAS injection rail characteristics

Number of sections	4
Number of electro valves operating one section	2
Coil resistance	6 Ω
Supply voltage	12 V
Opening delay time	1,5 ms
Outlet ferrule diameter	4 mm

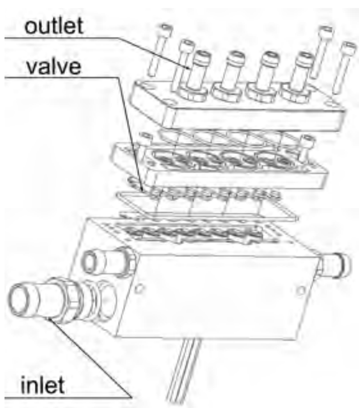

Fig. 3.3 Drawing of the PEGAS injection system assembly

Photo. 3.4 PEGAS injection rail

The applied transducer had one degree of reduction at which LPG evaporated and the preset pressure was maintained. Fuel consumption decreased the pressure in the reducer chamber. As a result, the valve opened and a new portion of LPG entered. Later, the fuel flew through the nozzle into the reducer chamber and evaporated, absorbing a heat from the coolant [50].

3.5 Measuring systems

During the experimental research the following values were stabilized: coolant temperature, engine speed, intake manifold pressure. The test control unit for engine allowed changing gas injection control parameters.

For the test, it was necessary to retrofit the test stand with additional systems and to modify the engine intake system. Firstly, the intake manifold was properly prepared. There were made holes in the four distances from the combustion chamber in which were mounted injection nozzles of 4 mm in diameter (fig. 3.4). The distance was measured along the symmetry axis of the intake pipe, which reflects the actual path the air-fuel mixture comes. The nozzles were connected with the injector pipes of 200 mm with the propane-butane injection system.

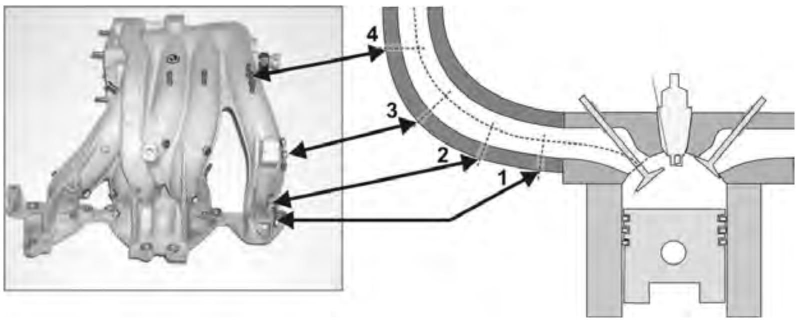

Fig. 3.4 Location of the nozzles in the intake pipes

Tab. 3.8 Types of nozzle mounting used in the research

Distance from the combustion chamber	Symbols
115 mm	L_{w1}
170 mm	L_{w2}
230 mm	L_{w3}
310 mm	L_{w4}

Additional pressure sensors were mounted at the test stand. During the testing, gas pressure was recorded at three points: socket injection rail, injection nozzle and inlet pipe of the fourth cylinder in the section with the injection nozzle. These results were used to calibrate the engine model. In addition, there was recorded the pressure in the other inlet pipes, the indicated pressure in the fourth cylinder and the position of the crankshaft (tab. 3.8).

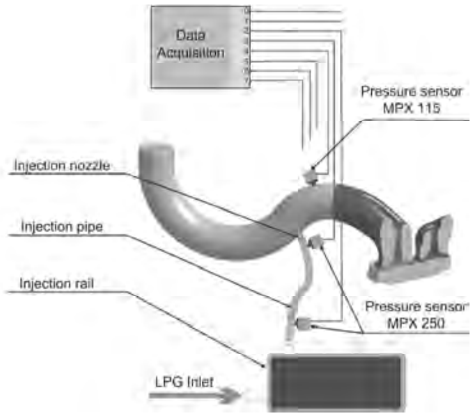

Fig. 3.5 Diagram of the measurement system and photo showing where the pressure sensors in the inlet system and gas supply system were mounted

Tab. 3.8 Sensors' properties

No	Place of the assembly, including the sensor	Recorded range	Calculation characteristics
0	camshaft position	-5±5V	-
1	indicated cylinder pressure (Optrand)	-0,5±5V	25º C 2,92 mV/psi 200º C 2,97 mV/psi
2	outlet ferrule in the injection rail MPX **250**	±5V	$\boxed{p=\left(\frac{1}{0{,}02}\cdot V_{out}+10\right)\cdot 0{,}01}$ bar
3	injection nozzle MPX **250**	0±5V	
4	manifold 1 MPX **115**	0±5V	$\boxed{p=\left(\frac{1}{0{,}045}\cdot V_{out}+\frac{0{,}475}{0{,}045}\right)\cdot 0{,}01}$ bar
5	manifold 2 MPX **115**		
6	manifold 3 MPX **115**		
7	manifold 4 MPX **115**		

The pressure was measured with the sensors manufactured by MOTOROLA of series MPXA6115A and MPXA6250A of a measuring range of 15-115 kPa and 15-250 kPa, respectively. These are piezoelectric pressure transducers and their technical properties are in Table 3.9.

A 16-channel data acquisition card by National Instruments NI-DAQPAD 6070 was used to record quick-changing signals on a personal computer. The data acquisition card has got 16 single or 8 varied channels of the maximum sampling rate of 1.25 MS/s. The measuring range of the input signal was 10 V. The measurements were recorded on a PC at a frequency of 10 kHz.

Tab. 3.9 Properties of MPX series sensor

Measuring range	15-115 kPa lub 15-250 kPa
Destructive pressure	400 kPa
Operation temperature	from -40 ºC to 125 ºC
Supply voltage	5 V
Supply current	6 mA
Measuring error	± 0,5 % of the measuring range
Sensitivity	45.9 mv/kPa
Response time	1 ms
Output current at full scale voltage	0,1 mA
Stand-by time	20 ms

To operate the card, a virtual gauge working in LabVIEW environment (figure 3.6) was developed. This environment, alike Borland C or Borland Pascal, is perfect for creating one's own software applications. The only difference is the way a source code of the program is developed. In other environments, the source code is a sequential textual record in a particular programming language (Basic, C, Pascal). The LabVIEW- based source code boils down to graphical presenting the operation of a function of input (from a keyboard and devices), output (into a screen, printer and devices), information handling and processing and connections between the blocks. Graphic language G presents the record of the program as icons, clamps and connections through which any virtual gauge can be built. Depending on your needs and software, it can be a virtual oscilloscope, spectrum analyzer, recorder, multimeter or other unusual instrument.

In order to measure the mixture composition in the exhaust system, a wide-band BOSCH LSU 4.2 lambda sensor was installed. Its measuring range of an air bearing ratio was 0.7 to 2.5. The air-fuel mixture composition can be read directly from the LM-1 digital meter by Innovate (photo 3.5). The tests were based on a PC with LogWorks2 programme supporting the gauge that recorded the up-to-date values of an excess air ratio (photo 4.3). The software has been supplied by its manufacturer.

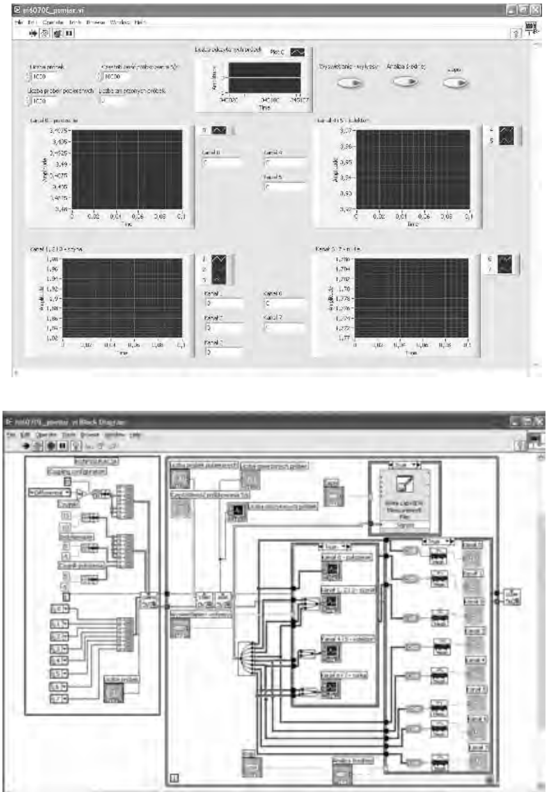

Fig. 3.6 View user panel and block diagram of the program for measuring data

Photo 3.5 LM-1 meter with a sensor LSU BOSH 4.2

Fig. 3.7 LogWorks 2 user interface

3.6 Results

Tab.3.10 Concentration of gas exhaust components obtained in the case of lean mixture fuelling (λ=1,1) for the distances of L_{w1} and L_{w2}.

α_w	L_{w1}			L_{w2}		
	CO [%]	**HC** [ppm]	**NO_x** [ppm]	**CO** [%]	**HC** [ppm]	**NO_x** [ppm]
-120	0,28	139	600	0,50	174	694
-110	0,31	146	577	0,48	238	645
-100	0,3	143	549	0,50	156	655
-90	0,3	137	542	0,42	144	681
-80	0,24	136	591	0,36	136	735
-70	0,25	133	606	0,37	136	738
-60	0,3	134	562	0,40	154	701
-50	0,33	133	514	0,540	138	655
-40	0,34	141	573	0,38	130	623
-30	0,32	140	591	0,30	126	698
-20	0,27	138	610	0,25	120	784
-10	0,28	134	605	0,23	121	793
0	0,28	142	618	0,26	121	713
10	0,32	143	626	0,26	119	674
20	0,28	143	629	0,24	114	673
30	0,28	152	618	0,29	159	671
40	0,32	144	592	0,30	114	571
50	0,34	142	532	0,33	114	575
60	0,31	135	536	0,27	104	675
70	0,26	178	554	0,19	103	712
80	0,27	142	609	0,20	112	738
90	0,31	153	598	0,33	122	702
100	0,35	143	556	0,44	127	637
110	0,38	151	515	0,49	142	631
120	0,38	155	513	0,48	149	665

Tab. 3.11 Concentration of gas exhaust components obtained in the case of lean mixture fuelling (λ=1,1) for the distances of L_{w3} and L_{w4}.

α_w	L_{w3}			L_{w4}		
	CO [%]	**HC** [ppm]	**NO_x** [ppm]	**CO** [%]	**HC** [ppm]	**NO_x** [ppm]
-120	-	-	-	-	-	-
-110	-	-	-	-	-	-
-100	-	-	-	-	-	-
-90	-	-	-	-	-	-
-80	-	-	-	-	-	-
-70	-	-	-	-	-	--
-60	-	-	-	-	-	-
-50	-	-	-	-	-	-
-40	1,17	1247	497	-	-	-
-30	0,85	241	583	-	-	-
-20	0,5	140	678	1,43	1479	274
-10	0,25	122	759	0,68	661	375
0	0,25	118	714	0,38	134	396
10	0,28	120	648	0,43	142	366
20	0,29	112	550	0,46	285	356
30	0,37	215	559	0,48	187	361
40	0,35	145	580	0,45	194	402
50	0,33	120	636	0,53	227	408
60	0,37	124	738	0,72	277	418
70	0,62	138	740	1,20	1175	407
80	0,61	191	729	1,65	2200	383
90	0,97	663	609	2,00	2490	348
100	1,37	1231	506	2,30	2170	277
110	1,62	1431	431	2,52	2080	204
120	1,67	1685	419	2,62	2060	167

Tab. 3.12 Concentration of gas exhaust components obtained in the case of lean mixture fuelling (λ=0,98) for the distances of L_{w1}, L_{w4}, L_{w3} and L_{w4}.

α_w	L_{w1}			L_{w1}		
	CO [%]	**HC** [ppm]	**NO_x** [ppm]	**CO** [%]	**HC** [ppm]	**NO_x** [ppm]
-120	1,44	180	967	1,53	172	997
-100	1,46	180	953	1,55	167	1077
-80	1,36	178	1007	1,43	164	1152
-60	1,44	178	967	1,48	162	1025
-40	1,46	181	891	1,33	159	1133
-20	1,41	182	949	1,24	160	1330
0	1,47	188	986	1,26	161	1293
20	1,42	193	1019	1,29	161	1164
40	1,46	192	824	1,31	157	972
60	1,42	175	745	1,18	156	1156
80	1,3	173	852	1,26	162	1067
100	1,5	179	951	1,49	156	1035
120	1,43	176	941	1,66	165	968

α_w	L_{w3}			L_{w4}		
	CO [%]	**HC** [ppm]	**NO_x** [ppm]	**CO** [%]	**HC** [ppm]	**NO_x** [ppm]
-120	3,16	1526	113	-	-	-
-100	2,89	1255	163	-	-	-
-80	2,97	584	144	-	-	-
-60	3,01	1253	181	-	-	-
-40	2,38	210	326	3,61	1969	60
-20	1,62	187	875	1,42	243	167
0	1,24	183	1146	1,35	178	674
20	1,27	165	966	1,39	169	744
40	1,37	165	988	1,4	178	728
60	1,5	178	1025	1,91	203	443
80	1,92	180	650	2,93	1366	323
100	2,68	270	267	-	-	-
120	2,99	926	196	-	-	-

4. Simulation

4.1 Introduction

The system applied, i.e. massive computing power computer and research software to carry out the simulation tests is presented in this chapter. Its further part describes the engine model and its assumptions.

4.2 Engine test stand

Nowadays, it is very popular to model the phenomena that occur in an engine. Solving complex problems is possible thanks to the method known as computational fluid dynamics (CFD). STAR-CD is the software, developed by CD Adapco [84], which enables calculations using computational fluid dynamics [6, 11, 15, 28, 54, 76]. Discretization of the analyzed volume by dividing it into cells of a finite volume and the numerical solution of partial differential equations determined pressure gradients, temperature or speed in the case of single and multi-phase flows.

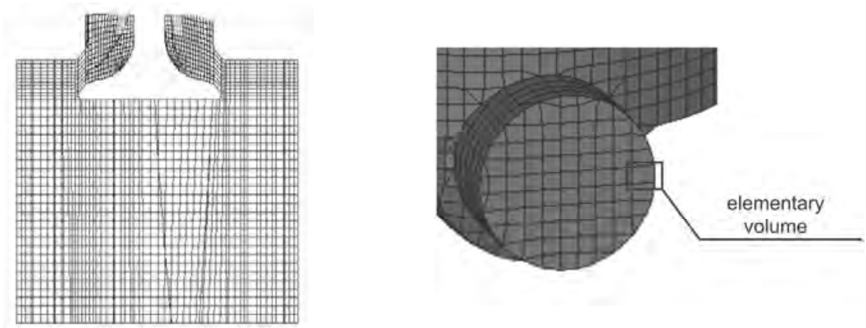

a) **b)**

Fig. 4.1 Geometric discretization: a) a model of a cylinder with a valve [84], b) basic volume

The software in use has a complex graphical user interface. It is also possible to type commands to do particular operations. Figure 4.2 presents its user interface.

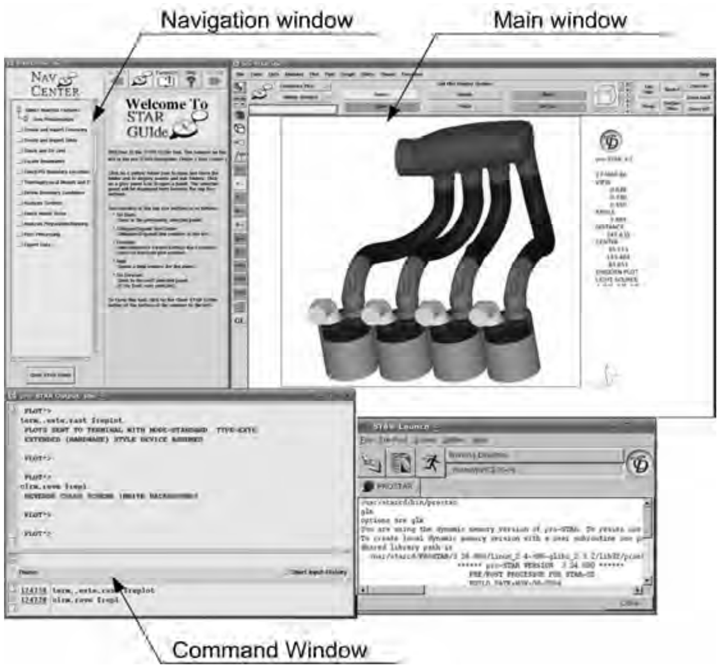

Fig. 4.2 Star-CD user interface

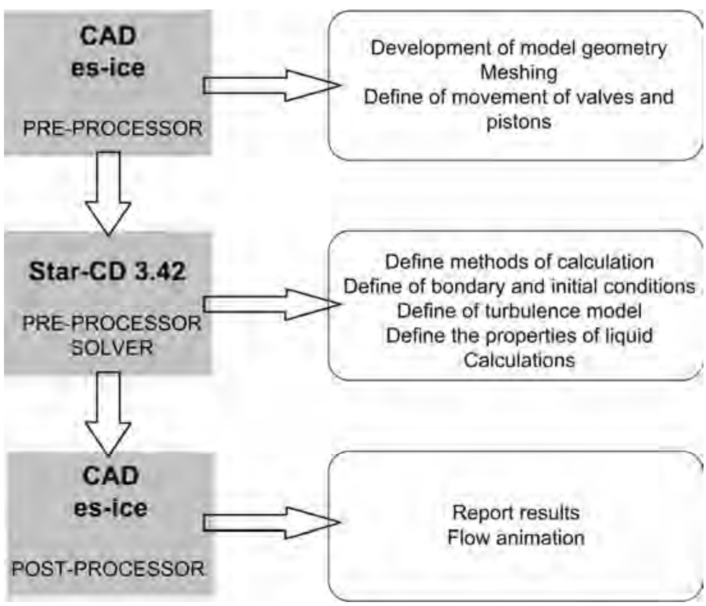

Fig. 4.3 Diagram of simulation research

Pre-processing includes all the activities necessary to start numerical calculations, i.e.

- development of the geometry of a model,
- development of a model mesh (discretization in space),
- defining boundary conditions,
- defining initial conditions,
- defining a gas and its parameters.

A solver enables calculations at discrete points of the system, specified thanks to the developed calculation mesh with a required time discretization. It also includes, e.g.

- mixing of gases,
- a model of ideal gas density,
- turbulent flow phenomena.

Post-processing

This stage of the simulation tests concentrates on working out graphically the results obtained. There were made the characteristics and diagrams of the analyzed quantities in a given area and time (due to a transient process analysis.)

The applied computer research system was based on the Dell Precision 470 workstation with two processors of a timing frequency of 3 GHz each and a software Star CD v 3.24 with a module es-ice and CAD software. The operating system for calculations was Linux Suse.

4.3 Assumption for the engine model

Gas flow calculations were carried out according to the Navier-Stokes equations (4.1, 4.2) that describe the principle of mass and momentum conservation for the compressible fluid in tensor notation [83]:

$$\frac{\partial \rho}{\partial t} + \frac{\partial}{\partial x_j}(\rho, u_j) = s_m \tag{4.1}$$

$$\frac{\partial \rho u_i}{\partial t} + \frac{\partial}{\partial x_j}(\rho u_j u_i - \tau_{ij}) = -\frac{\partial p}{\partial x_i} + s_i \tag{4.2}$$

where:

$\boldsymbol{t}$ – time,

$\boldsymbol{x_i}$ – Cartesian coordinate system (i =1, 2, 3),

$\boldsymbol{u_i}$ – absolute velocity into the direction of x_i,

$\boldsymbol{p}$ – pressure,

$\boldsymbol{\rho}$ – density,

$\boldsymbol{\tau_{ij}}$ – stress tensor component,

$\boldsymbol{s_m}$ – mass source,

$\boldsymbol{s_i}$ – momentum source component.

The main equation for total enthalpy was the sum of mechanical conversion energy and chemical-and-thermal enthalpy.

$$\frac{\partial \rho H}{\partial t} + \frac{\partial}{\partial x_j}(\rho u_j u_i + F_{h,j} - u_i \tau_{ij}) = -\frac{\partial p}{\partial x_i} + s_i u_i + s_h \qquad (4.3)$$

where:

$$H = \frac{1}{2} u_i u_i + h \qquad (4.4)$$

$\boldsymbol{s_h}$ – energy source,

$\boldsymbol{F_{h,j}}$ – energy stream diffusion into the direction of x_j.

The delivery equation for total enthalpy was solved in accordance with the recommendations for CFD modeling. This means that the Eckert number was calculated that formulates a temperature impact according to the following formula:

$$H = \frac{U^2}{c_P T} \qquad (4.5)$$

where:

$\boldsymbol{U}$ – velocity,

$\boldsymbol{C_p}$ – specific heat,

$\boldsymbol{T}$ – temperature.

Due to turbulent flow, it was necessary to define a suitable model of turbulence. Star-CD software provides many models of turbulence that fall into three categories:

- Eddy Viscosity models,
- Reynolds Stress models,
- Large Eddy Simulation models.

The model for large values of Reynolds numbers designated as high-Reynolds number k-ε model [star methodology] was applied for the calculations. This choice resulted from an analysis of research literature on simulation of combustion engines. The k-ε model is currently the most widely used in CFD calculations, which is supported, e.g. in the works [22, 27, 29, 80]. In this case, the equation for k and ε need to be solved apart from the basic delivery equations. The adopted model of turbulence is described by the following equations:

- turbulence kinetic energy k

$$\frac{\partial}{\partial t}(\rho k) + \frac{\partial}{\partial x_j}\left[\rho u_j - \left(\mu + \frac{\mu_t}{\sigma_k}\right)\frac{\partial k}{\partial x_j}\right] = \\ = \mu\left(P + P_B\right) - \rho\varepsilon - \frac{2}{3}\left(\mu_t \frac{\partial u_i}{\partial x_i} + \rho k\right)\frac{\partial u_i}{\partial x_i} + \mu P_{NL} \tag{4.6}$$

where

$$P \equiv S_{ij}\frac{\partial u_i}{\partial x_j} \tag{4.7}$$

$$P_B \equiv -\frac{g_i}{\sigma_{h,t}} \cdot \frac{1}{\rho} \cdot \frac{\partial p}{xj} \tag{4.8}$$

$$P_{NL} = -\frac{\rho}{\mu_t} u_i^{'} u_j^{'} \frac{\partial u_i}{\partial x_j} - \left[P - \frac{2}{3}\left(\frac{\partial u_i}{\partial x_i} + \frac{\rho k}{\mu_t}\right)\frac{\partial u_i}{\partial x_j}\right] \tag{4.9}$$

where:

P_{NL}=0 – for a linear model,

σ_k - Prandtl number.

- energy dissipation ε

$$\frac{\partial}{\partial t}(\rho\varepsilon)+\frac{\partial}{\partial x_j}\left[\rho u_j\varepsilon-\left(\mu+\frac{\mu_t}{\sigma_\varepsilon}\right)\frac{\partial\varepsilon}{\partial x_j}\right]=$$

$$=C_{\varepsilon 1}\frac{\varepsilon}{k}\left[\mu_t P-\frac{2}{3}\left(\mu_t\frac{\partial u_i}{\partial x_i}+\rho k\right)\frac{\partial u_i}{\partial x_j}\right]+C_{\varepsilon 3}\frac{\varepsilon}{k}\mu_t P_B- \tag{4.10}$$
$$+C_{\varepsilon 2}\rho\frac{\varepsilon^2}{k}+C_{\varepsilon 4}\rho\varepsilon\frac{\partial u_i}{\partial x_i}+C_{\varepsilon 1}\frac{\varepsilon}{k}\mu_t P_{NL}$$

where:

σ_ε - Prandtl number,
$C_{\varepsilon 1,4}$ – turbulence model coefficients,
μ_t – kinematic viscosity.

The calculations were done for the assumed ideal gas density model where density was a function of pressure and temperature with respect to air and fuel. Fluid flow was defined as compressible. Gas mixture density was according to the formula:

$$\rho=\frac{p}{RT\left(\sum\frac{Y_m}{M_m}\right)} \tag{4.11}$$

where:

Y_m – mass share of m-time component,
M_m – mole mass of m-time component,
R – universal gas constant,
T – gas temperature

4.4 Engine model

The engine model includes an intake manifold with four cylinders (fig. 4.4). Its geometry was developed by means of software CATIA V5 according to technical documentation and the measurements of the intake manifold and head.

Fig. 4.4 Geometric model of the engine

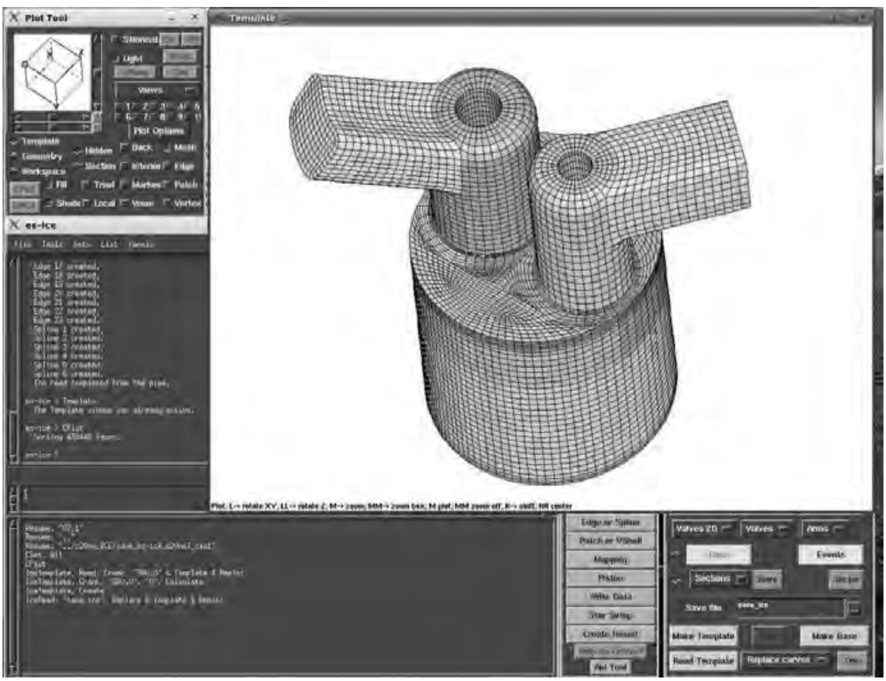

Fig. 4.5 User interface of the module es-ice in STAR-CD

The spatial discretization of the model and the movement of valves and pistons were done with a module *es-ice* of the STAR-CD software. The geometric model of surfaces and edges was imported into the programme. Then, a cell type and their local density in selected areas, including the vicinity of the intake and exhaust valves (fig. 4.7) were defined. This is necessary due to high velocity and pressure that occur right there. The efficiency and accuracy of these calculations is directly related to the quality of a generated mesh. According to the recommendations given in [37], a geometric discretization error decreases as the density of a mesh decreases, in accordance with the principle of C^n, where C is the coefficient of mesh density, while *n* is approximation scheme accuracy. The process of model generation with use of the *es-ice* programme is in figure 4.6.

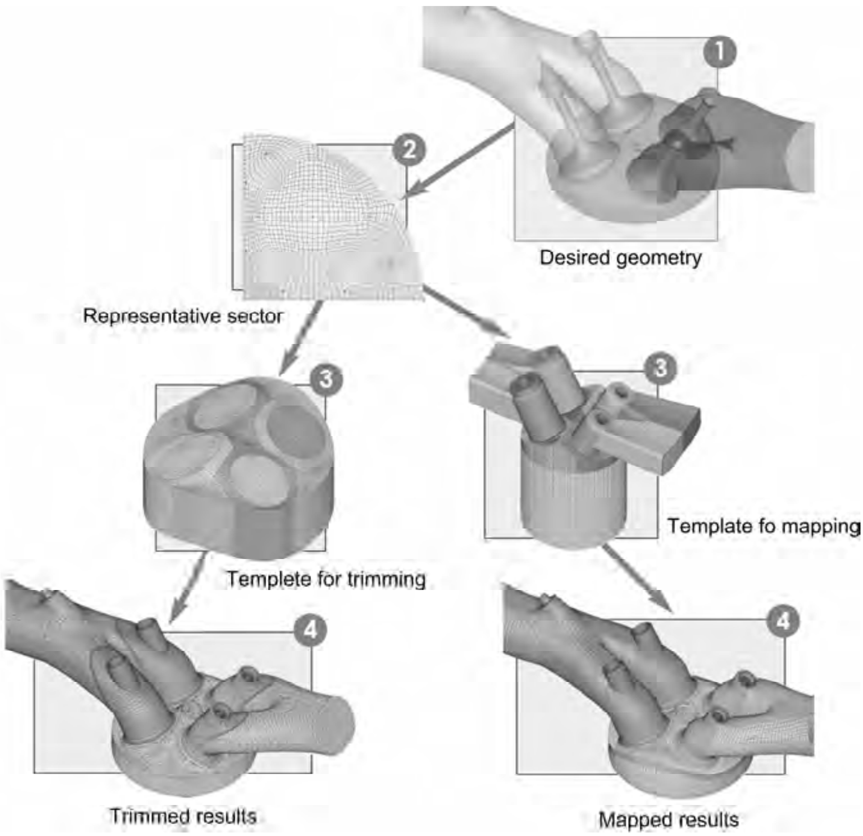

Fig. 4.6 Numerical discreditation [54]

In order to eliminate any discontinuities in geometry and to ensure the required accuracy of calculations, the correctness of a mesh generated was verified with a special function implemented in the *es-ice* module. Due to the complexity of the shape of a model, it was necessary to use many types of cells (fig. 4.7). Eventually, the mesh consisted of about 300 000 cells. Such a level of discretization of geometric calculations assured that the required accuracy and the time necessary to make calculations was simultaneously reduced. This numerical model was developed by the author.

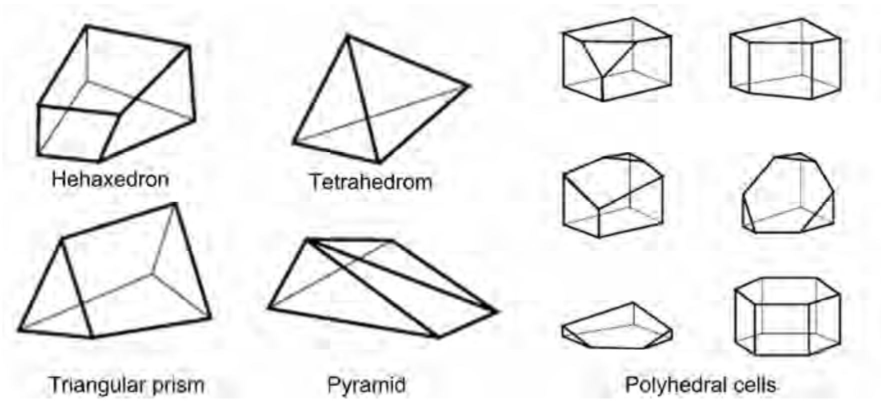

Fig. 4.7 Cell types used in the mesh

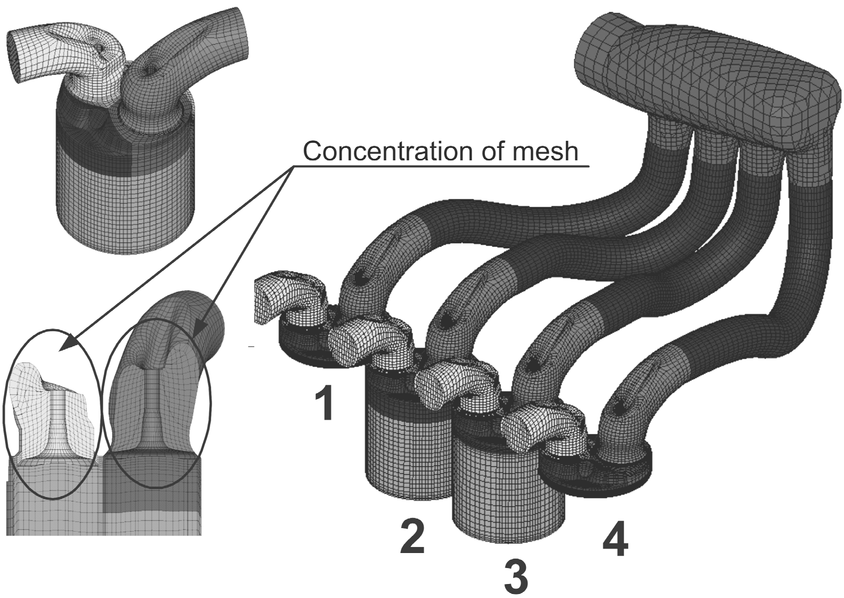

Fig. 4.8 Mesh

4.4.1 Boundary and initial condition

The simulation research reflected the operation conditions kept during the test stand research. The first step in determining the initial and boundary conditions was defining the movement of the valves and pistons in the *es-ice* module. Figure 4.9 shows the valve lift characteristics introduced into the model and was developed on the basis of the measurements of the real object. Movement of pistons was specified automatically by introducing a piston stroke and correlating it with the characteristics of temporary valve opening.

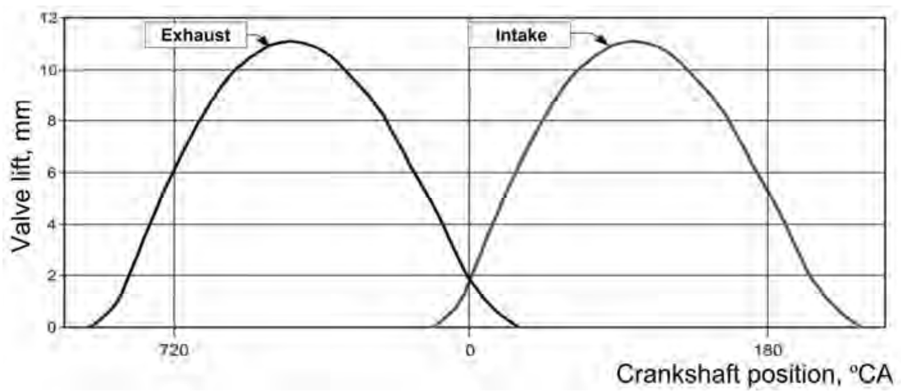

Fig. 4.9 Camshafts phases of C20LE Holden

During the simulation research, propane was the fuel to be injected; it is available directly from the libraries of the software in use. As described in Chapter 3, the gaseous injection system applied in the research was based on an injection rail that was connected with the intake manifold by injection pipes. In this case, the models of the injectors that are available in the programme can not be applied directly. Therefore, to map propane injection into the manifold model, a mesh corresponding to the geometry of the nozzles was developed. Based on the measurements done on a running engine, it was assumed that an injection pressure at the nozzle intake was 140 kPa and an injection time t_w (electronic impulse time) was 5.5 ms. The injection was done by a stroke function (fig. 4.10). In addition, the desired value of the mass of fuel injected was obtained by changing the roughness of the injection nozzle. This aimed at obtaining the required concentration in the cylinder at the end of the compression stroke. To ensure identical conditions of engine operation during the stand test, the pressure at the inlet to the intake manifold was assumed to be 40 kPa. A pressure of 100 kPa was assumed to be in the individual cylinder outlet pipes (fig. 4.11).

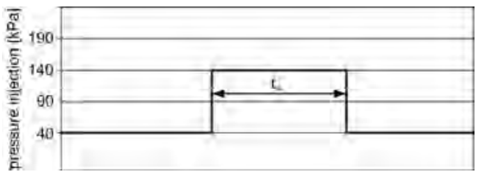

Fig. 4.10 Gas injection impulse

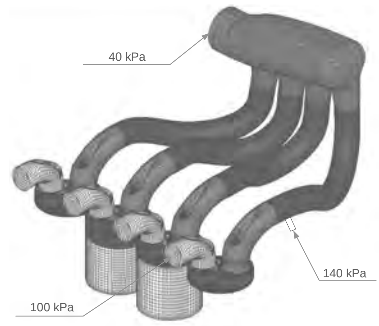

Fig. 4.11 Distribution of boundary conditions in the engine model

4.4.2 Time discretization

Time is the fourth independent variable that needs to be taken into account when dealing with non-stationary problems. All methods to solve such problems use the so-called “marching method” of calculation for the subsequent time steps. These steps may be treated as iterations to obtain a final state [36]. The appropriate selection of time step Δt guarantees that a time discretization error can be reduced, which translates directly into the results attained and provides reduced computation time. The excessive increase in a time step in STAR-CD is followed by the interruption of the calculation due to lack of stability. According to the rule given in [37], a method is assumed to be stable, if the measurement error ε (according to the formula in 5.12) used to assess average discrepancies at points ϕ of a spatial discretization of the index i, will decrease as n increases.

$$\varepsilon = \sqrt{\frac{1}{M}\sum_{i=1}^{M}(\phi_i^{(n)} - \phi_i^{(n-1)})^2}\ , \tag{4.12}$$

where:

ϕ - generalized, scalar variable intensity.

In the case study, simulation time step Δt was determined on the basis of test calculations. Finally, the stability of the calculation over the whole engine operation cycle was provided by a step $\Delta\varphi = 0.01^{\mathrm{o}}$ of crankshaft rotation, which is the same as time step Δt = 0.000011 s for an engine speed of 1500 rpm.

4.4.3 Stabilization of simulation condition

The initial simulations have shown that it is necessary to calculate several cycles of engine operation to obtain similar values of fuel concentration before and after the calculation. This follows from the geometry of the engine and the supply system used. A large volume of the intake manifold and the supply of gaseous fuel contribute to accumulating propane. Hence, it was necessary to make the calculations of 6 cycles of engine operation to stabilize the concentration of propane in the inlet manifold. The intensity of this phenomenon was increasing as the distance between the nozzles and the combustion chamber was increasing, which is confirmed by the figure below. It may be noted that the largest average concentration of propane in the manifold was obtained for the most remote injection nozzle.

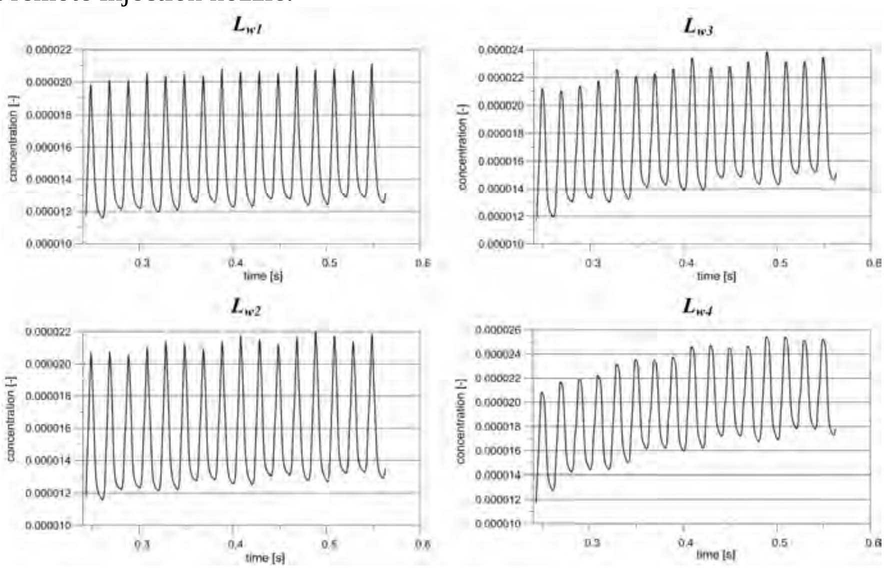

Fig. 4.12 Changes in time of propane average concentration in the inlet manifold

The maximum propane concentration was 0.0000254 for the most remote injection nozzle and 0.0000211 for the closest one (fig. 4.3). It should be noted that these results refer to the total volume of the intake manifold. Distribution of fuel in the intake manifold will be presented in the next chapter.

.

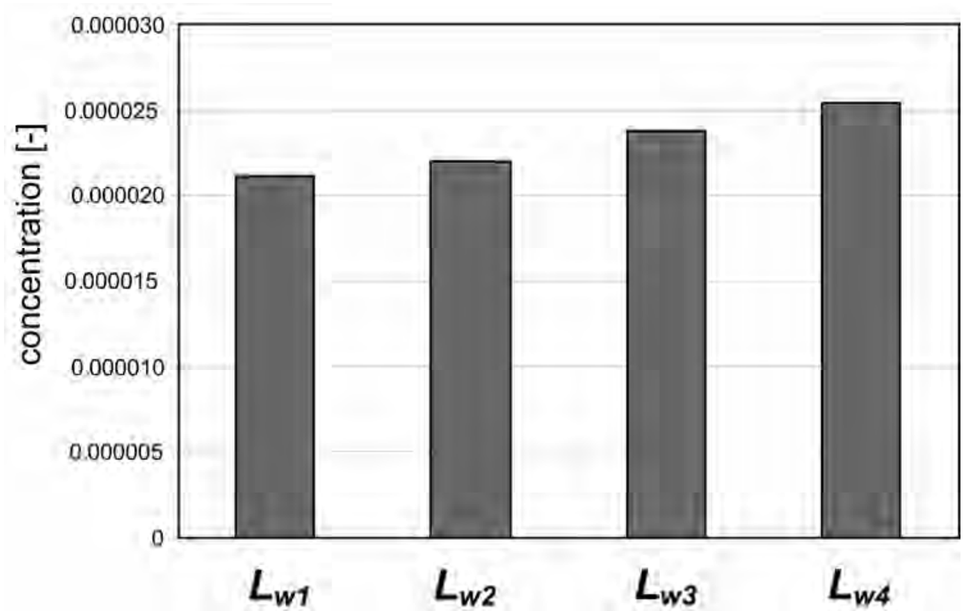

Fig. 4.13 The average concentration of propane in the inlet manifold for the subsequent distances of the nozzles from the intake valve axis

5. Testing

5.1 Introduction

This chapter describes the research objectives and the experiment plan to conduct experimental research. The further part of this section provides the results obtained on how the distance L_w between an injection nozzle and an inlet valve axis, and an early injection angle α_w influence the emission of toxic components

5.2 Research assumption

The fuel was dosed once during an operation cycle (fig. 5.1). Depending on the preset value of an early injection angle α_w, the fuel was injected when the intake valve was closed or open.

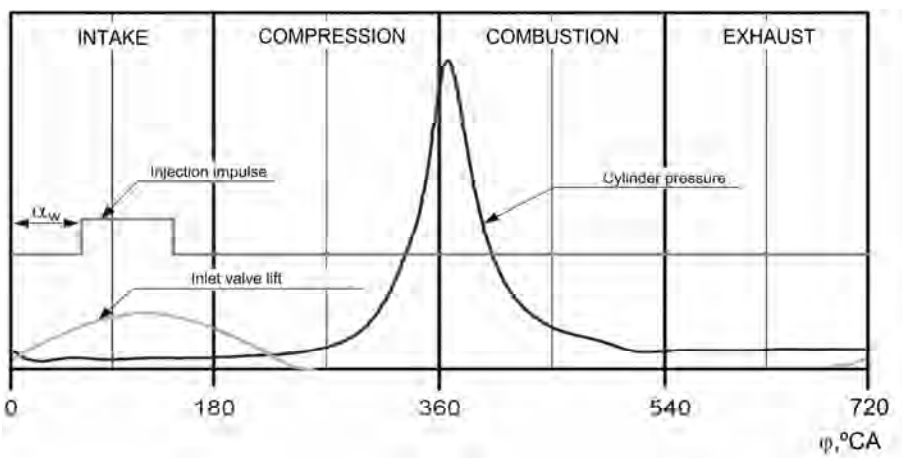

Fig. 5.1 Time courses of cylinder pressure, intake valve lift and an injection signal as a function of crankshaft rotation

The flow phenomena in the inlet are more intense for small loads [35, 69]. A charge exchange process is characterized by two significant backflows through the inlet valve into the intake manifold. A significant difference in pressure between the cylinder and the intake manifold deteriorated a filling process. Filling efficiency η_v, which in SI engines increases as load increases due to a throttle in an inlet system, is also important (fig. 5.2).

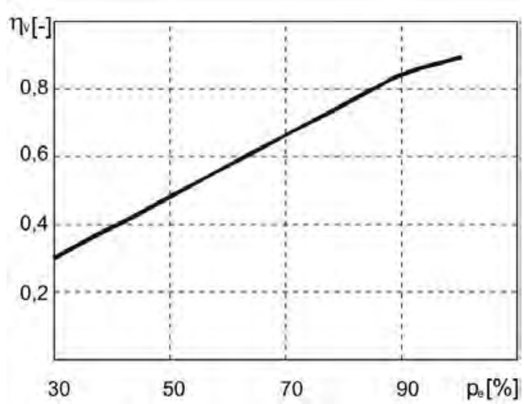

Fig. 5.2 SI engine filling characteristics [69]

For small loads, the adjustment of an early injection angle can enhance fuel delivery into a cylinder, which results from the fact that an injection angle is narrower than an intake valve opening angle. Particular attention should be paid to the backflows from the cylinder (fig. 5.3). A wide range of early injection angles was selected on purpose because the distance between the injector nozzle and combustion chamber changed.

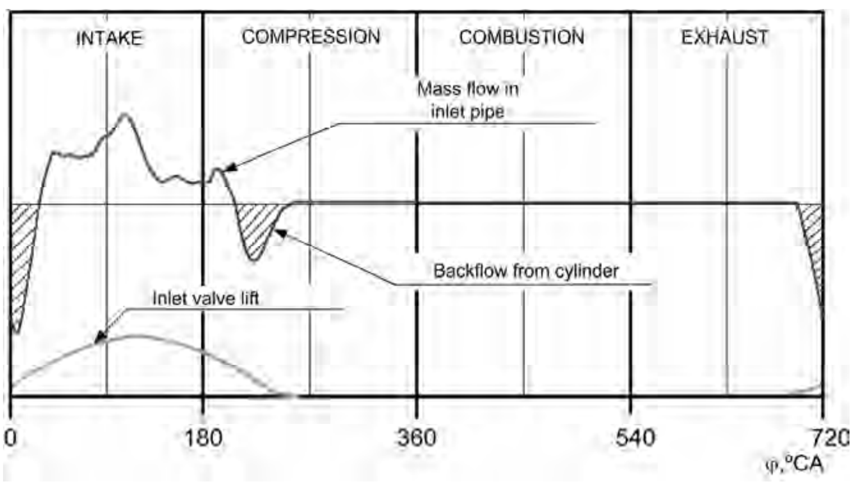

Fig. 5.3 Time course of mass flow rate through the inlet valve and of the inlet valve lift as a function of crankshaft rotation.

The doctoral dissertation [35] demonstrated that the regulation of a start injection angle significantly affects engine performance with respect to the value of torque generated and emissions of toxic components in exhaust gas. Based on the literature, the impact of α_w can already be identified during testing every 20 degrees of crankshaft rotation [42] in the case of fuelling the engine by a rich mixture. However, when a lean mixture is used, it is necessary to select more measurements points as an angle of injection start changes. The reason for this is that here the adjustment of α_w affects much fuel distribution in a cylinder, mixture homogenization, and as a result combustion [94]. The measurements were done every 10° CA. The change of an angle of injection start ranged between -120 ÷ 120° CA for the both mixture compositions, which allowed the fuel to be dosed during a closed or open intake valve.

The results given in [35] confirm that an optimal advance ignition angle α_z is 20° for the adopted engine working conditions. An engine thermal state was determined by a coolant temperature of 80° C that equaled a thermostat opening temperature, an air temperature inside the intake manifold of 38 ± 2° C and a lubricating oil temperature of 80 ± 2° C. The propane-butane temperature was 60 ± 3° C as a result of the applied pressure regulator-vaporizer.

5.3 Experiment plan

The experimental research was done under steady operation state according to the assumptions outlined in Chapter 2 to verify how the distance between the propane-butane injection nozzle and combustion chamber influences operating parameters. For each installation place, a injection start angle α_w was changed within the range from -120 ° to 120 ° CA (fig. 5.4) against a piston top dead position (the beginning of an intake stroke). The value of α_w was changed every 20° CA and 10° CA for an excess air ratio λ = 0.98 and λ = 1.1, respectively (fig. 5.5).

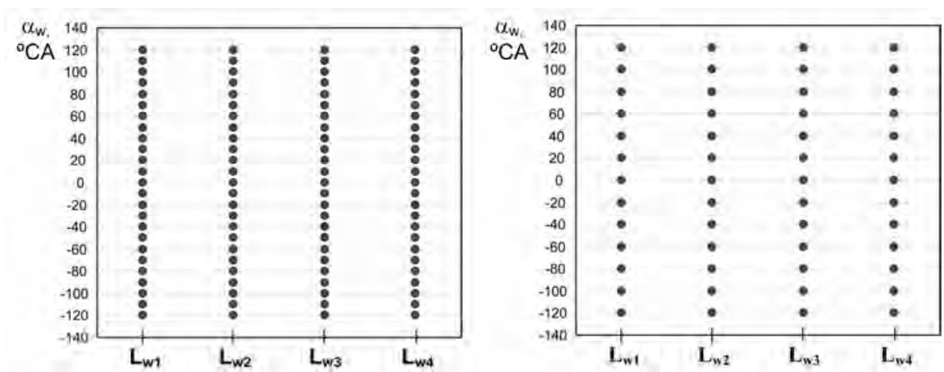

a)

b)

Fig. 5.4 Graphic chart of the research plan: excess air ratio λ = 1.1, b) excess air ratio λ = 0.98

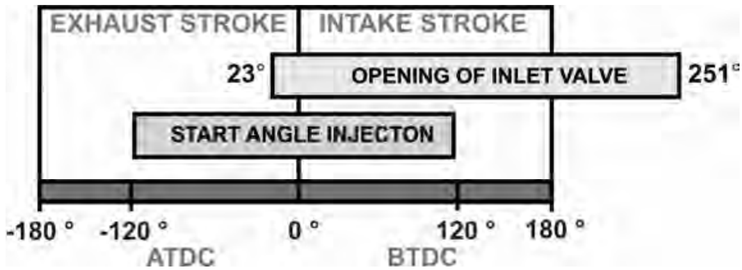

Fig. 5.5 Range of changes in an injection start angle

A constant air-fuel mixture composition was assumed for each operation point. If the place for mounting the injection nozzle in the intake manifold and an early injection angle were changed, the deviation of an excess air ratio λ from the set value was noted. In order to maintain the assumed mixture composition, injection time was rectified (fig. 5.5).

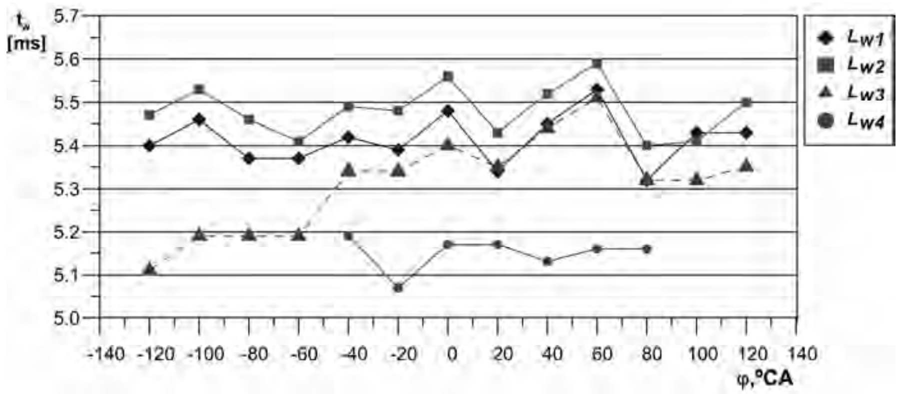

Fig. 5.6 Injection time for the subsequent variants of injection nozzle installations for a mixture composition λ = 0.98

The following values were measured in each measurement points designated by the location of the injection nozzle ($\mathbf{L}_{w1}$, $\mathbf{L}_{w2}$, $\mathbf{L}_{w3}$, $\mathbf{L}_{w4}$) and an early injection angle:

- indicated pressure in the 4th cylinder,
- intake manifold pressure,
- pressure in the inlet pipe supplying propane-butane into the intake manifold,
- concentration of toxic components in exhaust gases (nitrogen oxides, carbon monoxide, hydrocarbons)
- excess air ratio.

5.4 Results

Figures 5.7-5.12 show how the emissions of toxic components depend on the place where an injection nozzle is mounted, and on an injection start angle. The results are presented with respect to an engine fuelled by a rich mixture of λ = 0.98 and a lean mixture of λ = 1.1. The test results are presented as a function of crankshaft rotation. The value of 0º CA refers to the position of a crankshaft at a piston top dead center of an intake stroke. The other variants of nozzle mounting were labelled as $\boldsymbol{L_{W1,\,2,\,3,\,4}}$.

The concentration of toxic gases obtained in the case of rich mixture fuelling.

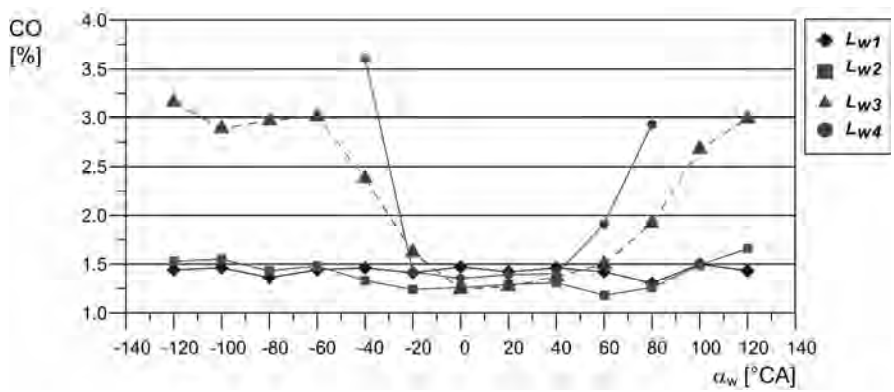

Fig. 5.7 Dependence of carbon monoxide in the exhaust gases on the early injection angle α_w and the distance between the injection nozzle and combustion chamber L_w for a rich mixture of λ = 0.98

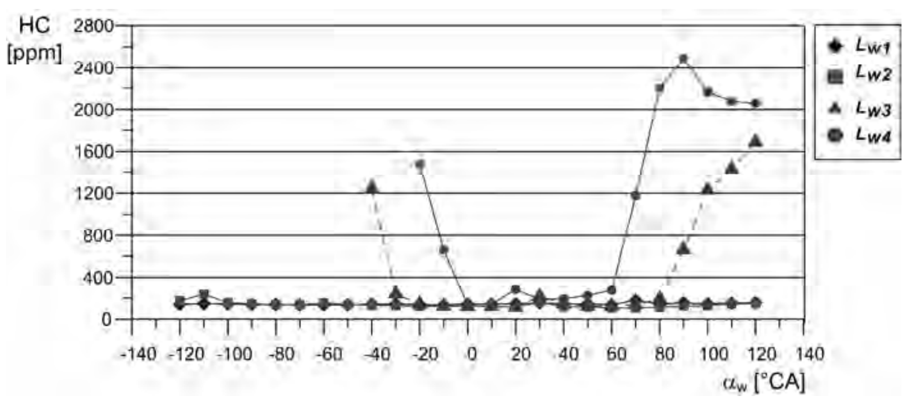

Fig. 5.8 Dependence of hydrocarbons in the exhaust gases on the early injection angle α_w and the distance between the injection nozzle and combustion chamber Lw for a rich mixture of λ = 0.98

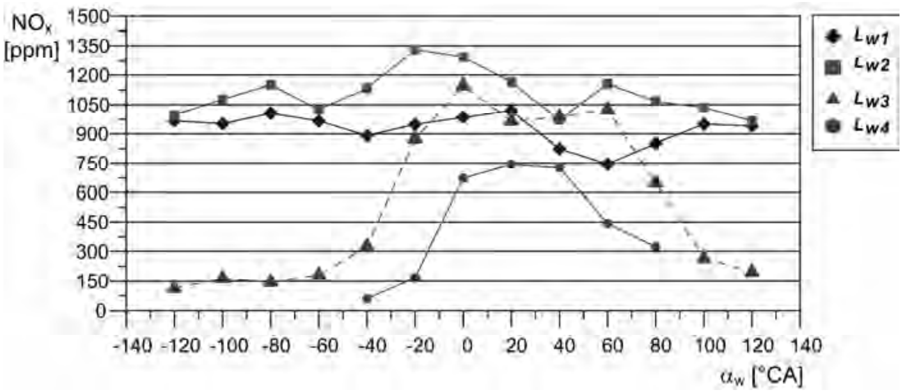

Fig. 5.9 Dependence of nitrogen oxide in the exhaust gases on the early injection angle α_w and the distance between the injection nozzle and combustion chamber L_w for a rich mixture of $\lambda = 0.98$

The concentration of toxic gases obtained in the case of lean mixture fuelling.

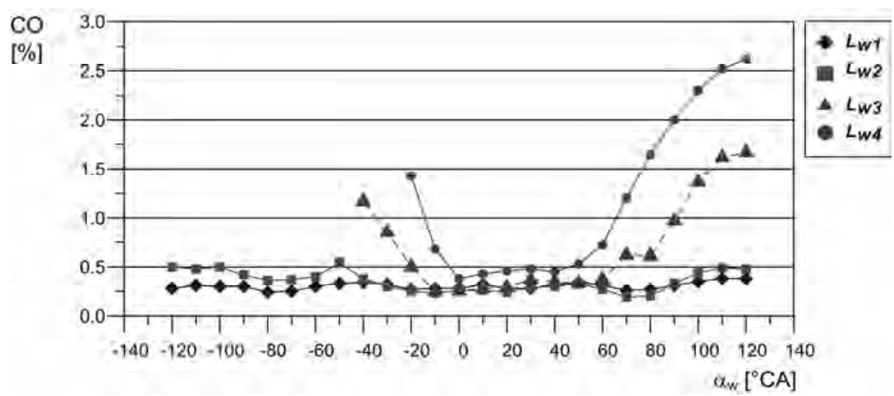

Fig. 5.10 Dependence of carbon monoxide in the exhaust gases on the early injection angle α_w and the distance between the injection nozzle and combustion chamber L_w for a lean mixture of $\lambda = 1.1$.

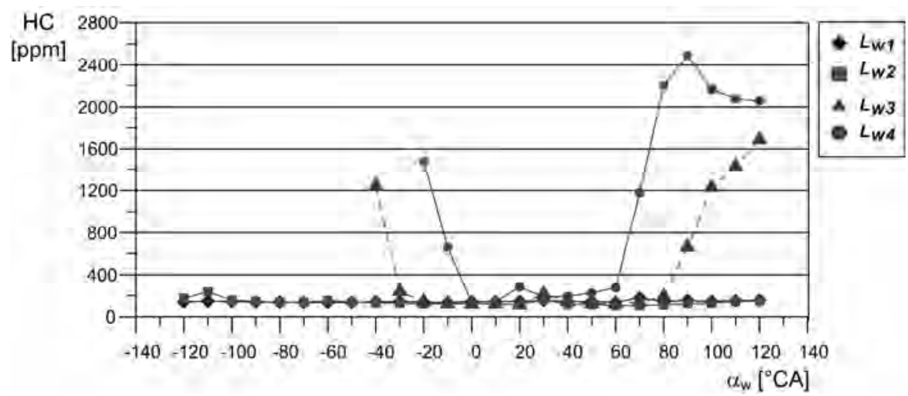

Fig. 5.11 Dependence of hydrocarbon in the exhaust gases on the early injection angle α_w and the distance between the injection nozzle and combustion chamber L_w for a lean mixture of $\lambda = 1.1$.

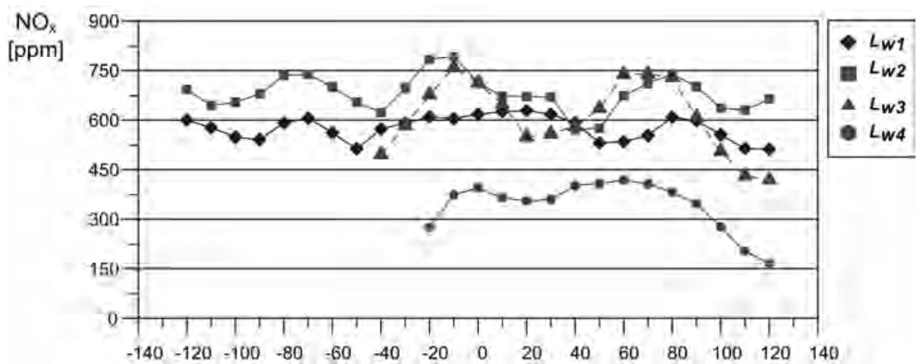

Fig. 5.12 Dependence of nitrogen oxides in the exhaust gases on the early injection angle α_w and the distance between the injection nozzle and combustion chamber L_w for a lean mixture of $\lambda = 1.1$.

5.5 Analysis

A reference point in a comparative analysis of the test stand results attained was the results obtained during the engine operation when the distance between the injection nozzle and combustion chamber L_{w1} was the shortest both for fuelling by a rich and lean mixture.

As an indicator of the quantitative increase of toxic gases concentration was the quotient of the concentration of measured exhaust gas component (CO, HC, NO_x) obtained at a given point of the engine defined by L_w and α_w against the value obtained for the first variant of the injection nozzle installation L_{w1}.

$$\phi = \frac{x_{Lwx}}{x_{Lw1}} \tag{5.1}$$

where:

ϕ – concentration relative value,

x_{Lwx} – value of exhaust gas component concentration obtained for $L_{w2,3,4}$,

x_{Lw1} – value of exhaust gas component concentration obtained for L_{w1}.

Figures 5.13-5.18 show the impact of an early injection angle on the relative values analyzed.

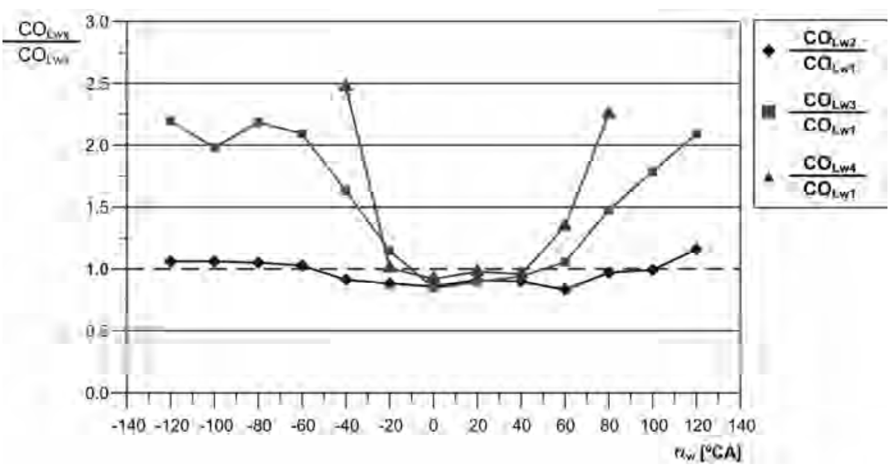

Fig. 5.13 Dependence of the relative concentrations of carbon monoxide in the exhaust gas on an early injection angle α_w for the subsequent variants of nozzle installation in the case of a rich mixture of λ=0.98

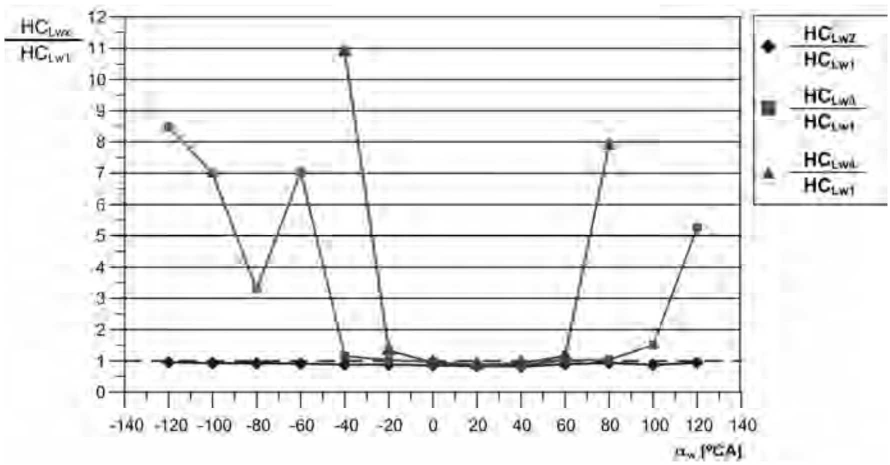

Fig. 5.14 Dependence of the relative concentrations of hydrocarbons in the exhaust gas on an early injection angle α_w for the subsequent variants of nozzle installation the case of a rich mixture of λ=0.98

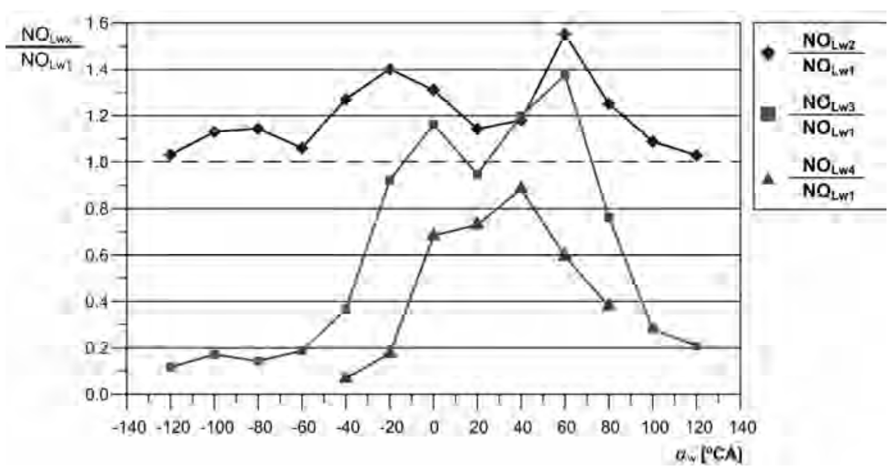

Fig. 5.15 Dependence of the relative concentrations of nitrogen oxides in the exhaust gas on an early injection angle α_w for the subsequent variants of nozzle installation in the case of a rich mixture of λ=0.98

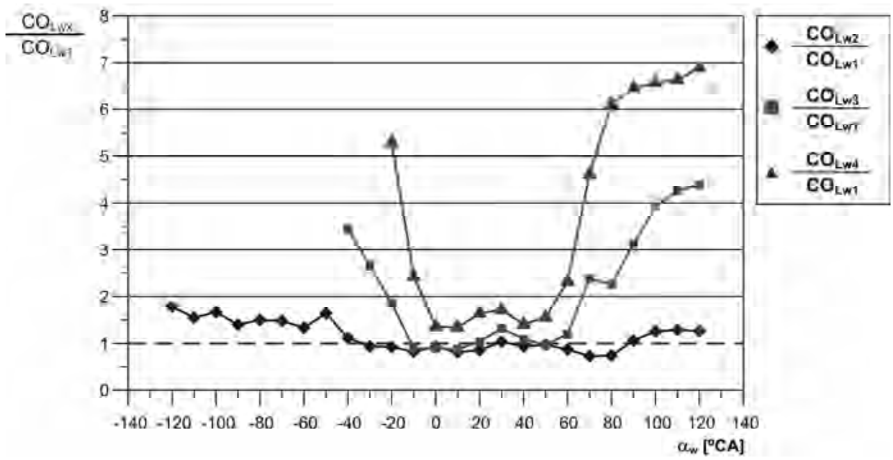

Fig. 5.16 Dependence of the relative concentrations of carbon monoxide in the exhaust gas on an early injection angle α_w for the subsequent variants of nozzle installation in the case of a lean mixture of λ=1.1

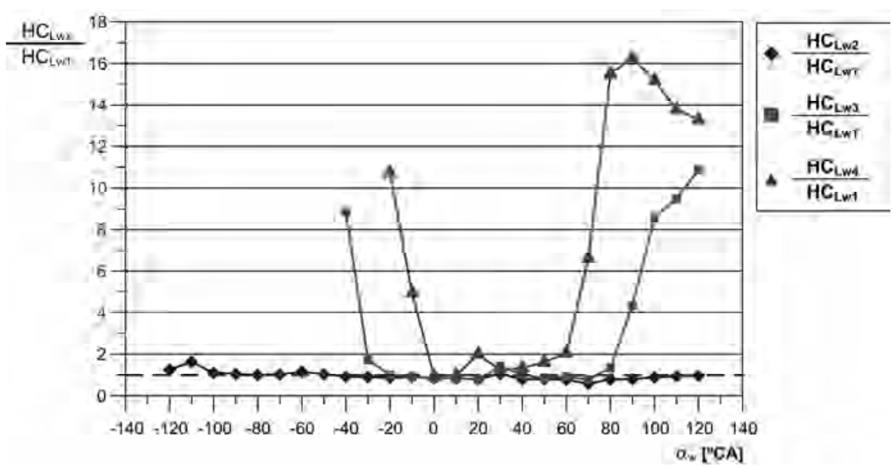

Fig. 5.17 Dependence of the relative concentrations of hydrocarbons in the exhaust gas on an early injection angle α_w for the subsequent variants of nozzle installation in the case of a lean mixture of λ=1.1

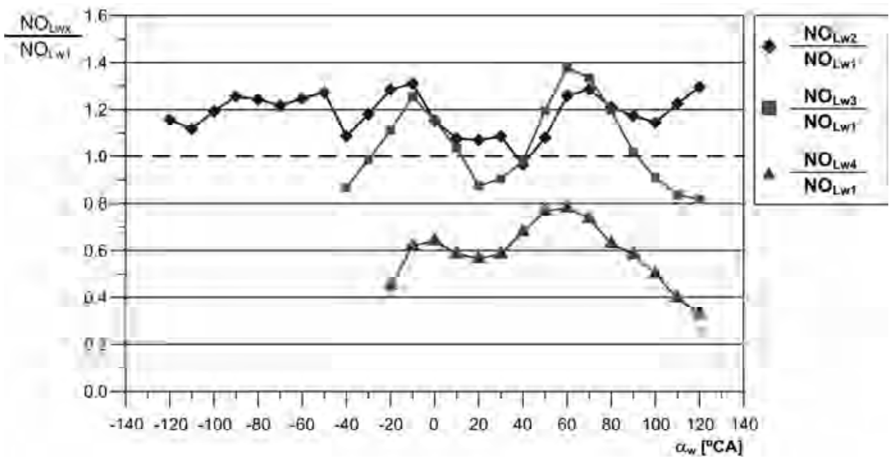

Fig. 5.18 Dependence of the relative concentrations of nitrogen oxides in the exhaust gas on an early injection angle α_w for the subsequent variants of nozzle installation in the case of a lean mixture of λ=1.1.

The following terms were used to describe the test stand results under analysis:

rich mixture - excess air ratio λ = 0.98,
lean mixture - excess air ratio λ = 1.1,
early injection angle - the beginning of fuel injection that corresponds to the beginning of the injection angle ranging from -120 to 0° CA with respect to an early intake stroke,
middle injection angle - the beginning of fuel injection that corresponds to the beginning of the injection angle ranging from 0 to 40° CA with respect to an early intake stroke,
late injection angle - the beginning of fuel injection that corresponds to the beginning of the injection angle ranging from 40 to 120° CA with respect to an early intake stroke,
L_{w1}, L_{w2}, L_{w3}, L_{w4} - variants of nozzle distances.

The analysis was done by comparing the test stand results for L_{w2}, L_{w3}, L_{w4} with L_{w1}. During the tests, stable engine operation was obtained after the nozzles were mounted at the distances L_{w1}, L_{w2}, L_{w3} within the whole range of the changes of the early injection angle of λ = 0.98, and for L_{w1}, L_{w2} at λ = 1.1.

For the middle injection angles when a rich mixture was used to fuel the engine, changes of 30% in the concentration of carbon monoxide, unburned hydrocarbons and nitrogen oxides in the exhaust gases were noted, compared with L_{w1} (fig. 5.13-5.15). However, for early and late injection angles α_w, if L_w increased, the changes in the concentration of exhaust gas components analyzed were much more intensive due to the changes in the distance between the injection nozzles and combustion chamber. For the distance of L_{w3}, the whole range of changes in the angle α_w was tested. However, reducing the early and increasing the late injection angles contributes to a greater impact of the distance L_w on exhaust gas composition. For the boundary angles, the concentration of carbon monoxide increased more than twice, the concentration of unburned hydrocarbons increased more that eight-times and the concentration of nitrogen oxide was reduced by 0.8 compared with L_{w1}. For L_{w4}, the tests were done within the range of α_w = (-40-80) CA, as for this range a stable engine operation was obtained.

For the middle injection angles, the concentration of carbon monoxide and unburned hydrocarbons changed by 30% with respect to L_{w1}. However, in the case of the relationship of relative emissions of nitrogen oxides (fig. 5.15) throughout the whole analyzed range, the distance of the injection nozzle causes more significant changes than an early injection angle.

Based on the analysis of the relative concentration of toxic gases measured during lean-burn engine power (fig. 5.16-5.15), a greater impact of the distance L_w was noted already for middle injection angles. Referring to figure 5.16, which shows the relative emission of carbon monoxide, a change in the distance has got a significant impact within the early and late injection angles. For the angle of α_w = 120° and the distance L_{w4} = 310 mm, CO concentrations increased by seven times. For the middle injection angles, the distance of the injection nozzle also influenced exhaust gas composition more than an early injection angle α_w. The change amounted to 80% (HC emissions, L_{w1}, α_w =20º) and was greater than in the case of rich mixture fuelling.

The relative emissions of hydrocarbons as shown in figure 5.17 changed similarly as a result of the distance change between the injection nozzle and the intake valve axis, as it was for the relative emissions of carbon monoxide. Maximum values were obtained for the boundary angles α_w and the distance L_{w4}. For the angle of α_w=120º, the concentration of unburned hydrocarbons increased by eighteen times, whereas for the angle of α_w=-40º the increase equalled eleven times.

Regarding the relative emissions of nitrogen oxides, the greatest impact of the distance of the nozzles from the intake valve axis was noted when the engine worked at the distance of L_w where the concentration decreased within the entire range of the angle α_w.

Based on figures from 5.13 to 5.18, it was noted that within the range of the middle early injection angles for both mixtures (rich and lean), the relative values of the emissions of measured exhaust gas components were the least. However, they were more sensitive to the geometrical factor for fuelling the engine by a lean mixture.

Changing the distance between the injection nozzle and the inlet valve axis changes exhaust gas composition more significantly than changing an early injection angle.

5.6 Significance of impact

The evidence that the distance between the injection nozzle and the inlet valve axis is an important factor in the concentration of toxic components in exhaust gas is supported by the fact that the hypothesis of equality of average values from two variants of injection was refuted.

The null hypothesis: $$H_0 : x_1 - x_2 = 0 \qquad (5.1)$$

The following measurement data was analyzed.

For the subsequent measurement values X, the mean value was calculated:

$$\overline{X} = \frac{1}{n}\sum_{i=1}^{N} x_i \;, \qquad (5.2)$$

where the number of “n" records was 5 in the case of the analyzed signals of extremely low frequency (CO, HC, NO_x).

Standard deviation was calculated using the formula:

$$\sigma_x = \sqrt{\frac{\sum_{i-1}^{N}[x(i) - \overline{X}]^2}{n-1}} \qquad (5.3)$$

To prove it, the Student's t-test was applied. The H_0 hypothesis of the equality of the average values from two series of measurements was verified. Thus, the value of $t_{1,x}$, was calculated according to the formula:

$$t_{1,x} = \frac{\overline{X}_1 - \overline{X}_2}{\sqrt{\frac{\sigma_{x1}^2}{n_1} + \frac{\sigma_{x2}^2}{n_2}}} \qquad (5.4)$$

where:

x: 2, 3, 4 – subsequent variants of $\boldsymbol{L_w}$.

Then, a significance level α for the subsequent tested cases was calculated.

The statistical relevance of the results attained was based on the value of a significance level α, which is the decreasing rate of reliability of the results.

A boundary value of an acceptable error level was a significance level of α=0.05.

The calculated value $t_{1,x}$ was compared with a quantile of the t-Student's distribution equalling 2.306 for $t_{1-p/2}$=0.975, a number of degrees of freedom N=N1 + N2-2 = 8, the significance level α = 0.05 (a two-sided critical area). In the case of inequality:

$$t_{1,x} \geq t_{1-p/2} \tag{4.5}$$

the null hypothesis of equality of two mean values was rejected.

Tables 5.1-5.3 provide the findings concerning the significance level of toxic emission changes resulting from the changes in the distance between the injection nozzle and the inlet valve axis. In each case, a test on the significance of the differences between the mean value obtained for $\boldsymbol{L_{w1}}$ and the values obtained for $\boldsymbol{L_{w2}}$, $\boldsymbol{L_{w3}}$, $\boldsymbol{L_{w4}}$ was done. The value of significance level α was calculated. The analysis was done for each early injection angle α_w and an excess air ratio λ = 1.1. Blank spaces in the tables correspond to the values of the angle α_w for which stable engine operation was not obtained.

The mean values of the concentrations of nitrogen oxides obtained for $\boldsymbol{L_{w1}}$ and $\boldsymbol{L_{w2}}$ are different at a given level with respect to the changes of the early and late injection angles. Comparing the concentrations of nitrogen oxides in the exhaust gas measured during engine operation for $\boldsymbol{L_{w1}}$ and $\boldsymbol{L_{w4}}$, the significance attained was less than 0.05 for all the early injection angles α_w.

With respect to the mean values of carbon monoxide emissions, the significance level of changes was noted for the early injection angles (between -120 and -40º CA) and the late injection angles (between 60 and -120º CA) in the case of all the tested variants. However, in the case of the early injection angles ranging from -30 to 50° CA, the null hypothesis was not rejected in some cases.

The analysis of the changes in hydrocarbon emissions showed also a significant impact of injection nozzle distance $\boldsymbol{L_w}$. However, the null hypothesis was maintained for all the cases examined ($\boldsymbol{L_{w1}}$ vs. $\boldsymbol{L_{w2}}$, $\boldsymbol{L_{w1}}$ vs. $\boldsymbol{L_{w3}}$, $\boldsymbol{L_{w1}}$ vs. $\boldsymbol{L_{w4}}$) and for certain early injection angles α_w.

It was shown that the significance of the differences of mean values for the changes in late injection angles is below the assumed level of α = 0.05 for the all measured exhaust gas components. With regard to the individual components of exhaust gas (CO, HC, NO_x), the distance between the injection nozzle and the inlet valve axis changed the exhaust gas composition more than the change in an injection start angle. The results of simulation research into gaseous fuel injection and filling the engine to clarify the mechanisms that increase the amount of toxic components in exhaust gas will be discussed in the further part of the monograph.

Tab. 5.1 The results of a significance level of the changes in nitrogen oxide emissions (NO_x) between the distance L_{w1} and the subsequent tested distances

Injection angle α_w	L_{w1} **vs.** L_{w2}	L_{w1} **vs.** L_{w3}	L_{w1} **vs.** L_{w4}
-120	**0,0096**	**-**	**-**
-110	**0,0389**	**-**	**-**
-100	**0,0054**	**-**	**-**
-90	**0,0016**	**-**	**-**
-80	**0,0014**	**-**	**-**
-70	**0,0019**	**-**	**-**
-60	**0,0016**	**-**	**-**
-50	**0,0015**	**-**	**-**
-40	0,1067	0,0655	**-**
-30	**0,0051**	0,8273	**-**
-20	**0,0008**	0,0926	**0,0006**
-10	**0,0007**	0,0031	**0,0006**
0	**0,0092**	**0,0276**	**0,0006**
10	0,1192	0,5537	**0,0006**
20	0,1488	0,0575	**0,0006**
30	0,0903	0,1361	**0,0006**
40	0,4668	0,7446	**0,0006**
50	0,1566	**0,0197**	**0,0006**
60	**0,0014**	**0,0010**	**0,0006**
70	**0,0010**	**0,0014**	**0,0006**
80	**0,0021**	**0,0103**	**0,0006**
90	**0,0047**	0,7650	**0,0006**
100	**0,0190**	0,1977	**0,0006**
110	**0,0035**	**0,0463**	**0,0006**
120	**0,0011**	**0,0301**	**0,0006**

Tab. 5.2 The results of a significance level of the changes in carbon monoxide (CO) between the distance L_{w1} and the subsequent tested distances

Injection angle α_w	L_{w1} **vs.** L_{w2}	L_{w1} **vs.** L_{w3}	L_{w1} vs. L_{w4}
-120	**0,0006**	-	-
-110	**0,0006**	-	-
-100	**0,0006**	-	-
-90	**0,0007**	-	-
-80	**0,0007**	-	-
-70	**0,0007**	-	-
-60	**0,0009**	-	-
-50	**0,0006**	-	-
-40	**0,0415**	**0,0006**	-
-30	0,2585	**0,0006**	-
-20	0,2585	**0,0006**	**0,0006**
-10	**0,0166**	0,3056	**0,0006**
0	0,2585	0,3056	**0,0025**
10	**0,0071**	0,1828	**0,0016**
20	**0,0415**	0,7244	**0,0006**
30	0,5600	**0,0117**	**0,0006**
40	0,2585	0,3056	**0,0009**
50	0,5600	0,7244	**0,0006**
60	**0,0415**	**0,0604**	**0,0006**
70	**0,0033**	**0,0006**	**0,0006**
80	**0,0033**	**0,0006**	**0,0006**
90	0,2585	**0,0006**	**0,0006**
100	**0,0012**	**0,0006**	**0,0006**
110	**0,0007**	**0,0006**	**0,0006**
120	**0,0009**	**0,0006**	**0,0006**

Tab. 5.3 The results of a significance level of the changes in hydrocarbons (HC) between the distance L_{w1} and the subsequent tested distances

Injection angle α_w	L_{w1} vs. L_{w2}	L_{w1} vs. L_{w3}	L_{w1} vs. L_{w4}
-120	**0,0006**	-	-
-110	**0,0006**	-	-
-100	**0,0157**	-	-
-90	0,1361	-	-
-80	1,0000	-	-
-70	0,4973	-	-
-60	**0,0020**	-	-
-50	0,2703	-	-
-40	**0,0318**	**0,0006**	-
-30	**0,0111**	**0,0006**	-
-20	**0,0033**	0,8538	**0,0006**
-10	**0,0157**	0,2855	**0,0006**
0	**0,0017**	**0,0010**	0,5674
10	**0,0010**	**0,0012**	0,9263
20	**0,0007**	**0,0007**	**0,0006**
30	0,1361	**0,0006**	**0,0108**
40	**0,0007**	0,8183	**0,0020**
50	**0,0007**	**0,0139**	**0,0006**
60	**0,0007**	**0,0318**	**0,0006**
70	**0,0006**	**0,0006**	**0,0006**
80	**0,0007**	**0,0006**	**0,0006**
90	**0,0007**	**0,0006**	**0,0006**
100	**0,0059**	**0,0006**	**0,0006**
110	**0,0660**	**0,0006**	**0,0006**
120	0,1931	**0,0006**	**0,0006**

6. Simulation research

6.1 Introduction

This chapter presents the simulation research results of the impact of the distance between the injection nozzle and combustion chamber, and an injection start angle on a filling process in a multicylinder engine. Later, the results attained were analyzed with respect to mixture homogenization.

6.2 Research assumption

The simulation research was to explain why engine operation is diversified due to varied distances L_w between an injector nozzle and a combustion chamber and the changes in an injection start angle α_w. Precise mapping of the distribution of an air-fuel mixture in a cylinder is crucial due to the process of its ignition. Air-fuel mixture formation in a spark-ignition engine is a process that depends on many variables. To clarify why the increased emissions of toxic gases occur, is closely connected with how a fuel is distributed in a combustion chamber [16]. The cases described in literature confirm that simulation research based on computational fluid dynamics is compatible with test stand results, which also applies to alternative-fuels-based engines. The work in [78] presented the results of the research into the effect of CNG injection nozzle geometry on a filling process.

6.3 Experiment plan

The analysis of the phenomena that occur in an intake manifold and in particular combustion chambers in a multi-cylinder engine can explain how a geometric factor, i.e. the distance between an injection nozzle and a combustion chamber influences engine filling.

Due to much time necessary to make calculations, the tests were done for the four distances L_w between the injection nozzles and combustion chamber without changing an injection start angle α_w. These distances corresponded to the values within the scope of test stand research. Injection time for these distances remained the same. The research scope is shown in figure 6.1. No combustion model research was conducted.

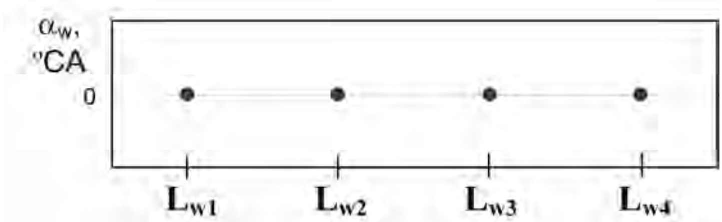

Fig. 6.1 Scope of the simulation research

6.4 Results

6.4.1 Fuel distribution in the intake manifold

The following figures present the simulation results obtained. These results relate to the processes inside the intake manifold and combustion chambers during gas fuelling for the distance of $\boldsymbol{L_{w1}}$.

°CA	
0	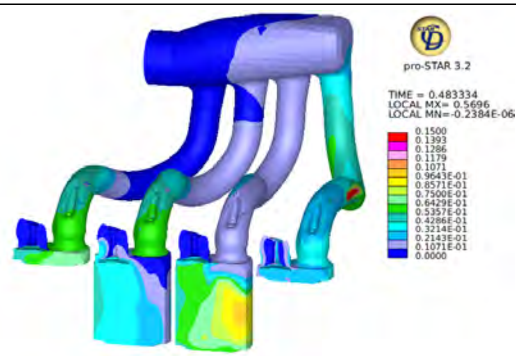
20	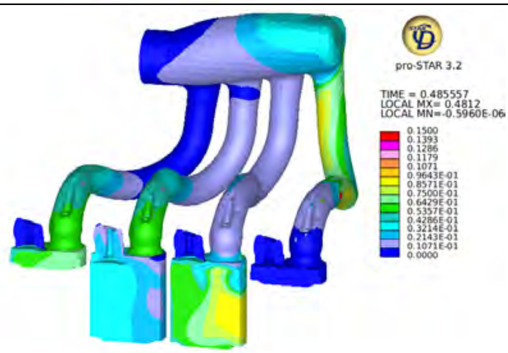

Fig. 6.2 Time course of fuel concentration distribution

40

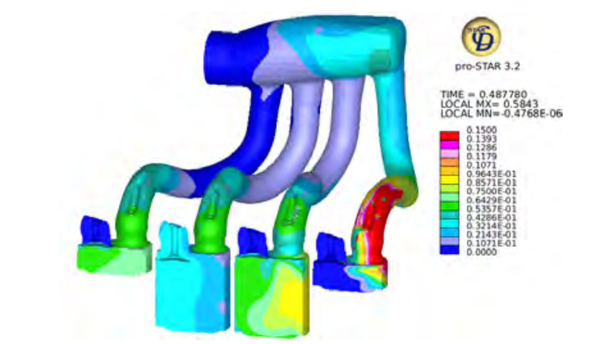

60

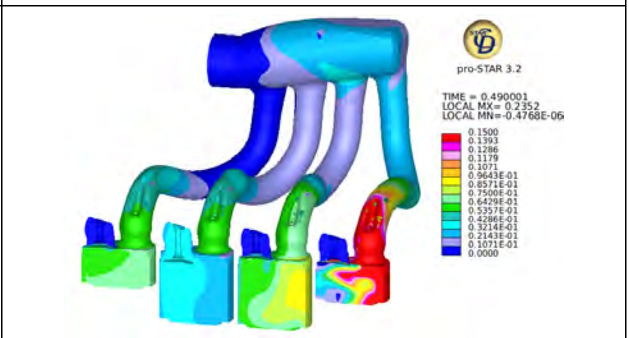

80

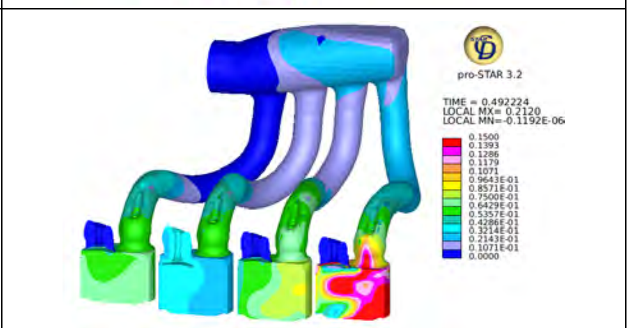

100

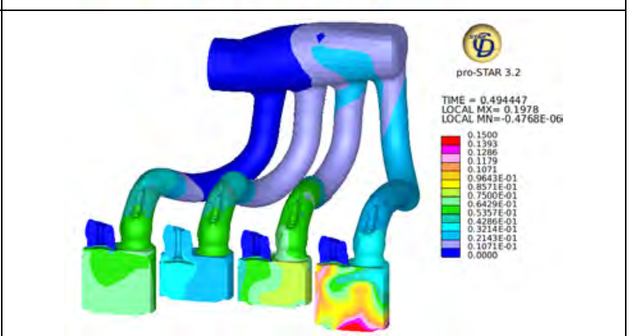

Fig. 6.2 Time course of fuel concentration distribution - continued

120	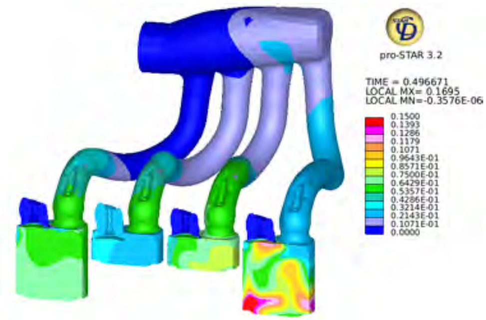
140	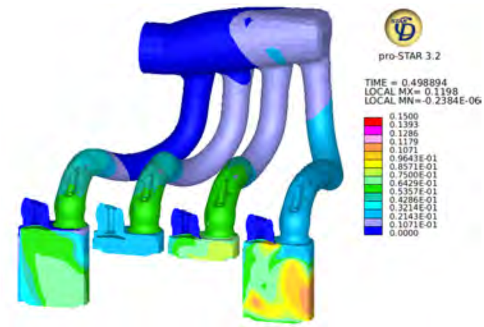
160	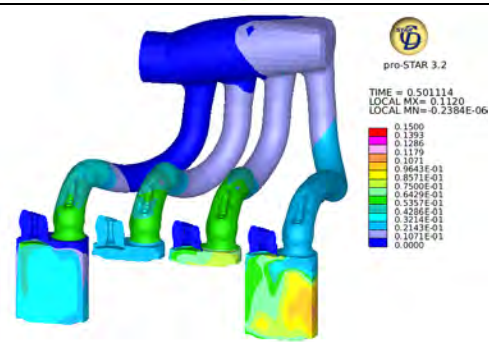
180	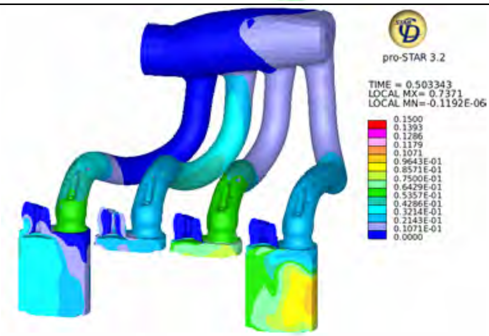

Fig. 6.2 Time course of fuel concentration distribution - continued

<table>
<tr><td>200</td><td>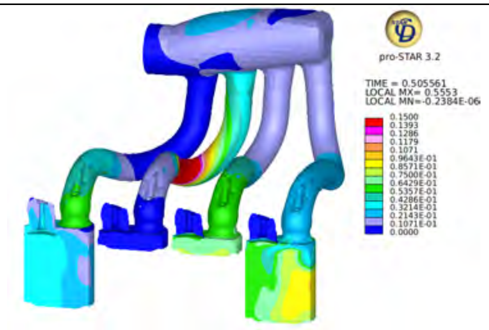
</td></tr>
<tr><td>220</td><td>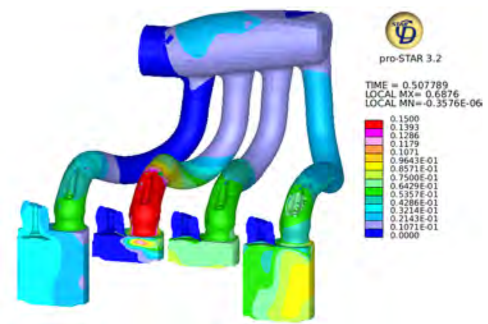
</td></tr>
<tr><td>240</td><td>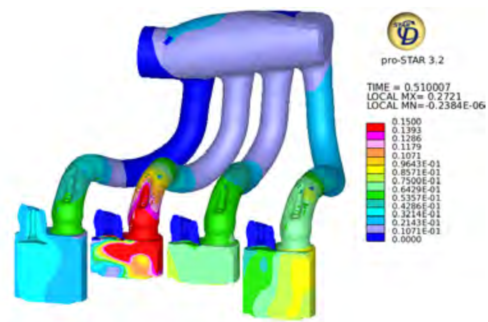
</td></tr>
<tr><td>260</td><td>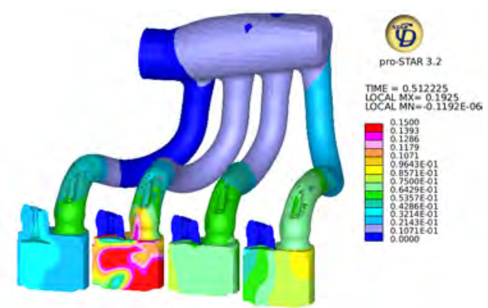
</td></tr>
</table>

Fig. 6.2 Time course of fuel concentration distribution - continued

<table>
<tr><td>280</td><td>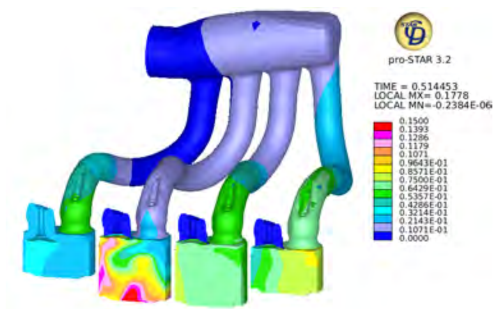
</td></tr>
<tr><td>300</td><td>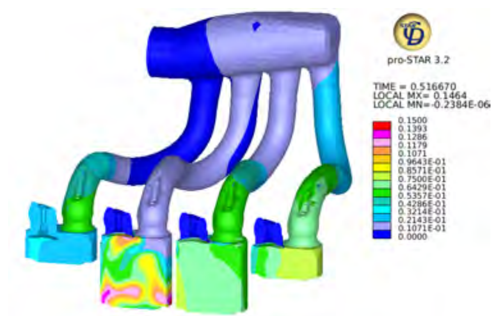
</td></tr>
<tr><td>320</td><td>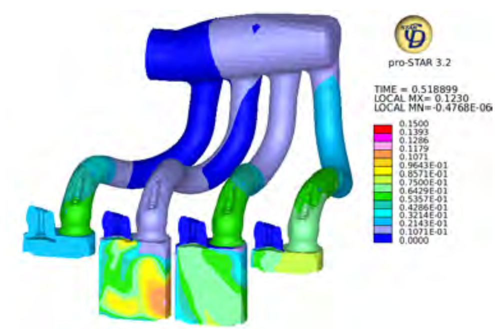
</td></tr>
<tr><td>340</td><td>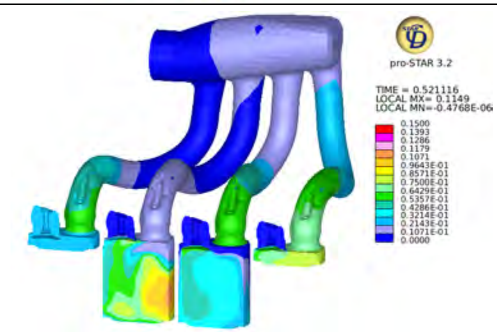
</td></tr>
</table>

Fig. 6.2 Time course of fuel concentration distribution - continued

360	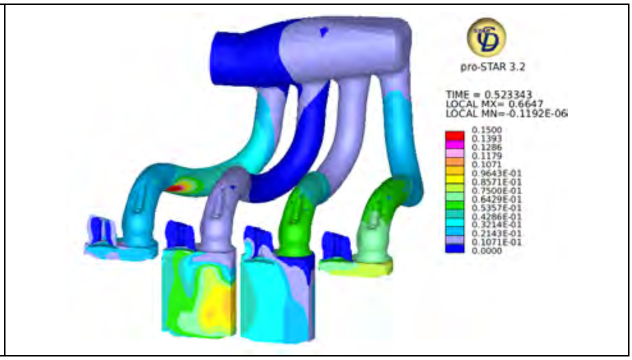

Fig. 6.2 Time course of fuel concentration distribution - continued

Figure 6.2 shows the fuel concentration in the model for the successive values of crankshaft rotation angle during fuelling at point $\boldsymbol{L_{w2}}$.

It can be noted that after starting the injection, in the case of the 0° angle which corresponds to the start of filling stroke of the 4th cylinder, the intake pipe is filled with an air-fuel mixture from the previous cycle. Due to the lack of combustion, the average concentration is about 3.2%. The opening of the intake valve which took place at 23º before TDC caused a backflow from the combustion chamber to the intake pipe both for an angle of 0º and 20º. At the same time, the still lasting injection in some areas enriched the mixture that moved in the pipe to reach its maximum of about 15%. At that time, the fuel concentration in the intake manifold increased to reach an average value of 1.8.

For an AC angle of 40°, the flow was reversed and the mixture entered the cylinder. The fuel injection continued and additionally enriched the mixture. The turbulence that occurred in the manifold (due to its shape) makes the inflowing fresh air mix with the mixture in the manifold. At the same time along the axis of the manifold, a small spin occurred that moved the mixture accumulated at the inlets into the inlet pipes. This rotational motion, however, was not as intense as clean air could continuously flow into the inlet pipes. For the angles between 60º and 180º CA, the diluted mixture of fresh air and air-fuel mixture that was pushed into the collective manifold during the initial backflow flew into the inlet pipe. At this time, after the injection of gas, i.e. an angle of 80° after TDC, a leaner air-fuel mixture flew into the cylinder and diluted the mixture already accumulated in the cylinder.

During the final stage of the filling stroke, i.e. after 180° OWK, there was a further backflow of the air-fuel mixture through the intake valve. Some amount of the fuel remained in the inlet pipe of the analyzed cylinder and the collective manifold, and then it entered the adjacent cylinders in the subsequent engine operation cycles. In some areas near the intake valve, the fuel concentration was around 6%. By contrast, its concentration in the collective manifold was about 1%. The distance between the injection nozzle and the combustion chamber (the design parameter of the gaseous injection system) significantly influences this phenomenon. Increasing this distance can increase the mass of the fuel remaining in the inlet pipe after the inlet valve closes.

The filling process of the 2nd cylinder looked alike. The backflow from the cylinder at the beginning of the injection helped significantly increase the amount of fuel in the collective manifold (difference between 180º and 200º CA). Definitely, the smallest amount of fuel was pushed into the collective manifold in the 1st cylinder. Simultaneously, due to the fact that this cylinder was the closest to the air inlet, fresh air and not a mixture, as it was for the other cylinders, flew into the inlet pipe during suction.

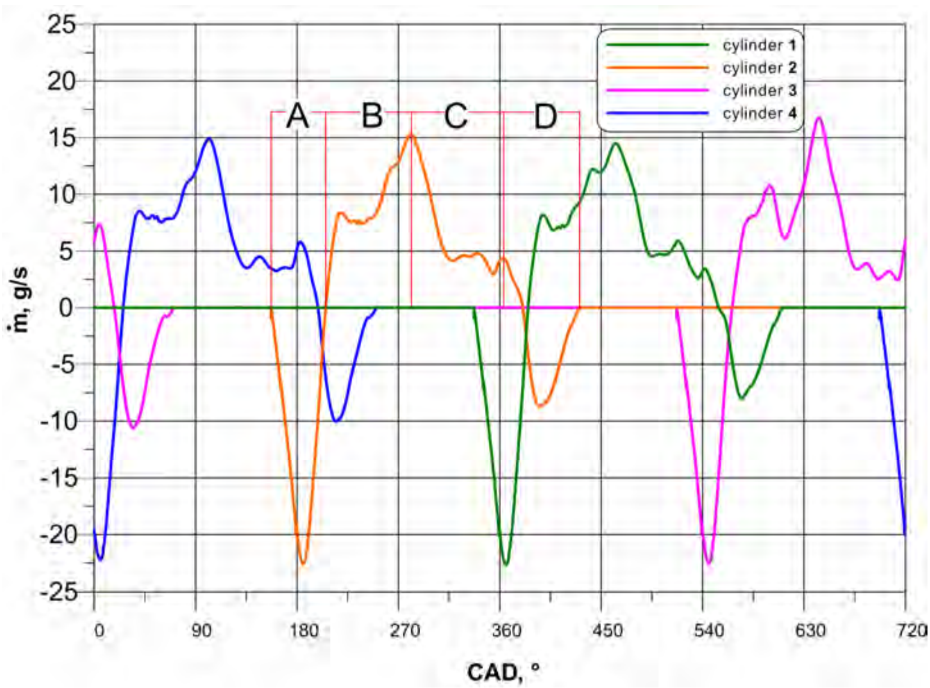

Fig. 6.3 Mass flow rate through the intake valves in each cylinder as a function of a crankshaft rotation angle

The mass flow rate through the intake valves in each cylinder during an operation cycle is given in figure 6.3. It was noted that in each case at the initial stage of the intake stroke, a return flow from the cylinder to the intake manifold (A) followed. It reaches -23 g/s and is similar for all the cylinders.

Next, the mass flow rate increased intensively up to about 8 g/s (B). This value was maintained for approximately 30 degrees of crankshaft rotation. Then, due to wave phenomena in the intake manifold and the movement of the piston, the mass flow reached its maximum value, though not the same for each cylinder. Its highest value (17 g/s) was for the 3rd and 4th cylinder, while the lowest one (14 g/s) was for the 1st cylinder.

In the next phase (C), the mass flow rate decreased and its value set at about 4 g/s through about 45 ° CA. For each cylinder, however, the mass flow was different. This was caused by the wave phenomenon in the intake pipes. As a result, the greatest amount of the mixture flew out of the 3rd and 4th cylinder and the smallest from the 1st one.

Then, because the piston was moving up and the intake valve was opened, there was another backflow from the cylinder (D). The value of mass flow rate in this case was -10 g/s on average for all the cylinders and was more than twice less than the backflow at the beginning of the intake stroke. The mass flow rates at this stage were different for the subsequent cylinders. The highest value was noted for the 3rd cylinder (-11 g/s), while the lowest one was -8 g/s for the 1st cylinder.

6.4.2 Fuel distribution in the combustion chamber

The following figures show the fuel distribution in the combustion chambers for subsequent options of mounting the nozzles L_w. Two representative cylinder sections were selected (fig. 6.4). The results refer to the fuel concentration at the moment of ignition, i.e. 20 degrees of crankshaft rotation before TDC. Next, the following were shown: a fuel weight change, an average fuel concentration change and a change in the fuel concentration in the combustion chamber at the spark plug as a function of the crankshaft rotation angle.

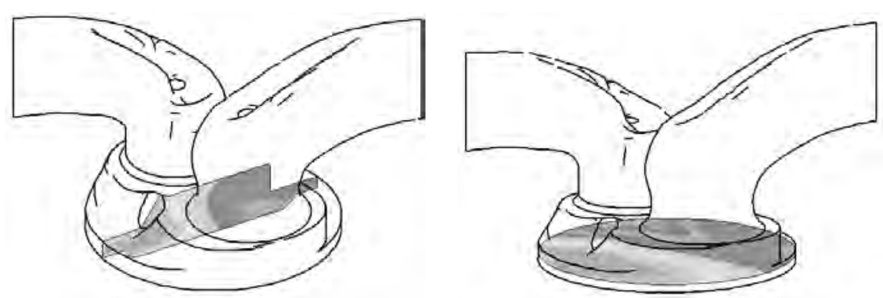

a) b)

Fig. 6.4 Examined sections of the combustion chamber: section I - longitudinal, b) section II – cross

Figures 6.5-6.28 illustrate the simulation results for the subsequent cylinders according to the numbering adopted in Chapter 4 (fig. 4.8).

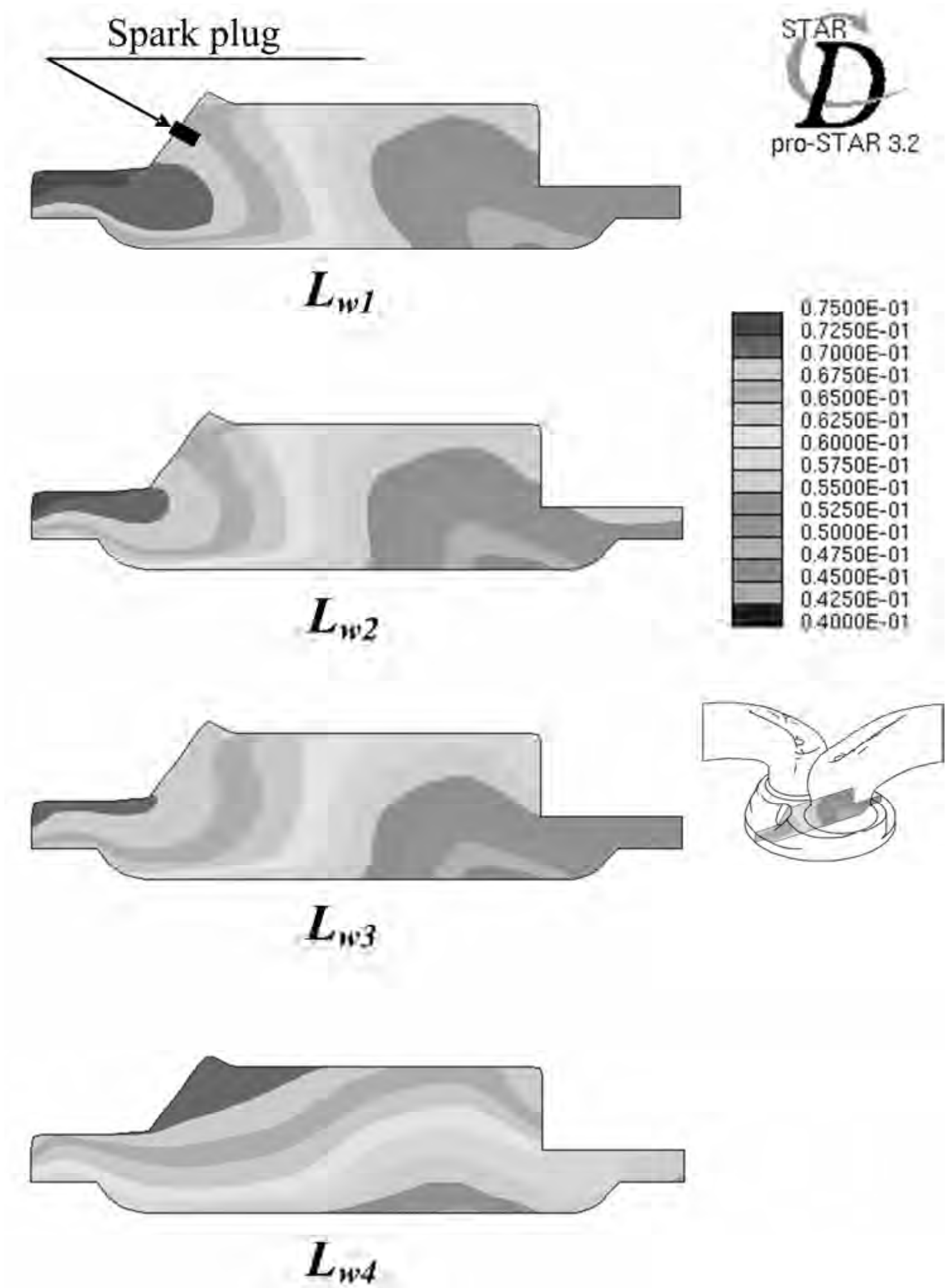

Fig. 6.5 The fuel distribution in the 1st cylinder in section I for the variants of nozzle installation.

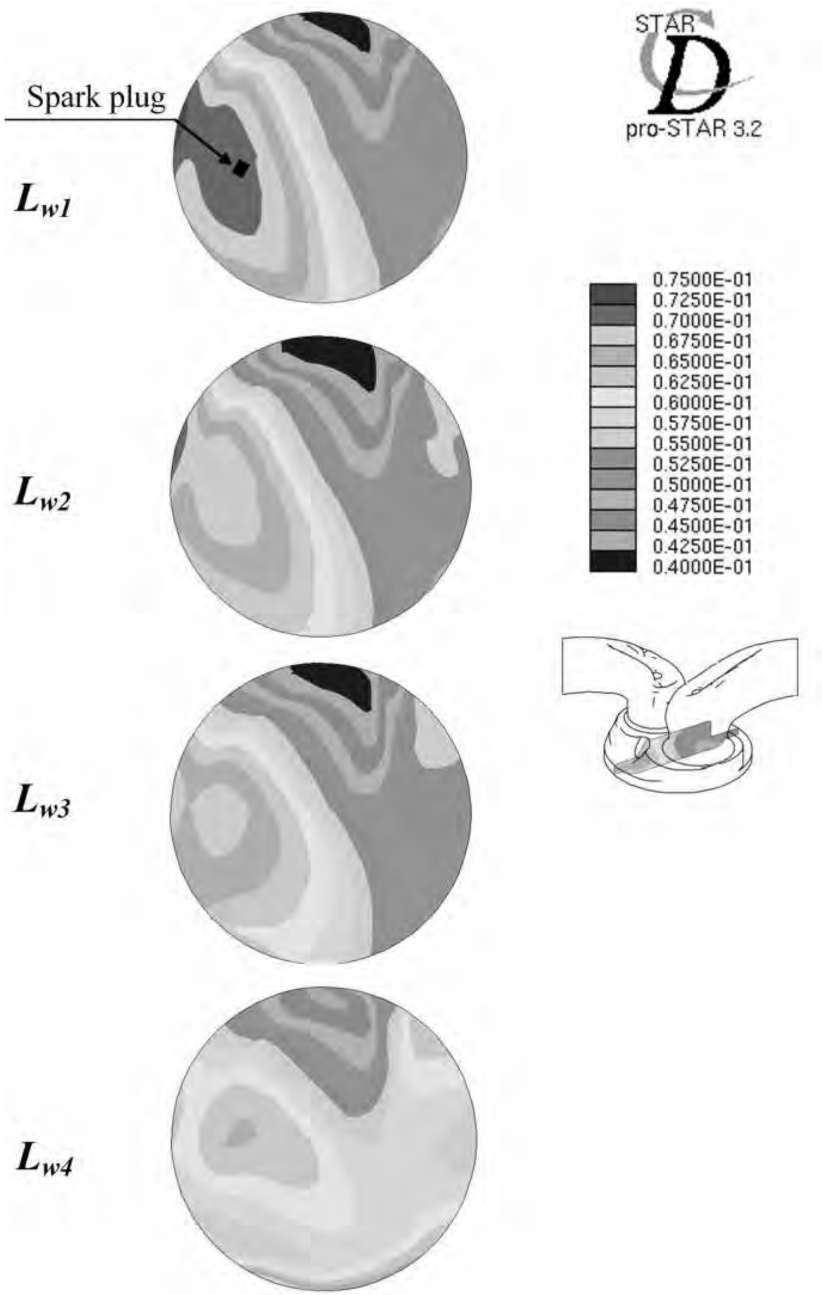

Fig. 6.6 The fuel distribution in the 1st cylinder in section II for the variants of nozzle installation

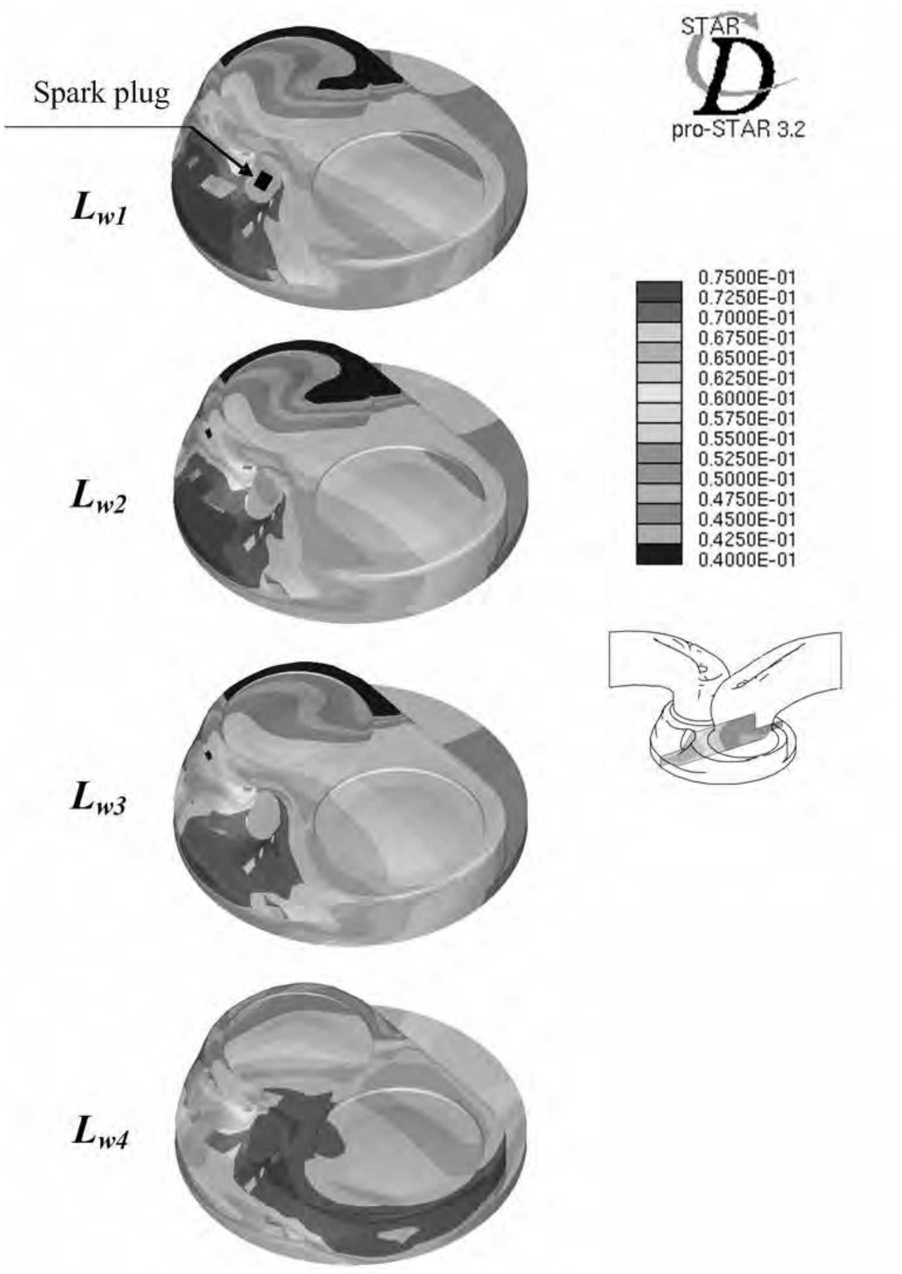

Fig. 6.7 The fuel distribution in the 1st cylinder for the variants of nozzle installation

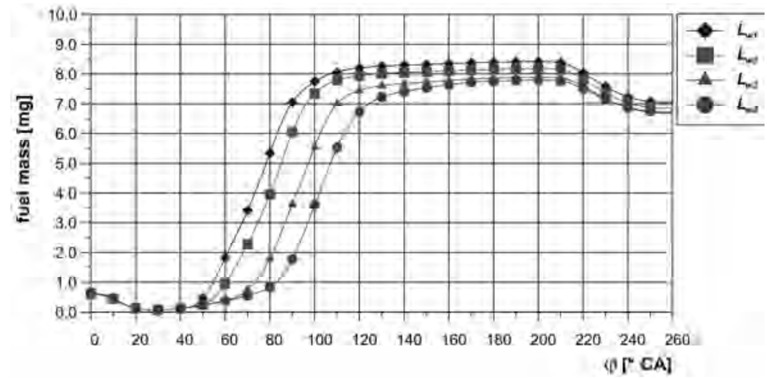

Fig. 6.8 Fuel mass in the 1st cylinder as a function of the crankshaft rotation angle for the subsequent distances of the injection nozzles from the inlet valve axis

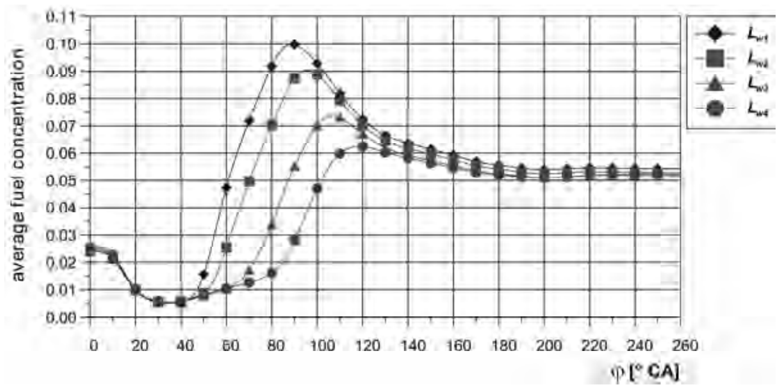

Fig. 6.9 Average fuel concentration in the 1st cylinder as a function of the crankshaft rotation angle for the subsequent distances of the injection nozzles from the inlet valve axis

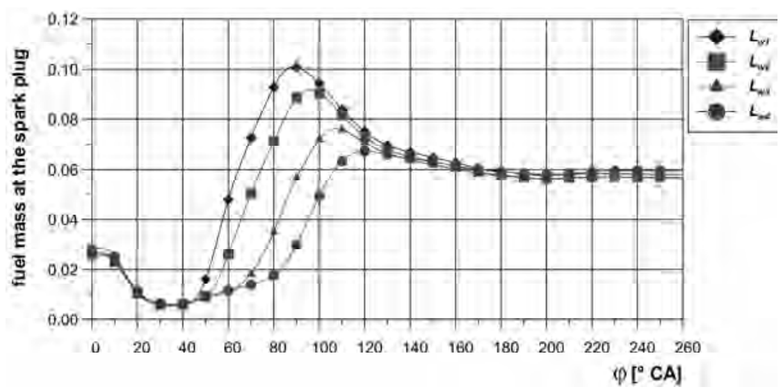

Fig. 6.10 Fuel mass at the ignition plug in the 1st cylinder as a function of the crankshaft rotation angle for the subsequent distances of the injection nozzles from the inlet valve axis

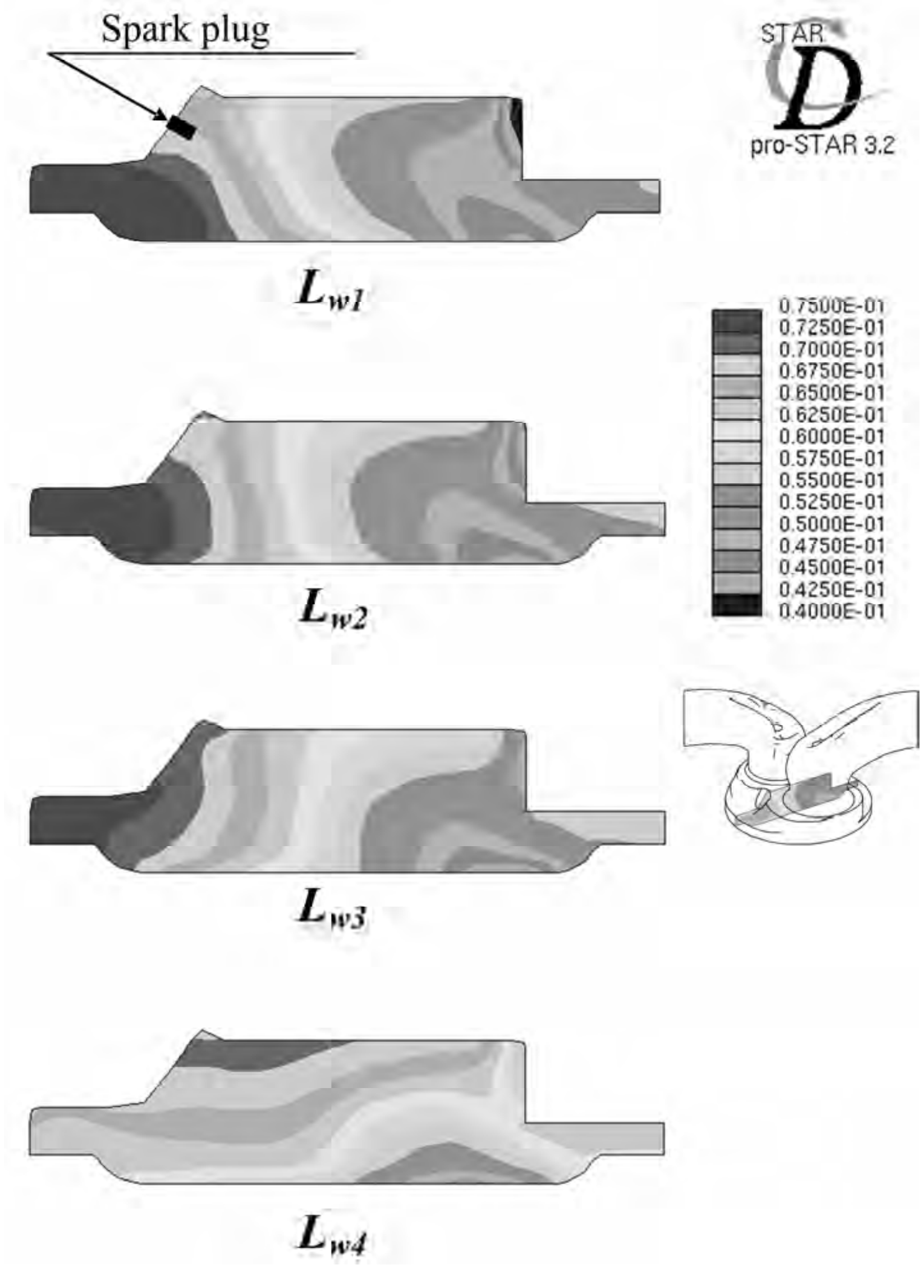

Fig. 6.11 The fuel distribution in the 2nd cylinder in section I the variants of nozzle installation

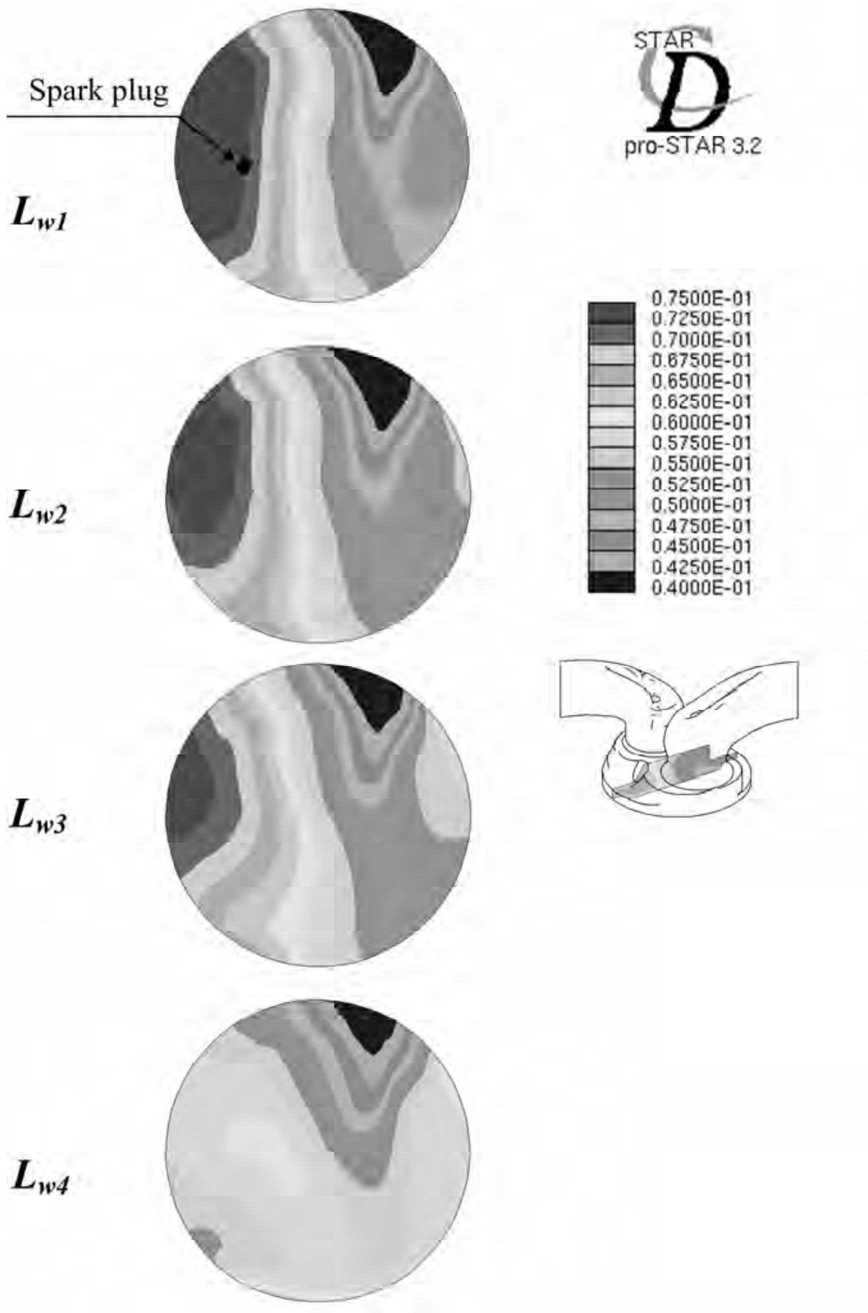

Fig. 6.12 The fuel distribution in the 2nd cylinder in section II for the variants of nozzle installation

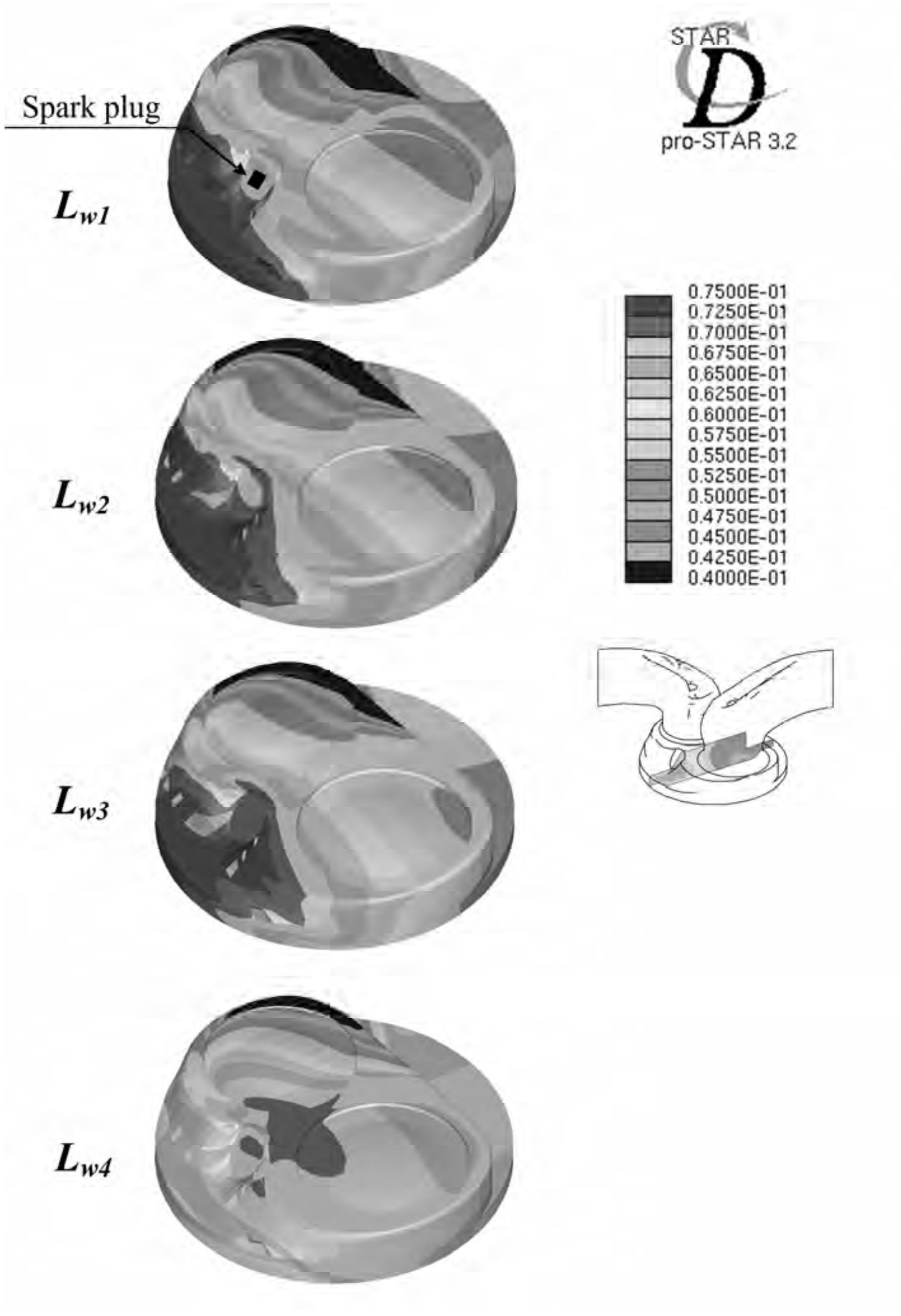

Fig. 6.13 The fuel distribution in the 2nd cylinder the variants of nozzle installation

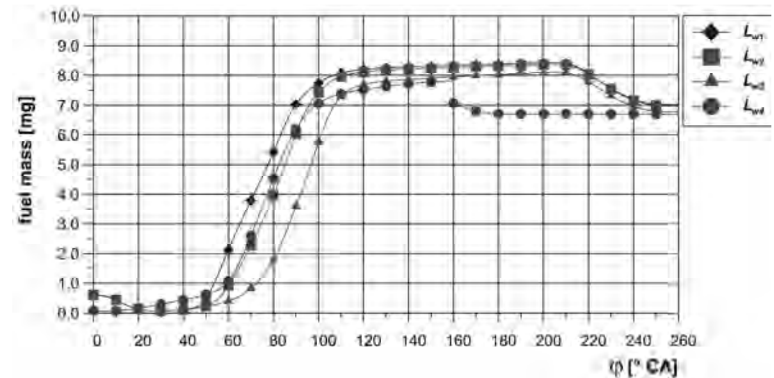

Fig. 6.14 Fuel mass in the 2nd cylinder as a function of the crankshaft rotation angle for the subsequent distances of the injection nozzles from the inlet valve axis

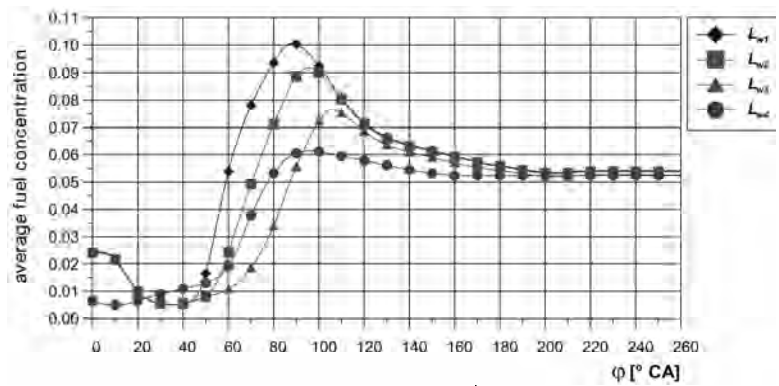

Fig. 6.15 Average fuel concentration in the 2nd cylinder as a function of the crankshaft rotation angle for the subsequent distances of the injection nozzles from the inlet valve axis

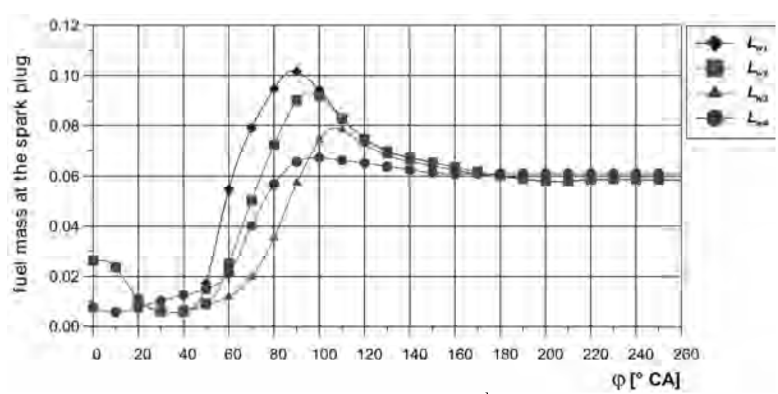

Fig. 6.16 Fuel mass at the ignition plug in the 2nd cylinder as a function of the crankshaft rotation angle for the subsequent distances of the injection nozzles from the inlet valve axis

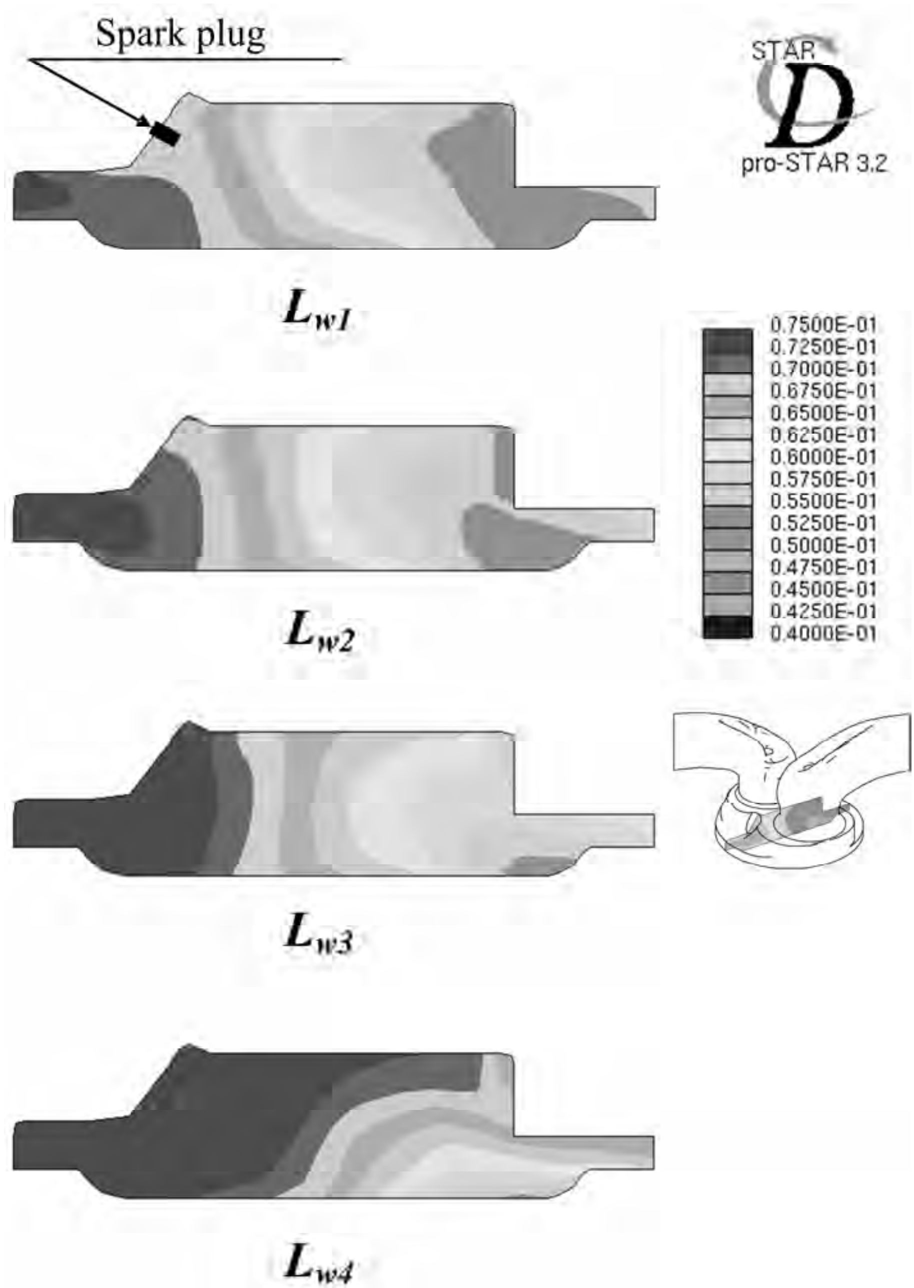

Fig. 6.17 The fuel distribution in the 3rd cylinder in section I for the variants of nozzle installation

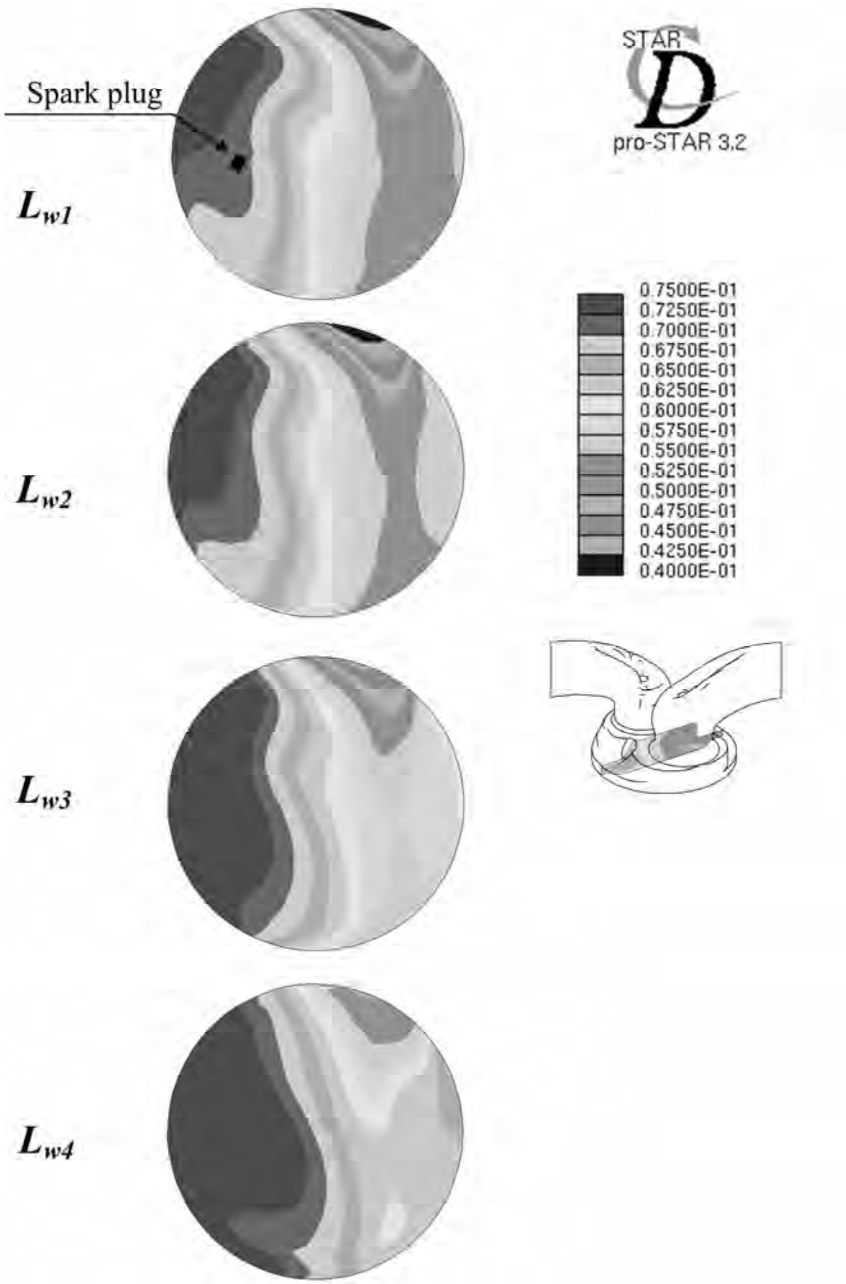

Fig. 6.18 The fuel distribution in the 3rd cylinder in section II for the variants of nozzle installation

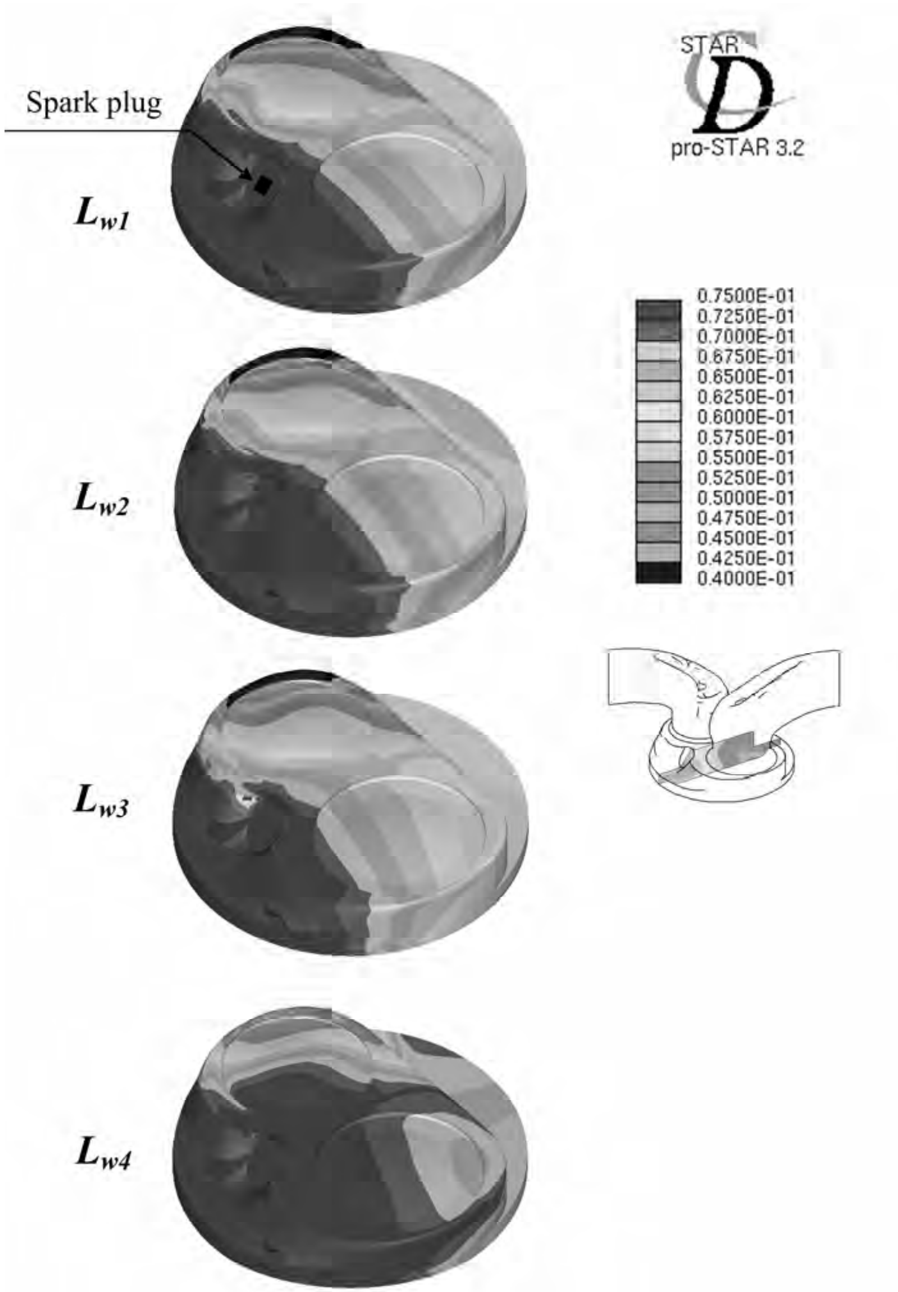

Fig. 6.19 The fuel distribution in the 3rd cylinder for the variants of nozzle installation

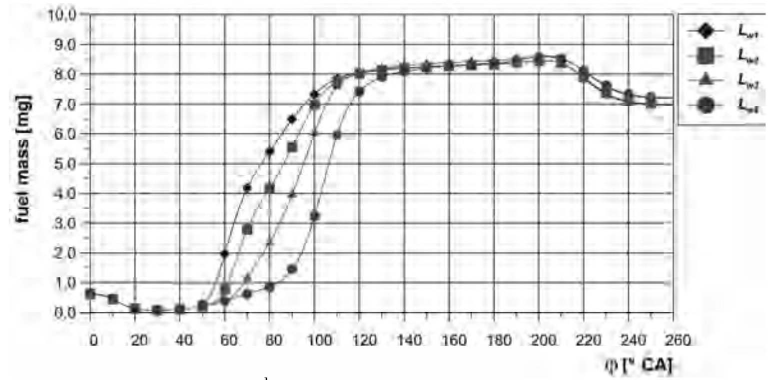

Fig. 6.20 Fuel mass in the 3rd cylinder as a function of the crankshaft rotation angle for the subsequent distances of the injection nozzles from the inlet valve axis

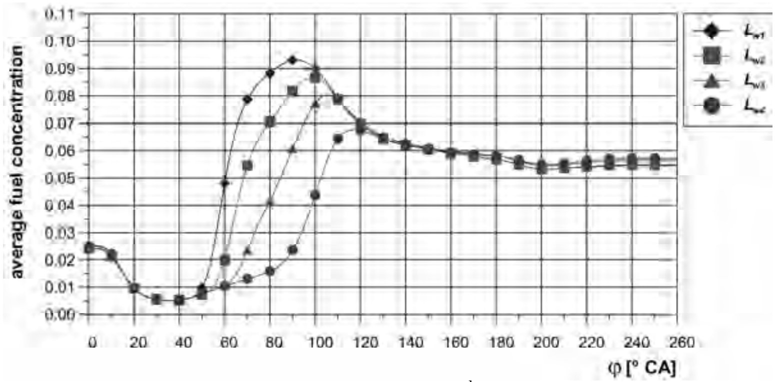

Fig. 6.21 Average fuel concentration in the 3rd cylinder as a function of the crankshaft rotation angle for the subsequent distances of the injection nozzles from the inlet valve axis

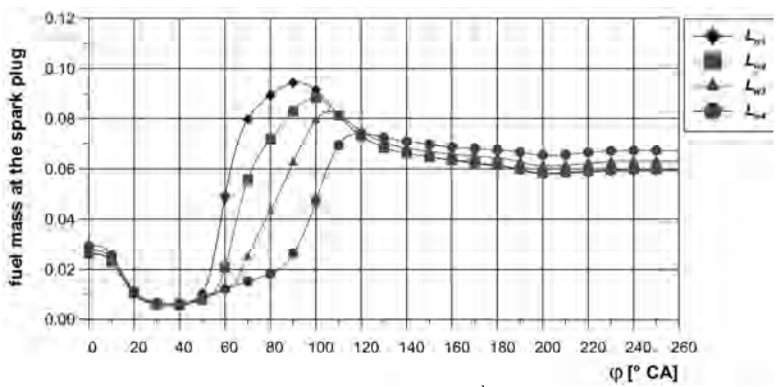

Fig. 6.22 Fuel mass at the ignition plug in the 3rd cylinder as a function of the crankshaft rotation angle for the subsequent distances of the injection nozzles from the inlet valve axis

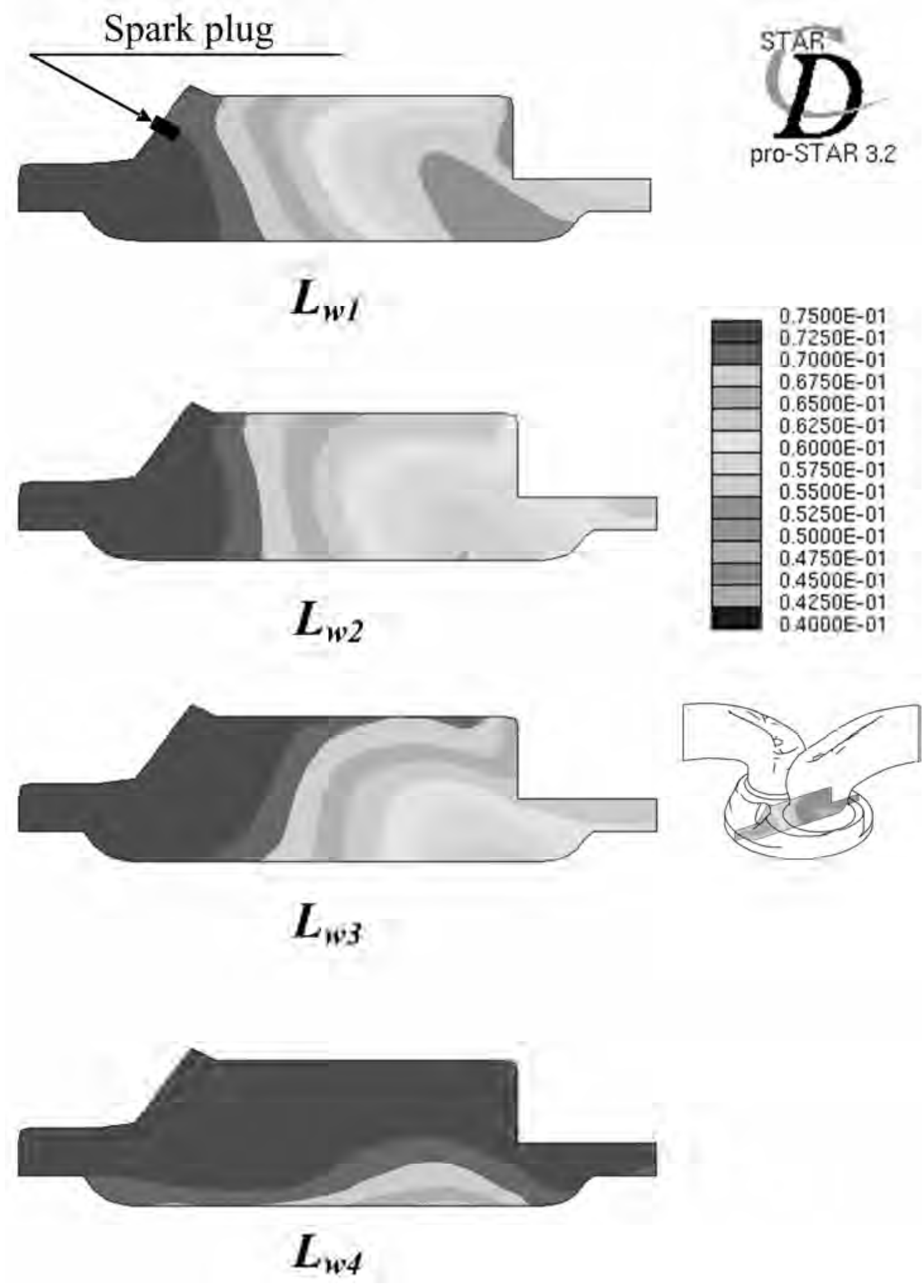

Fig. 6.23 The fuel distribution in the 4th cylinder in section I for the variants of nozzle installation

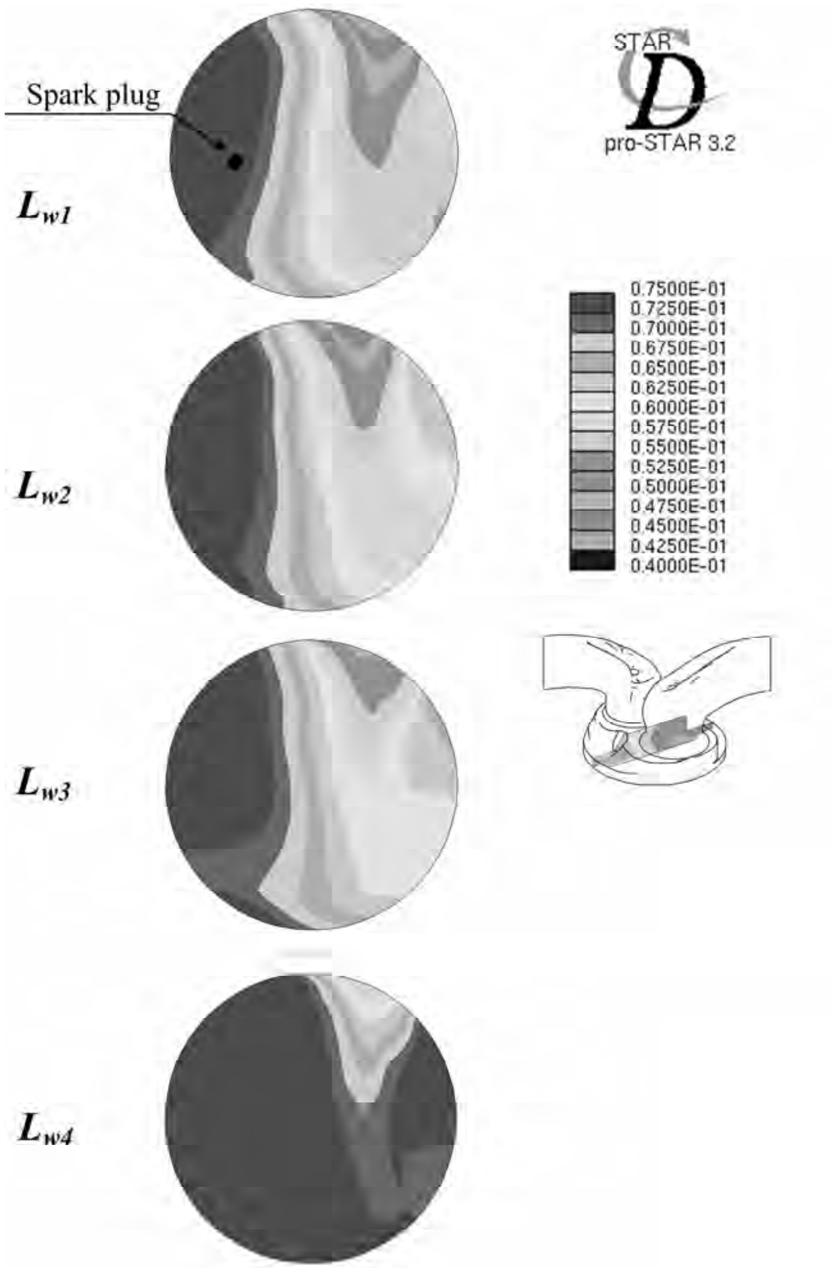

Fig. 6.24 The fuel distribution in the 4th cylinder in section II for the variants of nozzle installation

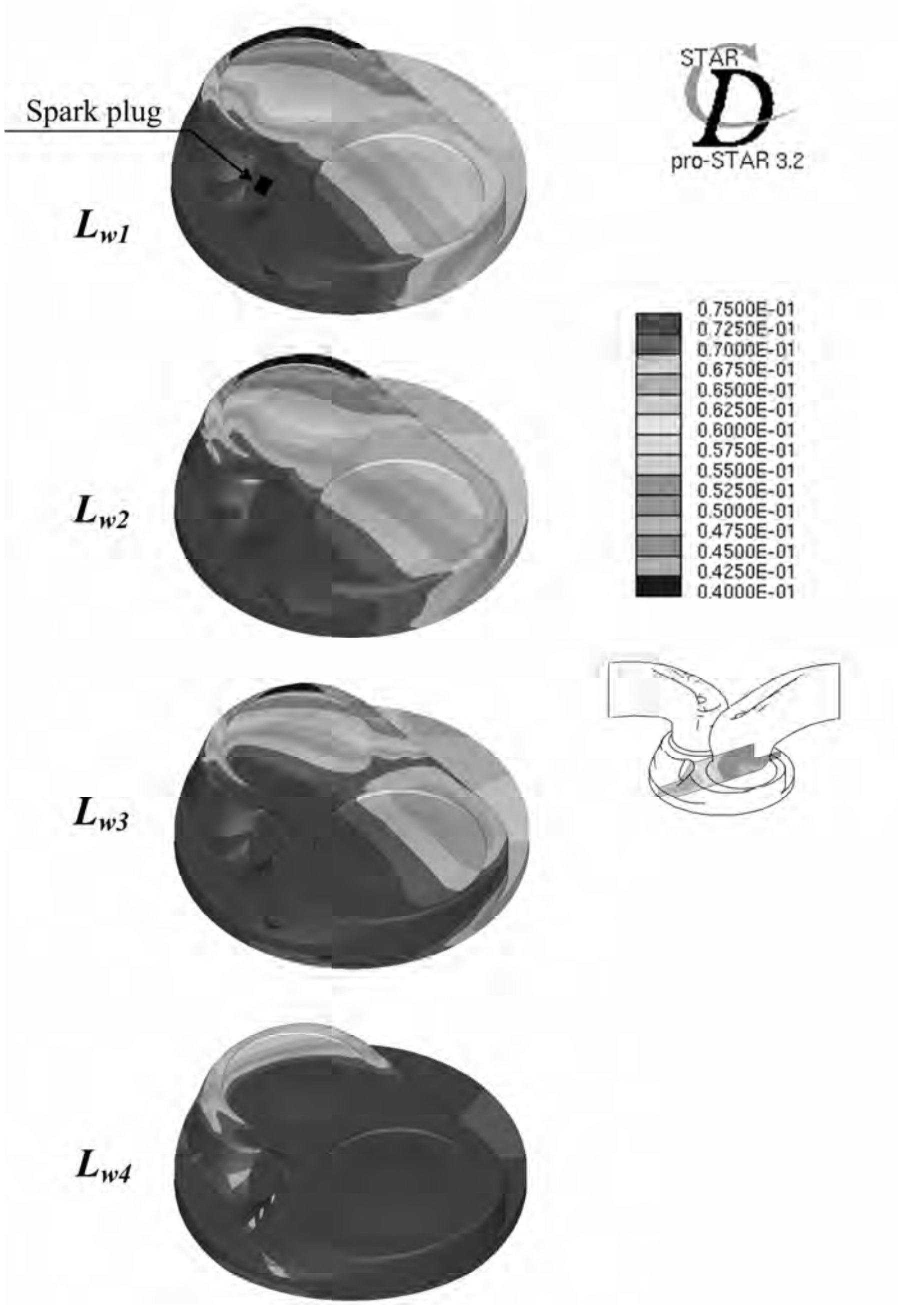

Fig. 6.25 The fuel distribution in the 4th cylinder for the variants of nozzle installation

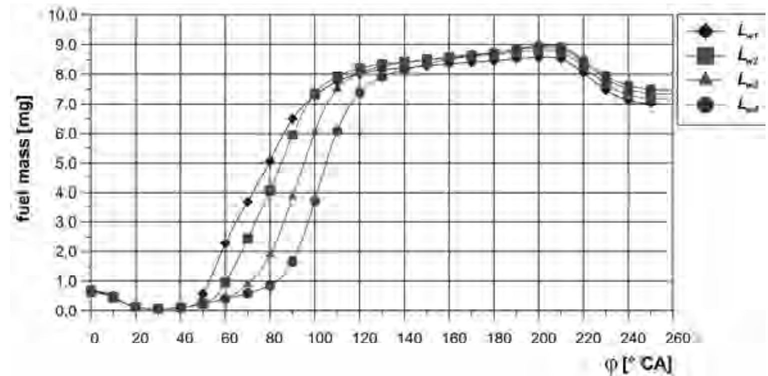

Fig. 6.26 Fuel mass in the 4th cylinder as a function of the crankshaft rotation angle for the subsequent distances of the injection nozzles from the inlet valve axis

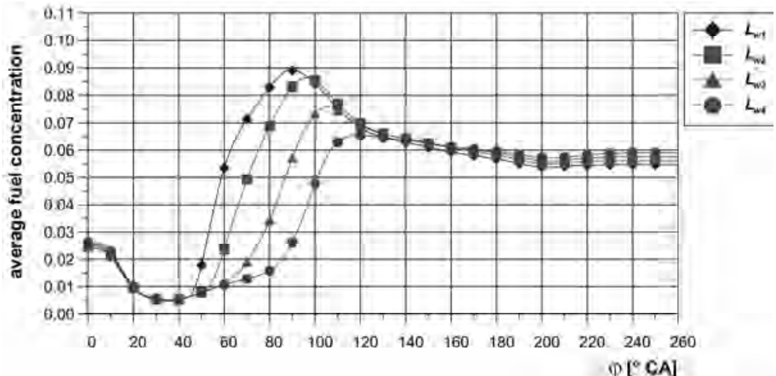

Fig. 6.27 Average fuel concentration in the 4th cylinder as a function of the crankshaft rotation angle for the subsequent distances of the injection nozzles from the inlet valve axis

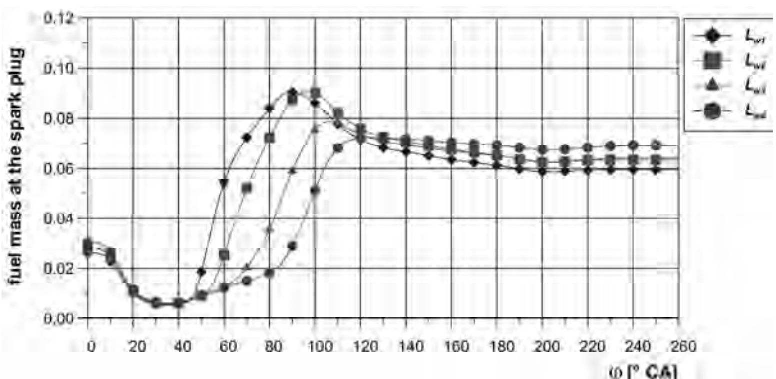

Fig. 6.28 Fuel mass at the ignition plug in the 4th cylinder as a function of the crankshaft rotation angle for the subsequent distances of the injection nozzles from the inlet valve axis

6.5 Analysis

6.5.1 Homogenization of the air-mixture in the cylinder

Figures 6.30 and 6.31 show the average fuel concentration and the discrepancy between its maximum and minimum local concentration in each cylinder at the moment of ignition (20^o before TDC of a compression stroke). The charts below show the subsequent cylinders for the four distances.

If the distance of the injection nozzle from the inlet valve axis in the first cylinder increased, the average fuel concentration in the combustion chamber decreased. Comparing the value obtained for the distance $\boldsymbol{L_{w1}}$, this decline was 0.0014, 0.0028 and 0.0033 for the distances $\boldsymbol{L_{w2}}$, $\boldsymbol{L_{w3}}$ and $\boldsymbol{L_{w4}}$, respectively.

A similar trend occurs in the second cylinder. However, the differences are smaller and the average concentration is less by 0.002 for $\boldsymbol{L_{w4}}$ as compared to $\boldsymbol{L_{w1}}$.

Based on the analysis of the change in the average fuel concentration in the 3rd and 4th cylinder because of the changed distance, a reverse situation in the 1st and 2nd cylinder can be noted. The more distant the injection nozzle was from the axis of the inlet valve, the higher the average concentration was. Examining the extreme cases ($\boldsymbol{L_{w1}}$ and $\boldsymbol{L_{w4}}$), the concentration values in the 3rd cylinder increased by 0.0024 and in the 4th cylinder by 0.0047.

Table 6.1 and figure 6.31 present the diversity of the fuel distribution in the combustion chambers (the discrepancy between the maximum and minimum local concentration). It can be noted for each cylinder tested that the distance between the injection nozzle and the intake valve axis enhanced the air-fuel mixture homogenization. The smallest difference, i.e. 0.02683, was noted in the 4th cylinder and the distance $\boldsymbol{L_{w4}}$; whereas the largest, i.e. 0.05359 in the 3rd cylinder and the distance $\boldsymbol{L_{w2}}$, which is evident in the fuel distribution in the cylinders in figures 6.5-6.27. In sections I and II and in the entire volume of the combustion chamber, the air-fuel mixture became homogeneous thanks to the distance between the injection nozzle and the intake valve axis.

This fact was also confirmed by figure 6.29 with a mapping of the velocity vectors at the end of the 3rd cylinder filling stroke. The fuel that was flowing through the manifold mixed additionally with air because of the movement around the intake pipe axis.

It can be concluded that the distance of the injection nozzle from the symmetry axis of the intake valve improves the air-fuel mixture homogenization in each cylinder.

Fig. 6.29 Mapping of the flow velocity vectors during the 3rd cylinder filling

Tab. 6.1 The average fuel concentration in the cylinders

	Cylinder 1	**Cylinder 2**	**Cylinder 3**	**Cylinder 4**
$\boldsymbol{L_{w1}}$	0,0545	0,0543	0,0544	0,0547
$\boldsymbol{L_{w2}}$	0,0531	0,0539	0,0548	0,0566
$\boldsymbol{L_{w3}}$	0,0517	0,0526	0,0562	0,0578
$\boldsymbol{L_{w4}}$	0,0512	0,0523	0,0568	0,0594

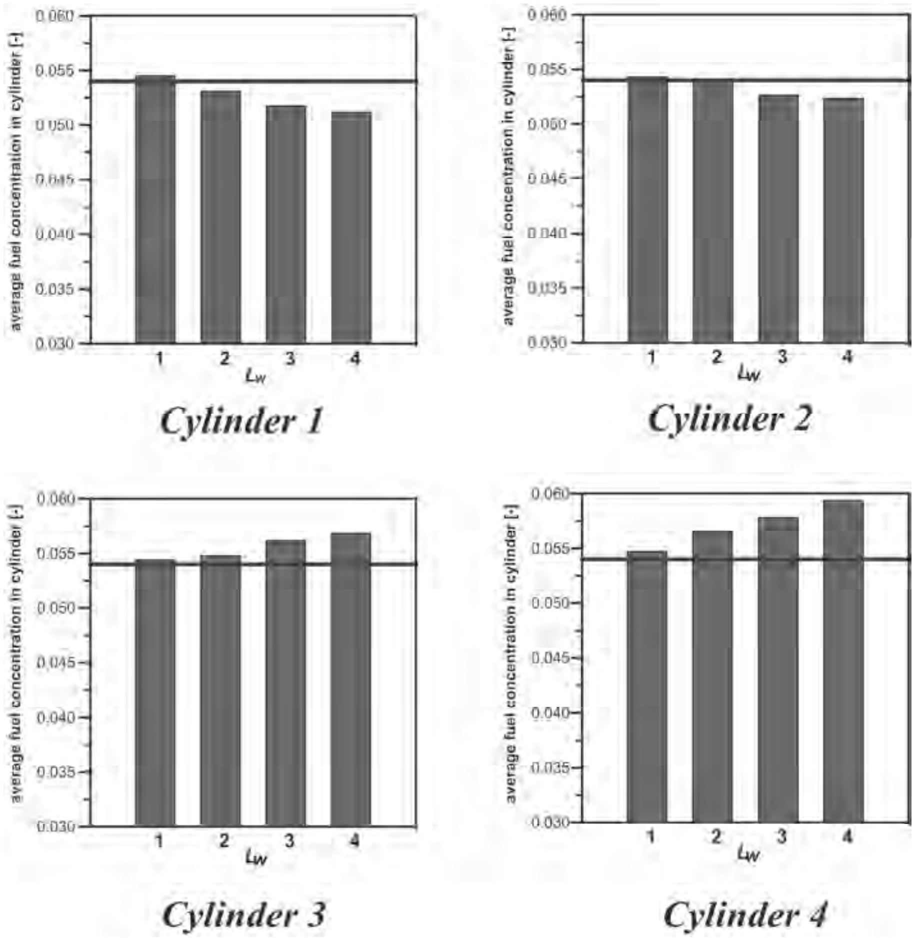

Fig. 6.30 Average fuel concentration in each cylinder for the tested distances L_w

Tab. 6.2 Differences of the fuel concentrations in the cylinders

	Cylinder 1	**Cylinder 2**	**Cylinder 3**	**Cylinder 4**
L_{w1}	0,04549	0,05214	0,05284	0,04457
L_{w2}	0,04768	0,05313	0,05359	0,04905
L_{w3}	0,04037	0,04656	0,05359	0,04343
L_{w4}	0,03119	0,03390	0,04516	0,02683

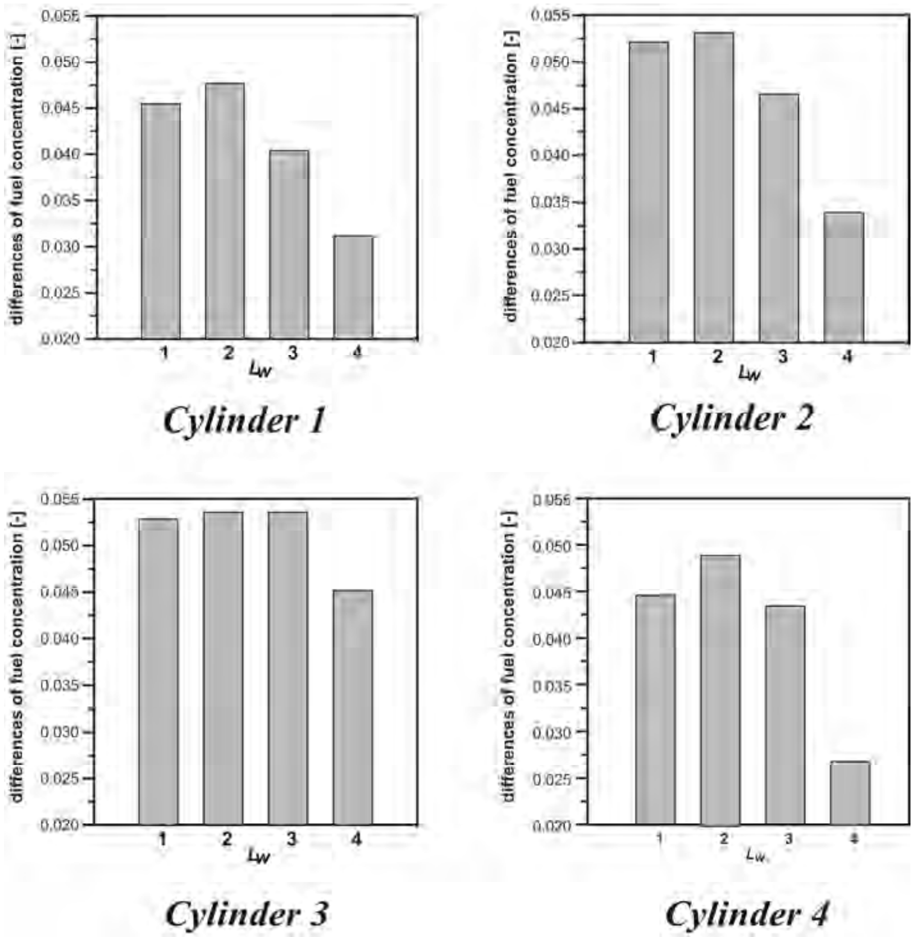

Fig. 6.31 Differences between the maximum and minimum local fuel concentration in each cylinder at ignition

6.5.2 Uneven fuel distribution for the individual

The analysis of the impact of the distance between the injection nozzle and the symmetry axis of the intake valve was demonstrated the dispersion of fuel between the cylinders.

Figures 6.32 and 6.33 and table 6.4 present the varied fuel mass in the cylinders according to the distances $\boldsymbol{L_w}$ for each cylinder. For the distance $\boldsymbol{L_{w1}}$, the unevenness of fuel distribution was the smallest. In this case, the 1st cylinder was supplied with the largest fuel mass - 7.084 mg and the uneven distribution (the difference between the maximum and minimum fuel mass in the cylinders) was 0.135 mg. Thus, it can be concluded that even in the case of a short $\boldsymbol{L_w}$ distance, the fuel is exchanged between the inlet pipes of particular cylinders when the engine operates at low speed and low load. As $\boldsymbol{L_w}$ increases, this phenomenon becomes more evident.

Figure 6.32 presents the varied fuel mass in relation to the average value of 7 mg. Starting from the distance $\boldsymbol{L_w}$, fuel dispersion is more intensive and the trend noted for the distance $\boldsymbol{L_{w1}}$ is reversed. The greatest discrepancies in fuel mass were noted between the 1st and 4th cylinder. These values are summarized in table 6.3.

Tab. 6.3 Uneven fuel distribution

Distance	Differences in fuel mass between the 1st and 4th cylinder
$\boldsymbol{L_{w1}}$	0,135 mg
$\boldsymbol{L_{w2}}$	0,334 mg
$\boldsymbol{L_{w3}}$	0,667 mg
$\boldsymbol{L_{w4}}$	0,880 mg

The phenomenon was caused by fuel exchange in the manifold between the inlet pipes in the individual cylinders. More fuel mass was supplied into the 3rd and 4th cylinder at the expense of the 1st and 2nd cylinder.

The intensity of backflows from the cylinder, which was given in figures 6.2 and 6.3, made the fuel injected to the collective manifold flow, especially when the injection nozzle was distant from the inlet valve. The design of the asymmetric intake manifold was also important. The air-fuel mixture was enriched in the cylinders mounted away from the fresh air inlet. The fuel concentration in the intake manifold, as shown in figure 6.2, reached locally higher values in the area adjacent to the inlet pipe of the 3rd and 4th cylinder.

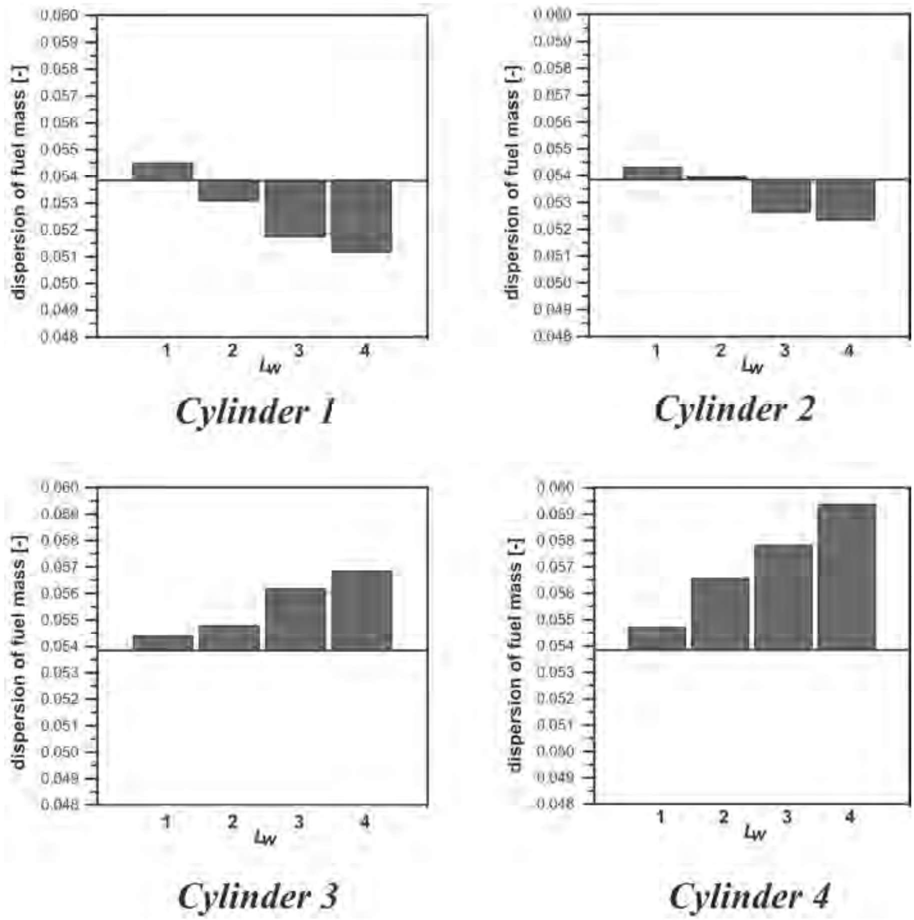

Fig. 6.32 The dispersion of fuel between the cylinders for the subsequent distances L_w

Tab. 6.4 Fuel mass in the cylinders in mg

	Cylinder 1	Cylinder 2	Cylinder 3	Cylinder 4
L_{w1}	7,084	7,005	6,963	6,949
L_{w2}	6,848	6,957	7,012	7,182
L_{w3}	6,676	6,790	7,191	7,343
L_{w4}	6,601	6,700	7,217	7,481

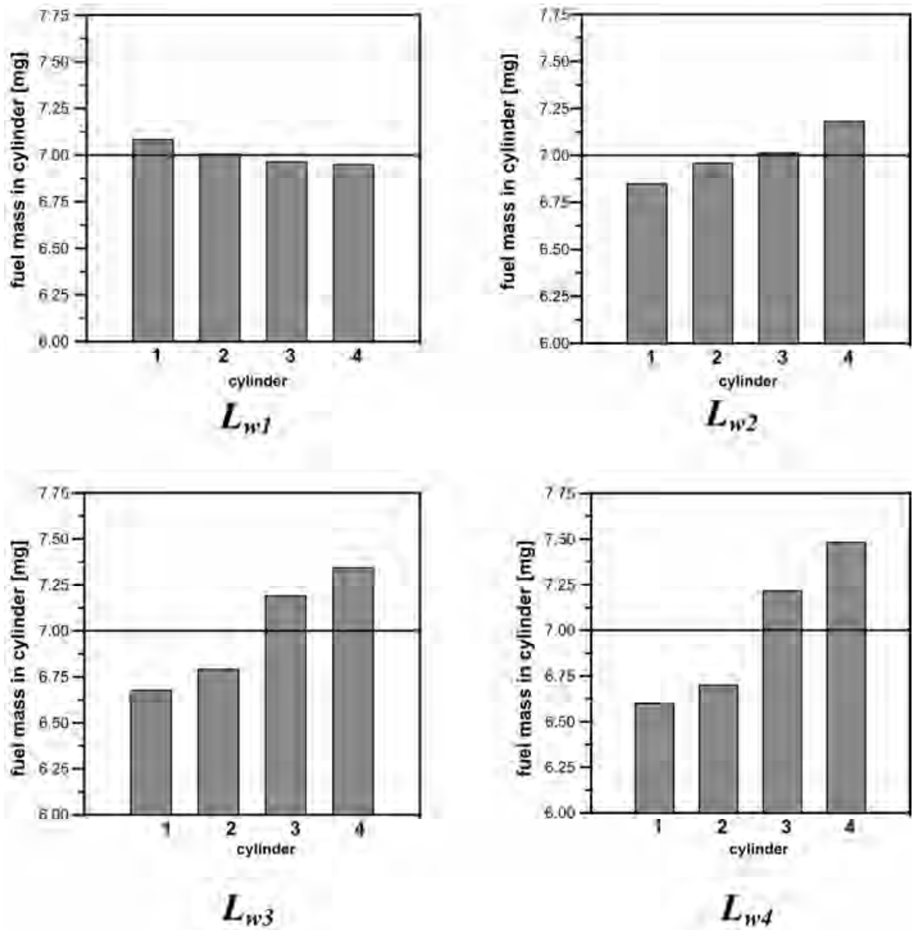

Fig. 6.33. Fuel mass in each cylinder for the tested distances of the nozzles

References

[1] AEGPL Europe: *Strategy to reduce CO_2 emissions from cars***,** AEGPL response to Commission's consultation, Reducing CO_2 from passenger cars and light-commercial vehicles, Final Report, Brussels, 2007.

[2] Almkvist G., Denbratt I., Josefsson G., Magnusson I.*: Measurement of fuel film thickness in the inlet port of an SI engine by laser induced fluorescenc*e. SAE Technical Paper nr 952483, 1995.

[3] Andrews M., Bracco F.: *Use of intake and exhaust measurements with computer simulation to investigate the evolution of the internal flow in a ported engine*. SAE Technical Paper nr 910262, 1991.

[4] Bahram K., Haworth D., Hubler.: *Multidimensional Port and In-Cylinder visualization Flow Calculations and Flow Vision Study in an Internal Combustion Engine with Different Intake Configurations*. SAE Technical Paper nr 941871, 1994.

[5] Balluchit L., Benvenutitj A., Di Benedettot M. D., Cardellinot S., Rossis C., Sangiovanni-Vincentellitti A.: *Hybrid Control of the Air-fuel ratio in Force Transients for Multi-point Injection Engines*, Proceedings of the 38th Conference on Decision & Control Phoenix, Arizona USA, 1999.

[6] Barański G., Wendeker M., Czarnigowski J., Jakliński P., Pietrykowski K., Grabowski Ł., Rola M.: *Simulation test of mixture formation in sequential CNG gas injection of SI engine*. Silniki Spalinowe 2007-SC2, 2007, str 25-34.

[7] Bass E., Bailey B., Jaeger S.: *LPG Conversion and HC Emission Specification of Light –Duty Vehicle*. SAE Technical Paper nr 932447, 1993.

[8] Bedford F., Hu X., Schmidt U.: *In-cylinder combustion modeling and validation using Fluent*. 14th Annual International Multidimensional Engine Modeling User's Group Meeting, Detroit, 2004.

[9] Begg S.M., Hindle M.P., Cowell T., Heikal M.R.: *Low intake valve lift in a port fuel-injected engine*. Energy, February 2008, str 1-9.

[10] Bielaczyc P., Szczotka A., Brodzinski H.: *Analysis of the exhaust emissions from vehicles fuelled with petrol or LPG and CNG alternatively*. Journal of Kones. Combustion Engines, Vol. B, No 1-2, 2001, str. 363-369.

[11] Blair G. P.: *Design and Simulation of Four-Stroke Engine*. SAE Order No. R-186, 1999.

[12] Bocheński C., Bocheńska A.: *Ocena zasobów ropy naftowej i perspektywy jej substytucji biopaliwami*. MOTROL, 2008, 10, str. 23–30.

[13] Cambell S., Clasen E., Chang C., Rhee K. T.: *Flames and liquid fuel in an SI engine cylinder during cold start*.

SAE Technical Papers nr 9611153, 1996.

[14] Ceviz M.A., Yuksel F.: *Cyclic variations on LPG and gasoline-fuelled lean burn SI engine*. Renewable Energy 31, str. 1950–1960, 2006.Costanzo V., Heywood J.: *Mixture preparation mechanisms in a port fuel injected engine*. SAE Technical Paper nr 2005-01-2080, 2005.

[15] Das S., Chmiel D.: *Computational and Experimental Study of In-Cylinder Flow in a Direct Injection Gasoline (DIG) Engine*. 11th International Multidimensional Engine modeling User's Group Meeting Agenda, Detroit, USA, March 2001.

[16] Deur J. M., Jonnawthuta S.: *The Combination of Detailed Kinetics and CFD in Automotive Applications*. Eleventh International Engine Combustion Multi-Dimensional Modeling Conference, Detroit, 2001.

[17] Dębowski S.: *Biuletyn specjalny Globtrex.com*. 18.06.2009.

[18] Dutczak J., Golec K., Papuga T.: *Niektóre problemy związane z wtryskowym zasilaniem silników ciekłym propanem-butanem*. Mat. VI Międzynarodowej Konf. Naukowej Silniki Gazowe 2003, Wydawnictwo Politechniki Częstochowskiej, Częstochowa 2003.

[19] Fijałkowski S., Nakonieczny K., Tarkowski P.: *Wstępna analiza egzergetyczna układu dolotowego wysokoprężnego silnika turbodoładowanego*, Konstrukcja, badania, eksploatacja, technologia pojazdów samochodowych i silników spalinowych. Teka Komisji Naukowo-Problemowej Motoryzacji PAN, 1997, z. 10, s. 61-72.

[20] Fontana G., Galloni E., Palmaccio R., Strazzullo L. Vittorioso G.: *Development of a New Intake System for a Small Spark-Ignition Engine. Modeling the Flow Through the Inlet Valve*. SAE Technical Paper nr 2003-01-0369, 2003.

[21] Ganesan V., Kale S. C.: *A Study of Steady Flow Through a SI Engine Intake System using CFD*. Journal of Institution of Engineers, India Vol 86, str. 61-65, July 2005.

[22] Go P., Zellat M.: *Simulation of Flow Field Generated by Intake Port, Valve and Cylinder Configurations and Comparison with Measurements and Applications*. SAE Technical Paper nr 940521, 1994.

[23] Gold M., Arcoumanis C., Whitelaw J., Gaade J., Wallace S.: *Mixture preparation strategies in an optical four-valve port-injected gasoline engine*. Int. J. Engine Research 2000, 1(1), str. 41–56.

[24] Grasso F.: *Three-dimensional model for spark ignition engine initial validation*. Meccanica 17 (1982), 201-210.

[25] Hacohen J., Belmont MR., Thurley R., Thomas J., Morris E., Buckingham D.: *Experimental and theoretical analysis of flame development and misfire phenomena in a spark-ignition engine*. SAE Technical Paper nr 920412, 1992.

[26] Hawryluk B.*: Stochastyczny model samochodowego silnika benzynowego w aspekcie stechiometrycznego składu mieszanki paliwowo-powietrznej*. Rozprawa doktorska, Politechnika Lubelska, 2001.

[27] Hentschel W., Block B., Hovestadt T., Meyer H., Ohmstede G., Richter V., Stiebels B., Winkler A.: *Optical Diagnostics and CFD-Simulations to Support the Combustion Process Development of the Volkswagen FSI Direct-Injection Gasoline Engine*. SAE Technical Paper nr 2001-01-3648, 2001.

[28] Heywood JB. *Internal combustion engine fundamentals*. McGraw-Hill International Editions, ISBN 0-07-100499-8; 1988.

[29] Hiroshi I., Masaaki J., Kunihumi S., Hatsuo N.: *An Analysis of Induction Port Fuel Behavior*. SAE Technical Paper nr 912348, 1991, Str. 1777-1786.

[30] Hollnagel C., Borges L.H., Muraro W.: *Combustion development of the Mercedes-Benz MY1999 CNG-Engine M366lag*. SAE Technical Paper nr 1999-01-3519,1999.

[31] Hosaka H. i in.: *Fuel injection control system for an automotive engine*. Patent USA, Nr 4967715, 1990.

[32] Idzior M.: *Influence of change quality engines passenger cars on toxic compounds exhaust emission*. Journal of KONES, Internal Combustion Engines 2003, vol. 10, 3-4.

[33] Idzior M., Lijewski P.: *Możliwości określenia jakości rozpylenia paliwa przez wtryskiwacze silników ZS metodą badania parametrów strugi rozpylonego paliwa*. Journal of KONES, Internal Combustion Engines 2002 No. 3-4 ISSN 1231- 4005, str. 104-112.

[34] Jakliński P.: *Badania wpływu parametrów sekwencyjnego wtrysku gazu propan-butan na pracę silnika o zapłonie iskrowym*. Rozprawa doktorska, Politechnika Lubelska, Lublin, 2005.

[35] Jakliński P., Czarnigowski J., Wendeker M.: *The effect of injection start angle of vaporized LPG on SI engine operation parameters.* SAE Technical Paper nr 2007-01-2054, 2007.

[36] Jaworski Z.: *Numeryczna mechanika płynów w inżynierii chemicznej i procesowej*. Akademicka Oficyna Wydawnicza EXIT, 2005.

[37] Jaworski A.: *Wpływ parametrów wtrysku sekwencyjnego układu zasilania ciekłym LPG na wybrane parametry użytkowe silnika spalinowego*. Rozprawa doktorska, Politechnika Rzeszowska, Rzeszów 2005.

[38] Kadota T., Mizatani S., Wu C., Hosimo M.: *Fuel droplet size measurement In the combustion chamber of motored SI engine via laser MIE scattering*. SAE Technical Paper nr 90047, 1990.

[39] Kamiński T.: *Ocena jakości procesu roboczego silnika o zapłonie iskrowym z wykorzystaniem światłowodowego czujnika interferencyjnego*. Rozprawa doktorska, Politechnika Lubelska, Lublin, 2005.

[40] Kelly-Zion P. i inni: *Liquid fuel behavior in port-injected SI engine.* Automotive Engineering International, January 1999.

[41] Kenihan S.: *Reducing the emissions from your council fleet*. Cities for Climate Protection Australia: An ICLEI program in collaboration with the AGO, http://www.iclei.org, 1999.

[42] Kato S., Hayashida T., Iida M.: *The Influence of Port Fuel Injection on Combustion Stability*. Yamaha Motor Technical Review, Technical Papers and Articles, 09.10.2008.

[43] Kowalewicz A.: *Tworzenie mieszanki i spalanie w silnikach o zapłonie iskrowym*. Wydawnictwa Komunikacji i Łączności, 1984.

[44] Latusek J., Burrahm R.: *Conversion of Two Small Utility Engines to LPG Fuel*. SAE Technical Paper Series nr 932447, 1993.

[45] Lee D., Cho S., Lee B., S. Ko, Park J., Choi J.: *Enhancement of volumetric efficiency in a gaseous LPG injection engine*. The 13th International Pacific Conference on Automotive Engineering, Gyeongju, South Korea, 2005.

[46] Lee D., Cho S., Lee B., Ko S., Choi J.: *Intake flow observation with gaseous LPG injection in a SI engine*. ILASS–Asia 2005, Oct. 13-14, 2005, Seoul, Korea.

[47] Lee J., Farrell P. V.: *Intake Valve Flow Measurements of an IC Engine Using Particle Image Velocimetry*. SAE Paper No. 930480, 1993.

[48] Lenz H.: *Mixture Formation in Spark Ignition Engines*. Springer Verlag, Wiedeń, 1992.

[49] Mahmood Z., Chen A., Yianneskis M., Ganti G.: *On the structure of steady flow through dual-intake engine ports*. International Journal for Numerical Methods in Fluids 1996, 23, str. 1085–1090.

[50] Majerczyk A., Taubert S.: *Układy zasilania gazem propan-butan LPG*. Wydawnictwa Komunikacji i Łączności, Warszawa, 2004.

[51] Makoto N., Hiroshi M., Katsuyuki O., Toshio Y.: *Improvement of fuel Behavior Model for Port-Injection Gasoline Engine*. The Fourth International Symposium COMODIA 98, 1998, str. 523-530.

[52] Małek A., Wendeker M., Czarnigowski J., Grabowski Ł., Jakliński P., Barański G., Sochaczewski R., Podleśny M.: *Stanowisko do badań prehomologacyjnych dla pojazdów wyposażonych w układ sekwencyjnego wtrysku gazu LPG*. PTNSS Congress-2007 P07-C148, Silniki Spalinowe PTNSS-2007-SC2, str. 290-299.

[53] Marchal C., Moréac1 G., Vovelle C., Mounaïm-Rousselle C., Mauss F.: *Soot modelling in automotive engines*. Proceedings of the European Combustion Meeting 2009.

[54] Materiały firmy CD Adapco.

[55] Materiały reklamowe firmy OPRTAND. Strona internetowa: www.optrand.com.

[56] Merkisz J., Mazurek S.: *Pokładowe systemy diagnostyczne pojazdów samochodowych OBD*. Wydawnictwo Komunikacji i Łączności, 2006.

[57] Merkisz J., Pielecha I.: *Alternatywne napędy pojazdów*. Wydawnictwo Politechniki Poznańskiej, 2006.

[58] Merkisz J., Pielecha I.: *Alternatywne paliwa i układy napędowe pojazdów*. Wydawnictwo Politechniki Poznańskiej, 2004.

[59] Merola S., Sementa P., Tornatore C., Vaglieco B.: *Effect of fuel film deposition on combustion process in PFI SI engine*. J. KONES Powertrain Transport 2007, 14(3), str. 395–402.

[60] Merola S., Sementa P., Tornatore C., Vaglieco B.M.: *Effect of the fuel injection strategy on the combustion process in a PFI boosted spark-ignition engine*. Science Direct, Energy, 2009, www.elsevier.com/locate/energy.

[61] Michalski M. Ł.: *Kierunki wykorzystania zasobów gazu ziemnego na świecie*. Rynek Energii – nr 1/2007.

[62] Minoru O., Yoshishige O.: *High Performance Engine Control System*. SAE Technical Paper nr 881154, 1988.

[63] Murali B. K., Bijucherian A., Mallikarjuna J. M.: *Effect of Intake Manifold Inclination on Intake Valve Flow Characteristics of a Single Cylinder Engine using Particle Image Velocimetry*. Proceedings of World Academy Of Science, Engineering and Technology Volume 34, ISSN 2070-3740, October 2008.

[64] Nakonieczny K., Fijałkowski S., Tarkowski P. *Semi-discrete FEM approach to modelling one dimensional gas dynamics*, Numerical methods in laminar and turbulent flow. Vol. 10, red. C. Taylor; J. Cross, Swansea, Pineridge Press, 1997, str. 903-913.

[65] Ney R.: *Zasoby ropy naftowej, Polityka Energetyczna*, Tom 9, Zeszyt specjalny 2006, PL ISSN 1429-6675.

[66] Niewczas A.: *Laboratorium silników spalinowych*. Politechnika Lubelska, 1996.

[67] Ommi F., Movahednejad E., Nekofar K.: *Theoretical and Experimental Study of Multi-Phase Flow in the Intake Port of a Port Fuel Injection Engine*. Leonardo Journal of Sciences, ISSN 1583-0233, Issue 14, January-June 2009, str. 31-49

[68] Orkisz M. i inni: *Wymiana ładunku w czterosuwowych silnikach tłokowych*. WKiŁ, Warszawa, 1991.

[69] Peters B., Gosman A. D.: *Numerical Simulation of Unsteady Flow in Engine Intake Manifolds*. SAE Paper 930609, 1993.

[70] Peters H., Spicher U.: *Numerical Analyses of the Combustion Process in a Spark-Ignition Engine*. The Japan Society of Mechanical Engineers, No.01-204 (20010701) p. 41, 2000.

[71] Polska norma PN-89/S-02006: *Pojazdy samochodowe, przyczepy i naczepy - Kategorie - Symbole i określenia*.

[72] Regulamin EKG ONZ Nr 83 Załącznik 114: *Jednolite przepisy dotyczące homologacji pojazdów w zakresie emisji zanieczyszczeń w zależności od wymagań paliwowych silnika*.

[73] Regulamin EKG ONZ Nr 115 Załącznik 114: *Jednolite przepisy dotyczące specjalnych układów doposażenia LPG (skroplonego gazu ropopochodnego), które mają być zainstalowane w pojazdach samochodowych dla wykorzystywania LPG do ich napędu*. Nowelizacja 3, Genewa 1995.

[74] Rola M., Wendeker M., Jakliński P., Czarnigowski J., Grabowski Ł., Szlachetka M.: *Badania symulacyjne układu zasilania gazem propan – butan silnika o zapłonie iskrowym*, PTNSS CONGRESS-2007 P07-C161, Silniki Spalinowe PTNSS-2007-SC3, str. 157-163.

[75] Shibata T., Matsui H., Tsubouchi M., Katsurada M.: *Evaluation of CFD Tools Applied to Engine Coolant Flow Analysis*. Mitsubishi Motors, Technical Review nr 16, 2004, www.mitsubishi-motors.com.

[76] Schöner N.: *LPG – The true Alternative*. Aral Autogas Manager Germany, Austria, 29.05.2009.

[77] Semin, Ismail A. R., Bakar R. A.: *Gas Fuel Spray Simulation of Port Injection Compressed Natural Gas Engine Using Injector Nozzle Multi Holes*. European Journal of Scientific Research ISSN 1450-216X, Vol.29 No.2, 2009, str.188-193.

[78] Semin, Ismail A. R., Bakar R. A.: *Simulation Investigation of Intake Static Pressure of CNG Engine*, Journal of Engineering and Applied Sciences 3 (9): str. 718-724, Medwell Journals, 2008.

[79] Shashikantha E., Parikh P.P.: *Spark ignition producer gas engine and dedicated compressed natural gas engine- technology development and experimental performance optimization*. SAE Technical Paper nr 1999-01-3515, 1999.

[80] Shojaeefard M.H., Noorpoor A.R.*: Flow Simulation in Engine Cylinder with Spring Mesh*, American Journal of Applied Sciences 5 (10), 2008, str. 1336-1343.

[81] Smith W. J., Timoney D. J., Lynch D. P.: *Emissions and Efficiency Comparison of Gasoline and LPG Fuels in a 1.4 Litre Passenger Car Engine*. SAE Technical Paper nr 972970, 1997.

[82] Sowa A.: *Samochodowe instalacje zasilania gazem*, Wydanie I, 2007, ISBN: 978-83-60863-30-5.

[83] Star-CD v. 3.24, Methodology.

[84] Tarkowski P.: *Metody badań zużycia rozpylaczy paliwa silników z Z.S.* Tendencje rozwojowe w konstrukcji, technologii i eksploatacji samochodów, Seminarium Techniczno-Naukowe MOTORYZACJA'96, 29.11-1.12. 1996, Lublin, Politechnika Lubelska, s. 101-108.

[85] Uzdowski M.: *Problematyka wykorzystania paliw alternatywnych do zasilania silników trakcyjnych*. MOTROL, 2008, 10, 143–146.

[86] Volvo Bi-Fuel LPG, vcc.volvocars.se/bifuel/index.htm

[87] Wendeker M.: *Adaptacyjne sterowanie wtryskiem benzyny w silniku samochodowym*. Państwowe Wydawnictwo Naukowe, Warszawa, 1999.

[88] Wendeker M.: *Sterowanie napełnianiem*. Lubelskie Towarzystwo Naukowe, Lublin 1999.

[89] Wendeker M.: *Sterowanie wtryskiem benzyny*. Lubelskie Towarzystwo Naukowe, Lublin 1999.

[90] Wendeker M., Jakliński P., Czarnigowski J., Filipek P.: *Investigation of the wideband SI lambda controlling system*, Journal of KONES Internal Combustion Engines No. 3-4, ISSN, 1231-4005, 2002.

[91] Wensing M., Kramer H., Munch K. U., Leipertz A.: *Mixture Formation and Combustion od Four-Valve SI Engine Investigation by Advanced Two-Dimensional Laser Measurement Techniques*. The Fourth Internatinal Symposium COMODIA 98, str. 379-385, 1998.

[92] Winterbone D. E., Pearson R. J.: *Design Techniques for Engine Manifolds Wave Action Methods for IC Engines*. Professional Engineering Publishing, UK, 2000.

[93] Yamato T., Hayashida M., Sekino H., Sugahara K.: *Effect of Injection Timing on the Performance of a Manifold Injection Gas Engine*, SAE Technical Paper nr 1999-01-3295, JSAE 9938050, 1999.

[94] Yasar, A., B. Sahin, H. Akilli, Aydin K.: *Effect of inlet port on the flow in the cylinder of an internal combustion engine*. Cukurova University, Adana, Turkey, Proc. I MechE Vol. 220, Part C: J. Mechanical Engineering Science, 2006.

[95] Yousufuddin S., Mehdi S. N.: *Performance and Emission Characteristics of LPG-Fuelled Variable Compression Ratio SI Engine*. Turkish J. Eng. Env. Sci., 32 (2008) TUBITAK, str. 7 – 12.

[96] Zhu G., Daniels C., Winkelman J.: *MBT timing detection and its closed-loop control using in-cylinder pressure signal*. SAE Technical Paper nr 2003-01-3266, 2003.

[97] Zhu G., Reitz R., Xin J., Takabayashi T.: *Modelling characteristics of gasoline wall films in the intake port of port fuel injection engines*. International Journal of Engine, Volume 2, Nr 4/2001, str. 231-248.

[98] www.vcc.volvocars.se/bifuel/print/lpg.htm.

[99] www.vcc.volvocars.se/bifuel/print/cng.htm.

[100] www.hilux4x4.co.za.

[101] www.0-60mag.com.

[102] www.bmwauto.net.

[103] www.hydrogencarsnow.com.

Symbols

CO	–	carbon monoxide
BDC	–	bottom dead center
TDC	–	top dead center
HC	–	hydrocarbons
LPG	–	Liquefied Petroleum Gas
L_w	–	distance of the injection nozzle from the inlet valve axis
n	–	engine speed
NO_x	–	nitrogen oxides
CA	–	crank angle
p_d	–	inlet manifold absolute pressure
p_g	–	pressure of LPG
t	–	time
T_{ch}	–	engine coolant temperature
t_{wtr}	–	injection time

α	–	level of significance
α_w	–	injection angle
ϕ	–	relative value of emissions
η_v	–	volumetric efficiency
φ	–	crank angle
λ	–	air fuel ratio
ρ	–	density
σ	–	standard deviation